Selection at Work in Plasmodium Falciparum: Lessons From the Expanded Acyl CoA Synthetase Gene Family and in Vitro Artemisinin Resistance.

Selection at work in *Plasmodium falciparum*: Lessons from the expanded acyl CoA synthetase gene family and *in vitro* artemisinin resistance

A dissertation presented

by

Allison Ross Demas

to

The Committee on Higher Degrees in Biological Sciences in Public Health

in partial fulfillment of the requirements

for the degree of

Doctor of Philosophy

in the subject of

Biological Sciences in Public Health

Harvard University

Cambridge, Massachusetts

April 2016

Dissertation Advisor: Professor Dyann F. Wirth Allison Ross Demas

Selection at work in *Plasmodium falciparum*: Lessons from the expanded acyl CoA synthetase gene family and *in vitro* artemisinin resistance

Abstract

Approximately one third of the world's population is at risk of contracting malaria. The World Health Organization estimates there were over 200 million news cases of malaria in 2015, resulting in nearly 500,000 deaths from this preventable disease. The majority of fatalities occur in Sub-Saharan Africa, where *Plasmodium falciparum* malaria causes severe disease in children under the age of five and pregnant women. In the last decade, increased anti-malaria interventions have resulted in substantial decreases in cases and fatalities. However, the recent emergence of artemisinin drug resistance in Southeast Asia threatens these gains, and the loss of another first-line antimalarial therapy would be a devastating setback.

The first goal of this work was to identify genetic markers of artemisinin drug resistance. Identifying the genetic determinants and molecular mechanisms of artemisinin resistance is crucial for understanding the emergence of this phenomenon and tracking the spread of these drug resistant parasites. Over the course of four years, we used an *in vitro* drug resistance selection approach to generate three independent artemisinin-resistant lines. Here we characterize those lines, and present Pfcoronin, a kelch13-like protein, as a novel candidate marker for artemisinin resistance. This study identifies additional non-

kelch13 molecular markers of artemisinin resistance, increases our understanding of how this resistance is acquired, and sheds light on the molecular mechanisms of artemisinin resistance in the parasite.

In contrast to *in vitro* selection, natural selection of parasites occurs during natural infection. Investigation of specific genes under selection in the parasite will increase our understanding of biological processes that provide a fitness advantage, and potentially identify novel pathways for therapeutic development.

Here, we focused on the acyl Co-A synthetase (ACS) gene family, previously shown to be under recent positive selection in *P. falciparum*. The signatures of recent positive selection identified in natural parasite populations suggest that particular ACS alleles may confer a selective advantage. Using molecular genetics approaches, we show distinct expression and localization patterns for individual ACS isoforms, and identify a growth defect in the ACS5 knockout line. Follow up studies characterize the fatty acid and metabolic profiles of individual ACS knockout lines, and point to a role for ACS5 in central carbon metabolism in *P. falciparum*.

Our investigation of the ACS gene family and their role in *P. falciparum* growth and metabolism led us to hypothesize a link between ACS activity and central carbon metabolism. In the final chapter, we explore the basic fatty acid and glucose requirements for *P. falciparum* growth *in vitro*, and present a metabolic profile for these starved parasites. Under starvation conditions, we were able to demonstrate fatty acid oxidation activity in the parasite. This is an unexpected finding, as this pathway was not previously annotated in the genome.

Taken together, these two projects tell a story of the selective pressures acting on *P. falciparum* parasites. Investigating *in vitro* selected artemisinin-resistant lines provides important insights into genetic markers and acquisition of resistance. Molecular and

biochemical characterization of a gene family under natural selection in *P. falciparum* increases our understanding of important metabolic pathways that support parasite growth.

Table of Contents

Listing of Figures

Chapter 1

Chapter 2

Chapter 3

Chapter 4

Chapter 5

Chapter 7

Listing of Tables

Chapter 2

Chapter 3

Chapter 4

Chapter 5

Chapter 7: Appendix

Acknowledgements

The work presented here would not have been possible without the love and support of many people. I would first like to thank my parents, Liz and Doug Demas, for their unwavering support of all my goals. I would not be where I am today without their love and encouragement. My brother and fellow grad student, Jeff Demas, has always been there for support and commiseration, and to show me how "real science" is done. In the end, we both win. I also want to thank my amazing boyfriend, Sam Greenblatt, who stuck it out through this impossibly difficult time, and emerged thoroughly convinced that I am, in fact, an evil scientist. I couldn't have done it without you.

Over the years, I have been privileged to work with many dedicated and brilliant professors, and their mentorship was instrumental to my development as a scientist. The work in this dissertation was carried out in the lab of Professor Dyann Wirth, and I am sincerely grateful for her support throughout my graduate school career. Dyann gave me the freedom to explore the craziest ideas, and her ability to always see the bigger picture helped focus and make sense of the science. Though I lost many quarters over the years, I am a better scientist for it. I especially want to thank her for being such a strong role model, and encouraging me to be part of the parasitology research community. Her passion and support of young scientists is inspiring.

I am also indebted to Professor Daouda Ndiaye at the Université Cheikh Anta Diop for my initial introduction to malaria research. The year I spent working with him in Senegal was transformative and motivated me to continue in parasitology. I would also like to thank Dr. Venkatachalam Udhayakumar at the Centers for Disease Control and Prevention. As a fellow in his lab, I learned how basic research informs public health policy, and I am so fortunate to benefit from his support and encouragement of my continuing studies.

I would also like to thank my Dissertation Advisory Committee, Professors Sarah Fortune, Dan Hartl, and Jay Mitchell, for their expert guidance over the years. Their input helped keep this project on track, and their incisive questions furthered my development as a researcher. I am also grateful to the Biological Sciences in Public Health program at HSPH, and the leadership of Professors Marianne Wessling-Resnick and Brenden Manning.

Fellow members of the Wirth Lab have been wonderful colleagues and friends over the years. In particular, Ulf Ribacke, Selina Bopp, Amanda Lukens, Rachel Daniels, Tomoyo Kato, Pam Magistrado, Angana Mukherjee, Jon Herman, Leila Ross, Lola Fagbami, and Wesley Wong: thank you all for your friendship, guidance, and support over the years. A very special thank you to the members of team ACS: Ulf, Selina, and Pam. This very collaborative project would not have been realized without your hard work, tequila shots, dark and stormies, and endless moral support. A special thank you to Sarah Volkman as well for her support in all things, scientific and otherwise, over the years. She is an amazing resource and wonderful mentor. I would also like to thank the other parasitology labs in IID. I am extremely fortunate to be part of such an exciting research community, and I have benefited greatly from the expertise of so many individuals in this group over the years.

I was incredibly lucky to be surrounded by fantastic classmates in the BPH program. Caeul Lim, Alex Sakatos, Michelle Rooks, Peter Wagner, Eylul Harputlugil, and Lear Brace: I could not have picked a better cohort, and I can't imagine having survived grad school without you all. We made it through (!!!) and made so many wonderful memories along the way. I feel so fortunate to call such amazing people my friends. Lastly, a very special thank you to my dear friends, Andrea Marcotte, Robyn Brosius, and Faith Hester-Reyes. Your visits and our trips over the years kept me sane and grounded, and I love you all.

Chapter 1: Introduction

1.1 Malaria: global burden, epidemiology, and clinical disease

In spite of ongoing global efforts to control and eradicate malaria, the disease remains a significant contributor to morbidity and mortality worldwide. More than a third of the world's population is at risk for malaria, and according to the most recent estimates, there were over 200 million new cases of malaria in 2015, resulting in approximately 500,000 deaths (World Health Organization 2015b). The most vulnerable populations shoulder the overwhelming majority of the malaria disease burden, with almost 90% of cases occurring in children and pregnant women in Sub-Saharan Africa (World Health Organization 2015b). The other endemic regions of the world are mostly tropical, including Southeast Asia, South America, and India (Figure 1.1.1). Despite a 50% decrease in mortality since 2000, the malaria community still faces new challenges to control efforts as we look ahead to the ambitious goal of eradication.

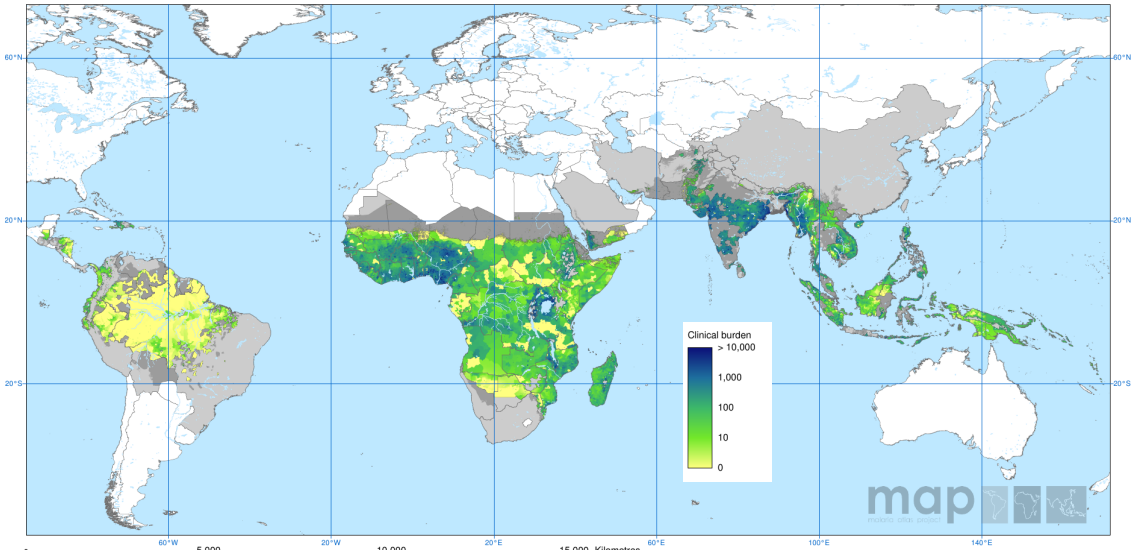

Figure 1.1.1. Mean clinical burden of *P. falciparum* malaria in 2007, expressed as the number of clinical cases per year per 5x5 km area (Hay & Snow 2006).

Malaria is caused by parasites of the genus *Plasmodium*, of which there are five species known to infect humans—*Plasmodium falciparum, P. vivax, P. ovale, P. malariae,* and *P. knowlesi*. *P. falciparum* is responsible for the majority of malaria deaths, while *P. vivax* is increasingly recognized as an important contributor to the global malaria burden (Breman & Brandling-Bennett 2011). Parasites are transmitted to the human host via the bite of female Anopheles mosquitoes. The *Anopheles gambiae* species complex is the most common vector for transmission of *P. falciparum* in Africa.

The majority of *P. falciparum* malaria cases are uncomplicated, manifesting as headache, fever, chills, nausea, and general malaise – not unlike the flu. In a minority of cases, especially in children under 5, more severe symptoms develop. Severe malaria symptoms include severe anemia, coma (indicative of cerebral malaria), metabolic acidosis, hypoglycemia, and death.

1.2 Public health interventions, control efforts, and the malaria eradication agenda

The complicated aspects of malaria transmission pose challenges to its control. Many successful control programs have focused on preventing the bite of infected mosquitoes. Bed nets create a physical barrier to transmission, while insecticide-based approaches, such as indoor residual spraying (IRS) or larvicidal spraying, kill the mosquito vector population en masse. Additional preventative measures, such as environmental modification, also target mosquito populations by eliminating their breeding areas.

One of the most effective tools in the arsenal against malaria is rapid treatment of cases. The World Health Organization (WHO) currently recommends Artemisinin Combination Therapy (ACT) to treat uncomplicated malaria cases, and intravenous artesunate for severe disease (World Health Organization 2015a). Artemisinin is a fast-acting and potent antimalarial, with a half-life of 2-5 hours (de Vries & Dien 1996). Administered in combination with a long-lasting partner drug (including amodiaquine, piperaquine, mefloquine, lumefantrine, sulfadoxine-pyrimethamine) parasite recrudescence is prevented and the efficacy of artemisinin is preserved.

The combination of these public health interventions, especially insecticide treated nets and increased coverage of effective anti-malarial therapy, has resulted in significant decreases in malaria cases and fatalities (World Health Organization 2015b). These gains are crucial and must be sustained in order to meet the ambitious goal of eradicating malaria in the near future. However, recent reports of emerging artemisinin resistance in Southeast Asia threaten these successes and are cause for alarm (Noedl et al. 2008; World Health Organization 2011).

1.3 Challenges to malaria control and eradication: drug resistance

The history of anti-malarial chemotherapy is fraught with cautionary lessons for current and future malaria control programs and treatment recommendations. Since the introduction of chloroquine in 1945, *P. falciparum* parasites have evolved resistance to nearly all major classes of antimalarials (World Health Organization 2010). Resistance to chloroquine evolved over many decades, while resistance to other drugs emerged on a much shorter time scale (Hyde 2005; Wongsrichanalai et al. 2002). Resistance to

atovaquone infamously developed during the clinical trials. Historically, resistance to many first-line antimalarials has developed independently in different geographical regions and then spread globally (Gregson & Plowe 2005; Wellems & Plowe 2001). As the evolution and spread of anti-malarial drug resistance is associated with increased risk of mortality, the prevention and containment of drug resistance must be considered a public health imperative (Trape 2001; Dondorp et al. 2011; World Health Organization 2011).

There are generally two means of drug resistance to consider in *P. falciparum*: mutations to the drug target itself, or alternate resistance mechanisms that render the drug less effective. Mutations in the target site decrease the efficacy of the compound. One such example is resistance to the anti-folate compounds, sulfadoxine and pyrimethamine (Gregson & Plowe 2005). Multiple mutations in dihydropteroate synthetase (*DHPS*) and dihydrofolate reductase (*DHFR*), the folate pathway enzymes targeted by sulfadoxine and pyrimethamine, respectively, modify the target of action and render the drugs less effective. These mutations evolved independently in South America and Southeast Asia, before spreading to Africa, leading to drug resistance worldwide.

Other resistance mechanisms include the increased efficacy of efflux pumps, which physically pump drugs away from their targets. Resistance to both chloroquine and mefloquine fall into this category. Chloroquine is predicted to act on the parasite by inhibiting detoxification of heme in the parasite digestive vacuole, an essential process for parasite growth (Wellems & Plowe 2001). The K76T mutation in the aptly-named Chloroquine Resistance Transporter (CRT) allows for effective efflux of the drug out of the parasite's digestive vacuole, decreasing its efficacy (Fidock et al. 2000; Wellems & Plowe 2001). In a second example, polymorphisms and copy number variation in the multidrug

resistance gene 1 (*Pfmdr1*), which encodes the gene product P-glycoprotein 1 (pgh1), are associated with antimalarial resistance (Reed et al. 2000; Duraisingh & Cowman 2005; Price et al. 2004). Pgh1 is a transporter localized to the food vacuole, similar to CRT. It is hypothesized to act by pumping cytosolic-acting drugs away from their targets of action, and into the parasite food vacuole for detoxification. *Pfmdr1* copy number variation is associated with increased mefloquine resistance (Price et al. 2004).

In the laboratory setting, drug resistance is measured by growing parasites in the presence of the drug of interest (Nzila & Mwai 2010). Measurements of parasite growth in serial dilutions of a drug can be used to generate a sigmoidal dose-response curve, from which one can calculate an EC_{50}, the effective drug concentration required to inhibit 50% of parasite growth. A shift in the dose-response curve, and a correspondingly higher EC_{50}, is indicative of *in vitro* drug resistance. These assays can be performed on parasites recently isolated from patients (*ex vivo*) to monitor drug resistance in malaria endemic settings. Clinically, drug resistance can be measured by reduced efficacy of a drug treatment, or treatment failure (parasite recrudescence) (World Health Organization 2010). Combined with molecular markers, these methods for assessing parasite drug susceptibility are used to monitor and track emergence of drug resistance globally.

Molecular epidemiology and *in vitro* drug resistance studies have identified many molecular markers associated with resistance to different antimalarial compounds. In the Wirth lab, a chemogenomics approach (*in vitro* drug resistance selection followed by whole genome sequencing of resistant lines) has been an effective method of identifying both drug targets and mechanisms of resistance (Wongsrichanalai et al. 2002; Lukens et al. 2014; Herman et al. 2015). It is important to note that identification of such resistance markers is not always

associated with clinical resistance or treatment failure in patients, but can be predictive of evolving resistance (Gregson & Plowe 2005). Currently, global surveillance efforts monitor molecular markers of drug resistance in many malaria-endemic regions with the goal of tracking resistance and informing public health and treatment policies.

As described above, ACTs are the current recommendation for first-line malaria treatment. The recent emergence of artemisinin resistance in Southeast Asia, coupled with reports of emerging resistance to the partner drugs used in ACTs, has the potential to create a public health disaster (Noedl et al. 2008; Dondorp et al. 2011; Spring et al. 2015; Leang et al. 2015). An estimated excess of 116,000 deaths would occur annually in a scenario of widespread ART resistance, with annual health costs in excess of US$32 million and productivity losses in excess of US$385 million, using conservative estimates (Lubell et al. 2014). According to WHO estimates, 21% of the 663 million malaria cases averted in sub-Saharan Africa between 2001 and 2015 were due to use of ACTs (World Health Organization 2015b). Loss of ACT efficacy due to drug resistance would mean 139 million more malaria cases in Africa. Research efforts to understand the molecular basis of artemisinin resistance and identify molecular markers are of high priority to help contain resistance, and prevent its spread worldwide.

1.4 Malaria parasite biology

Plasmodium parasites are unicellular eukaryotes, of the phylum Apicomplexa. These protozoan pathogens have a complicated life cycle alternating between the mosquito and human hosts (Figure 1.4.2). Infective sporozoites are released from the salivary glands of the mosquito when it bites a human, and must travel to the liver to multiply in hepatocytes.

This incubation stage generally lasts 7-14 days, during which time the infected individual is asymptomatic. Liver stage schizonts rupture and release merozoites into the bloodstream to begin the asexual intra-erythrocytic life cycle. Merozoites attach to and invade circulating red blood cells (RBCs). Once inside the RBC, the parasite develops from a ring, to a trophozoite, to a schizont over the course of 48hours. Asymmetric cell division segments the late schizonts into 8-32 daughter merozoites, which burst out to reinvade new RBCs. *P. falciparum* parasites, the focus of this dissertation, multiply exponentially over the course of these 48 hour cycles, causing the clinical symptoms associated with human disease (Miller et al. 2002).

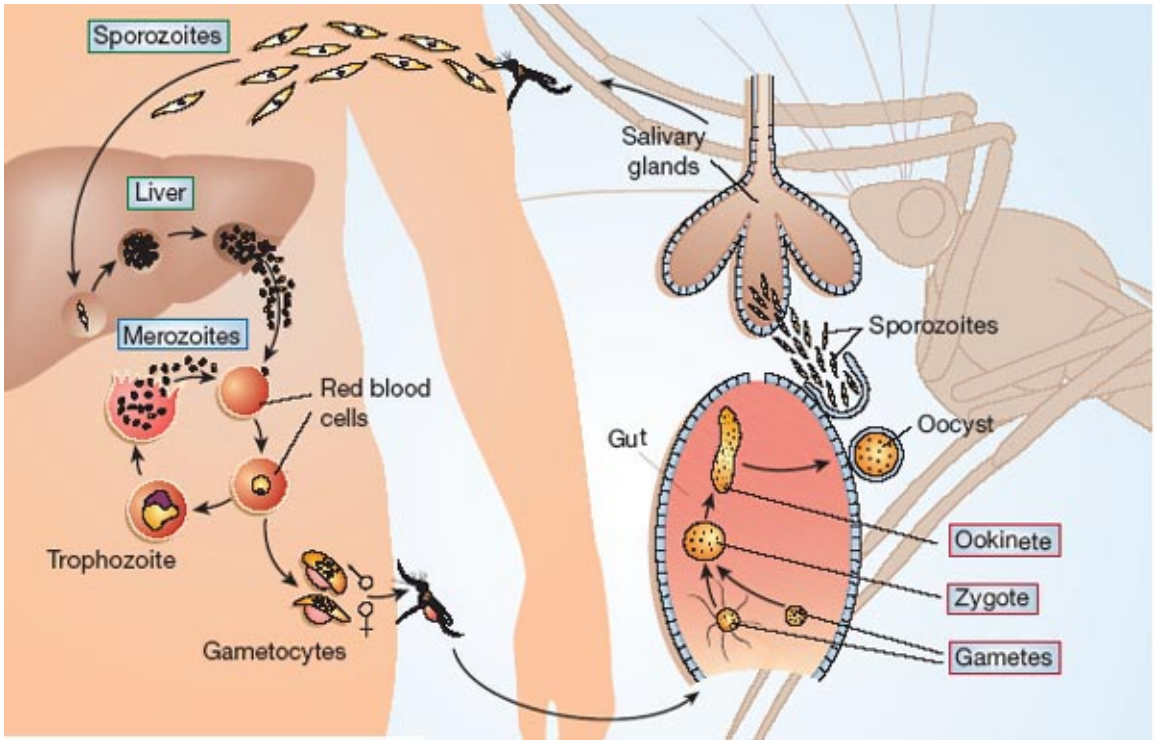

Figure 1.4.2. The complicated life cycle of *Plasmodium* parasites alternates between humans and *Anopheles* hosts (Ménard 2005).

A subset of these asexually replicating forms differentiates into gametocytes, the transmissible form of the parasite. Gametocytes are picked up through the bite of a new mosquito to begin the sexual stages of the parasite life cycle. Male and female gametes mate in the mosquito midgut, resulting in formation of a zygote. This diploid form allows for recombination of parasite genetic material. Zygotes develop into motile ookinetes, which migrate out of the mosquito midgut wall and develop into oocysts. Mature oocysts undergo many divisions over approximately 1-2 weeks, then rupture to release thousands of haploid sporozoites. *Plasmodium* sporozoites migrate to the mosquito salivary glands, ready to be injected into the next human host with the next blood meal and begin the cycle anew.

This dissertation will focus on *P. falciparum* parasites during the intra-erythrocytic stages of the asexual life cycle in the human host. Following invasion of merozoites into the RBC, parasites create their niche in the parasitophorous vacuole (PV) and begin substantial remodeling of the host cell to fit their needs, reviewed in (Maier et al. 2009). The parasite exports an impressive number of proteins across its plasma cell membrane and beyond the PV to the host cell cytoplasm and surface membrane. This exportome is responsible for altering the cytoskeleton and adherence properties of the host RBC. These parasite-directed modifications are important mediators of parasite virulence and disease pathology. For example, adherence of parasitized RBCs to the host endothelium (cytoadherence) is responsible for sequestration of parasites in the microvasculature of the brain and placenta, as seen in cerebral malaria and maternal malaria (Miller et al. 2002).

Sequencing of the *P. falciparum* genome in 2002 revealed minimalism in parasite metabolic functions inside the RBC (Gardner et al. 2002). For example, the parasite has lost the ability for *de novo* synthesis of amino acids and purines, instead relying exclusively on scavenging

from the host. The parasite maintains basic carbon metabolism pathways, including glycolysis, the TCA cycle, and the pentose phosphate pathway (MacRae et al. 2013; Oppenheim et al. 2014; Barrett 1997). *Plasmodium* minimalist metabolism necessitates a close relationship with the host, and this obligate intracellular pathogen is heavily reliant on uptake of nutrients to meet its needs (Landfear 2011; Saliba & Kirk 2001).

1.5 *Plasmodium* Lipids and Fatty Acids

Plasmodium lipids play essential roles in parasite growth and differentiation. Lipid membranes form the barrier between the host cell and the parasite, the membranes of the parasite's intracellular organelles, and the cytoplasmic networks inside the infected host RBC. They also play important roles in cell signaling, protein modification, and hemozoin formation (Vial & Ben Mamoun 2005).

Upon infection of a host RBC, the parasite dramatically alters both the content and the composition of the lipids. The parasite actively takes up precursor molecules from the host to supply its lipid biosynthesis pathways. The amount of phospholipids, the most abundant lipid class in *Plasmodium*-infected RBCs, increases to six times that of uninfected RBCs. Additional increases are reported in the neutral lipid pool of infected RBCs, including increases in fatty acids (FA), diacylglycerols (DAG), and triacylglycerols (TAG), though these species represent a very small fraction of the total lipid pool (Holz 1977; Vial & Ben Mamoun 2005; Vial & Ancelin 1998; Sherman 1979).

Completion of the genome sequence revealed that *P. falciparum* has all the required enzymes to perform bacterial-like Type II Fatty Acid Synthesis (FAS) (Gardner et al. 2002).

These enzymes are localized in the plastid-like apicoplast, a unique organelle characteristic of the Apicomplexan phylum (Waller et al. 1998). Early reports suggested that *P. falciparum* synthesizes 10-14 carbon chain fatty acids in *in vitro* culture of asexual stages (Surolia & Surolia 2001; Surolia et al. 2004; Ralph et al. 2004); however, these reports have been contradicted by subsequent studies demonstrating that crucial enzymes for Type II FAS, such as pyruvate dehydrogenase and FabI, are not essential for maintaining asexual replication (Pei et al. 2010; Yu et al. 2008; Vaughan et al. 2009). Interestingly, these gene knockouts did inhibit late liver stage growth, suggesting that Type II FAS is more important in this stage of the parasitic lifecycle (Vaughan et al. 2009). Transcription of these enzymes is indeed elevated in the liver stages (Tarun et al. 2008), compared to the minimal to undetectable mRNA expression in asexual stages (Bozdech et al. 2003). More recent metabolomics studies have used gas chromatography-mass spectrometry (GC-MS) to show that parasites grown with ^{13}C glucose *in vitro* do not produce ^{13}C labeled lipids, which supports the model of inactive Type II FAS during blood stages (Olszewski et al. 2010). This further emphasizes the importance of fatty acid scavenging from the host during the intra-erythrocytic life cycle, when the parasite must meet the significant fatty acid demands of sustained growth and replication (Vial & Ancelin 1998).

The parasite supplies the majority of its fatty acid requirements through scavenging pathways (Beaumelle & Vial 1988; Holz 1977). Serum FAs vary between human hosts, and the RBC membrane FA composition also changes with diet (Glatz et al. 1989; Nikkari et al. 1995). A mix of saturated and unsaturated fatty acids (not phospholipids or neutral lipids) is sufficient for maintaining *in vitro* growth of *P. falciparum* (Mitamura et al. 2000). *Plasmodium* has limited ability to modify these fatty acids, either by desaturation or elongation, and incorporate them into phospholipids and neutral lipids (Mi-Ichi et al. 2006).

Scavenged free fatty acids are activated through the addition of a coenzyme A moiety. This reaction is carried out by a family of enzymes known as the Acyl CoA Synthetases (ACS).

1.6 The *P. falciparum* Acyl CoA Synthetase Gene Family

The Acyl CoA Synthetase enzymes (EC: 6.2.1, fatty acid thiokinase) catalyze the activation of free fatty acids by a two-step reaction (Watkins 1997). The first step is the energetically favorable pyrophosphorolysis of adenosine triphosphate (ATP) to adenosine monophosphate (AMP), followed by thioesterification with Coenzyme A. Activation of free fatty acids is a crucial first step for entry into fatty acid synthesis, desaturation, and elongation pathways. In other systems, different isoforms of these enzymes are also known to regulate fatty acid uptake and transport (Black & DiRusso 2003), fatty acid entry into downstream metabolic pathways (Coleman et al. 2002), protein acylation (Ashrafi et al. 1998; Resh 1999), subcellular transport of proteins (Pfanner et al, Cell 1987), cell signaling (Faergeman & Knudsen 1997), and gene transcription (Black et al. 2000).

Plasmodium ACS enzymes mediate fatty acid scavenging. ACS activity is known to increase 20-fold in *P. knowlesi*-infected RBCs, and this activity is essential for asexual growth (Beaumelle & Vial 1988; Holz 1977). *Plasmodium* species, including the human-infecting species *P. falciparum*, *P. vivax*, and *P. knowlesi*, and the rodent-infecting species *P. berghei* and *P. yoelii*, have four ACS orthologs, known as ACS9-12 (Bethke et al. 2006). These four genes share homology to ACS genes from other systems, and they contain the characteristic ACS motif and AMP/ATP binding domains (Black et al. 1997). Interestingly, in *P. falciparum*, ACS9 has expanded to nine globally-conserved paralogs (ACS1a-ACS8) (Bethke et al. 2006). We recently identified a similar expansion in *P. reichenowi* (Figure 1.5.1; Nathan Hicks and

Selina Bopp, unpublished). This suggests that the ACS gene family expansion occurred after the *Laverania* clade split from the other *Plasmodium* species. Interestingly, the ACS9 gene in both species has expanded to a similar number of paralogs (thirteen in both *P. falciparum* and *P. reichenowi*), though not all expanded paralogs are identified in both species.

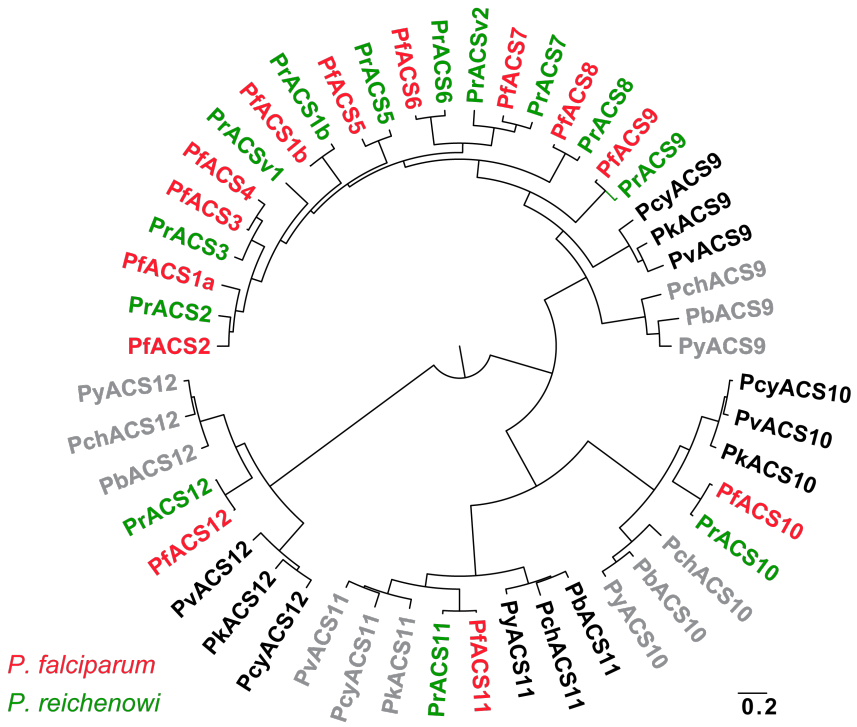

Figure 1.5.1. Phylogenetic tree shows the expansion of the ACS gene family in both *Plasmodium falciparum* (Pf) and *P. reichenowi* (Pr). ACS9, 10, 11 and 12 are conserved in *P. falciparum*, *P. reichenowi, P. yoelii* (Py), *P. chabaudi* (Pch), *P. berghei* (Pb), *P. vivax* (Pv), *P. knowlesi* (Pk), and *P. cynomolgi* (Pc). (Figure adapted from Nathan Hicks and Selina Bopp)

Gene duplications and expansions in *Plasmodium* have previously been associated with antigenic variation for immune evasion (Freitas-Junior et al. 2000) and drug resistance (Price et al. 2004). Specifically in *P. falciparum*, gene family expansions are implicated in both antigenic variation and cytoadherence (Gardner et al. 2002; Su et al. 1995; Fernandez

et al. 1999; Niang et al. 2009). In other systems, such gene duplication events are a significant source of genetic diversity, and may indicate novel functions in new paralogs (Ohno et al. 1968; Force et al. 1999; Lynch & Conery 2000).

Conserved ACS orthologs ACS9 and ACS10 have been shown to be under recent positive selection by Long Range Haplotype (LRH) Analysis (Van Tyne et al. 2011; Mu et al. 2010). This test of natural selection identifies long haplotypes that have not been broken down by recombination, indicating the presence of a mutation under recent positive selection (Sabeti et al. 2002). In the study by Van Tyne et al., ACS2, ACS8, ACS9, and ACS10 were shown to be highly divergent between Thai and Senegalese populations, with decreased single nucleotide polymorphism (SNP) diversity within each individual populations (Van Tyne et al. 2011). Together with a high divergence of non-synonymous SNPs between populations, this data suggests allelic variants that may confer selective advantage. Additionally, GWAS for phenotypes of drug resistance have found associations between ACS10 and artemisinin resistance (Van Tyne et al. 2011; Cheeseman et al. 2012). Integration of these different genomics approaches provides strong evidence that the ACS gene family, and thus lipid metabolism, is important for *P. falciparum* parasite fitness.

1.7 Overview of thesis chapters

The remarkable plasticity of the *Plasmodium falciparum* genome allows for adaptation in response to selective pressures and challenges efforts to combat this important human pathogen. In this dissertation, I present the findings from two very different projects, linked by the common theme of selective pressure at work in *Plasmodium falciparum*.

In Chapter 2, I will explore the selection effects exerted by artemisinin pressure *in vitro*. Over the course of four years, we selected three independent artemisinin resistant *P. falciparum* lines from Senegalese parent strains. These strains are found to be resistant by the $^{0\text{-}3h}$Ring Stage Survival Assay, and do not have the recently described kelch13 mutations associated with artemisinin resistance in Cambodia (Ariey et al. 2014). We present the findings of Whole Genome Sequencing of these selected parasites and their parental strains, and the thirteen candidate SNPs identified in the resistant lines.

The next three chapters investigate the acyl CoA synthetase (ACS) gene family and its role in *P. falciparum* fatty acid metabolism. The goal of this work is to explore an example of natural selection occurring in *P. falciparum*, as members of the ACS gene family have been shown to be under recent positive selection in the parasite. In Chapter 3, I present the findings of our initial descriptive study of the ACS gene family. We generated HA-tagged ACS lines in a 3D7 background, and used these strains to characterize the localization and expression profiles of several members of the ACS gene family *in vitro*. We identify specific differences in transcription, protein expression, and localization within the cell, suggesting that different ACS isoforms have distinct biological roles.

Chapter 4 comprises results from our continued study of the ACS gene family, using knockout lines to assess the function of individual ACS enzymes and their contributions to FA metabolism in the parasite. Specifically, we characterize a growth defect in the ACS5 knockout line, and use different biochemical approaches to determine the metabolic changes in the knockout that may be inhibiting parasite growth.

Finally, in Chapter 5, I take a step back, and look at FA metabolism in *P. falciparum* more generally, following up on observations about FA requirements for growth in different *in vitro* conditions. We determine the minimal nutrients required to support *P. falciparum* growth *in vitro*, and then measure the effects of this starvation on the overall metabolome of the parasite. We report evidence for an unexpected fatty acid oxidation pathway in *P. falciparum*, and discuss how this pathway may contribute to parasite energy requirements for sustained growth.

References

Ariey, F. et al., 2014. A molecular marker of artemisinin-resistant Plasmodium falciparum malaria. *Nature*, 505.

Ashrafi, K., Farazi, T.A. & Gordon, J.I., 1998. A role for Saccharomyces cerevisiae fatty acid activation protein 4 in regulating protein N-myristoylation during entry into stationary phase. *The Journal of Biological Chemistry*, 273(40), pp.25864–25874.

Barrett, M.P., 1997. The Pentose Phosphate Pathway and Parasitic Protozoa. *Parasitology Today*, 13(1), pp.11–16.

Beaumelle, B.D. & Vial, H.J., 1988. Correlation of the efficiency of fatty acid derivatives in suppressing Plasmodium falciparum growth in culture with their inhibitory effect on acyl-CoA synthetase activity. *Molecular and Biochemical Parasitology*.

Bethke, L.L. et al., 2006. Duplication, gene conversion, and genetic diversity in the species-specific acyl-CoA synthetase gene family of Plasmodium falciparum. *Molecular and Biochemical Parasitology*.

Black, P.N. et al., 1997. Mutational analysis of a fatty acyl-coenzyme A synthetase signature motif identifies seven amino acid residues that modulate fatty acid substrate specificity. *The Journal of Biological Chemistry*, 272(8), pp.4896–4903.

Black, P.N. & DiRusso, C.C., 2003. Transmembrane movement of exogenous long-chain fatty acids: proteins, enzymes, and vectorial esterification. *Microbiology and Molecular Biology Reviews*, 67(3).

Black, P.N., Faergeman, N.J. & DiRusso, C.C., 2000. Long-Chain Acyl-CoA-Dependent Regulation of Gene Expression in Bacteria, Yeast, and Mammals. *Journal of Nutrition*, 130, p.305S–209S.

Bozdech, Z. et al., 2003. The transcriptome of the intraerythrocytic developmental cycle of Plasmodium falciparum. *PLoS Biology*, 1(1).

Breman, J.G. & Brandling-Bennett, A.D., 2011. The challenge of malaria eradication in the

twenty-first century: Research linked to operations is the key. *Vaccine*, 29(SUPPL. 4), pp.D97–D103.

Cheeseman, I.H. et al., 2012. A major genome region underlying artemisinin resistance in malaria. *Science*, 336(79).

Coleman, R. et al., 2002. Do Long-Chain Acyl-CoA Synthetases Regulate Fatty Acid Entry into Synthetic Versus Degradative Pathways? *The Journal of Nutrition*, 132, pp.2123–2126.

Dondorp, A.M. et al., 2011. The Threat of Artemisinin-Resistant Malaria. *New England Journal of Medicine*, 365(12).

Duraisingh, M.T. & Cowman, A.F., 2005. Contribution of the pfmdr1 gene to antimalarial drug-resistance. *Acta Tropica*, 94(3), pp.181–190.

Faergeman, N.J. & Knudsen, J., 1997. Role of long-chain fatty acyl-CoA esters in the regulation of metabolism and in cell signaling. *Biochemistry Journal*, 323, pp.1–12.

Fernandez, V. et al., 1999. Small, clonally variant antigens expressed on the surface of Plasmodium falciparum-infected erythrocytes are encoded by the rif gene family and are the target of human immune responses. *Journal of Experimental Medicine*, 190(10), pp.1393–1403.

Fidock, D.A. et al., 2000. Mutations in the P. falciparum digestive vacuole transmembrane protein PfCRT and evidence for their role in chloroquine resistance. *Molecular cell*, 6(4), pp.861–71.

Force, A. et al., 1999. Preservation of duplicate genes by complementary, degenerative mutations. *Genetics*.

Freitas-Junior, L.H. et al., 2000. Frequent ectopic recombination of virulence factor genes in telomeric chromosome clusters of P. falciparum. *Nature*, 407.

Gardner, M.J. et al., 2002. Genome sequence of the human malaria parasite Plasmodium falciparum. *Nature*, 419.

Glatz, J.F.C., Soffers, A.E. & Katan, M.B., 1989. Fatty acid composition of serum cholesteryl esters and erythrocyte membranes as indicators of linoleic acid in man. *American Journal of Clinical Nutrition*, 49, pp.269–276.

Gregson, A. & Plowe, C. V, 2005. Mechanisms of Resistance of Malaria Parasites to Antifolates. *Pharmacol Rev*, 57(1), pp.117–145.

Hay, S.I. & Snow, R.W., 2006. The Malaria Atlas Project: Developing global maps of malaria risk. *PLoS Medicine*, 3(12), pp.2204–2208.

Herman, J.D. et al., 2015. The cytoplasmic prolyl-tRNA synthetase of the malaria parasite is a dual-stage target of febrifugine and its analogs. *Science Translational Medicine*, 7(288), pp.1–9.

Holz, G.G., 1977. Lipids and the malarial parasite. *Bulletin of the World Health Organization*, 55(2-3), pp.237–248.

Hyde, J.E., 2005. Drug-resistant malaria. *Trends Parasitol*, 21(11).

Landfear, S.M., 2011. Nutrient transport and pathogenesis in selected parasitic protozoa. *Eukaryotic Cell*, 10(4), pp.483–493.

Leang, R. et al., 2015. Evidence of falciparum malaria multidrug resistance to artemisinin and piperaquine in western Cambodia: dihydroartemisinin-piperaquine open-label multicenter clinical assessment. *Antimicrobial agents and chemotherapy*, 59(8), pp.2–5.

Lubell, Y. et al., 2014. Artemisinin resistance--modelling the potential human and economic costs. *Malaria journal*, 13, p.452.

Lukens, A.K. et al., 2014. Harnessing evolutionary fitness in Plasmodium falciparum for drug discovery and suppressing resistance. *Proceedings of the National Academy of Sciences of the United States of America*, 111(2), pp.799–804.

Lynch, M. & Conery, J.S., 2000. The evolutionary fate and consequences of duplicate genes. *Science*, 290(5495), pp.1151–1155.

MacRae, J.I. et al., 2013. Mitochondrial metabolism of sexual and asexual blood stages of the malaria parasite Plasmodium falciparum. *BMC Biology*, 11(67).

Maier, A.G. et al., 2009. Malaria parasite proteins that remodel the host erythrocyte. *Nature Reviews Microbiology*, 7.

Ménard, R., 2005. Knockout malaria vaccine ? *Nature*, 433(January), pp.6–7.

Mi-Ichi, F., Kita, K. & Mitamura, T., 2006. Intraerythrocytic Plasmodium falciparum utilize a broad range of serum-derived fatty acids with limited modification for their growth. *Parasitology*, 133, pp.399–410.

Miller, L.H. et al., 2002. The pathogenic basis of malaria. *Nature*, 415.

Mitamura, T. et al., 2000. Serum factors governing intraerythrocytic development and cell cycle progression of Plasmodium falciparum. *Parasitology International*, 49, pp.219–229.

Mu, J. et al., 2010. Plasmodium falciparum genome-wide scans for positive selection, recombination hot spots and resistance to antimalarial drugs. *Nature genetics*, 42(3), pp.268–71.

Niang, M., Xue, Y.Y. & Preiser, P.R., 2009. The Plasmodium falciparum STEVOR multigene family mediates antigenic variation of the infected erythrocyte. *PLoS Pathogens*, 5(2).

Nikkari, T. et al., 1995. Fatty acid composition of serum lipid fractions in relation to gender and quality of dietary fat. *Ann Med*, 27(4), pp.491–8.

Noedl, H. et al., 2008. Evidence of Artemisinin-resistant malaria in Western Cambodia. *New England Journal of Medicine*, 359(24), pp.2619–2620.

Nzila, A. & Mwai, L., 2010. In vitro selection of Plasmodium falciparum drug-resistant parasite lines. *The Journal of antimicrobial chemotherapy*, 65(3), pp.390–8.

Ohno, S., Wolf, U. & Atkin, N.B., 1968. Evolution from fish to mammals by gene duplication. *Heredeteria*, 59(6).

Olszewski, K.L. et al., 2010. Branched tricarboxylic acid metabolism in Plasmodium falciparum. *Nature*, 466.

Oppenheim, R.D. et al., 2014. BCKDH: The Missing Link in Apicomplexan Mitochondrial Metabolism Is Required for Full Virulence of Toxoplasma gondii and Plasmodium berghei. *PLoS Pathogens*, 10(7).

Pei, Y. et al., 2010. Plasmodium pyruvate dehydrogenase activity is only essential for the parasite's progression from liver infection to blood infection. *Molecular Microbiology*.

Price, R.N. et al., 2004. Mefloquine resistance in Plasmodium falciparum and increased pfmdr1 gene copy number. *Lancet*, 364, pp.438–447.

Ralph, S.A. et al., 2004. Tropical infectious diseases: metabolic maps and functions of the Plasmodium falciparum apicoplast. *Nature Reviews Microbiology*, 2(3), pp.203–216.

Reed, M.B. et al., 2000. Pgh1 modulates sensitivity and resistance to multiple antimalarials in Plasmodium falciparum. *Nature*, 403(6772), pp.906–909.

Resh, M.D., 1999. Fatty acylation of proteins: new insights into membrane targeting of myristoylated and palmitoylated proteins. *Biochimica et Biophysica Acta*, 1451, pp.1–16.

Sabeti, P.C. et al., 2002. Detecting recent positive selection in the human genome from haplotype structure. *Nature*, 419.

Saliba, K.J. & Kirk, K., 2001. Nutrient acquisition by intracellular apicomplexan parasites: Staying in for dinner. *International Journal for Parasitology*, 31, pp.1321–1330.

Sherman, I., 1979. Biochemistry of Plasmodium (malaria parasites). *Microbiol Rev*, 43, pp.453–495.

Spring, M.D. et al., 2015. Dihydroartemisinin-piperaquine failure associated with a triple mutant including kelch13 C580Y in Cambodia: An observational cohort study. *The Lancet Infectious Diseases*, 15(6), pp.683–691.

Su, X.-Z. et al., 1995. The large diverse gene family var encodes proteins involved in cytoadherence and antigenic variation of Plasmodium falciparum-infected erythrocytes. *Cell*, 82, pp.89–100.

Surolia, A. et al., 2004. "FAS"t inhibition of malaria. *Biochemistry Journal*, 383, pp.401–412.

Surolia, N. & Surolia, A., 2001. Triclosan offers protection against blood stages of malaria by inhibiting enoyl-ACP reductase of Plasmodium falciparum. *Nature Medicine*, 7(2).

Tarun, A.S. et al., 2008. A combined transcriptome and proteome survey of malaria parasite liver stages. *PNAS*, 105(1), pp.305–310.

Trape, J., 2001. The public health impact of chloroquine resistance in Africa. *American Journal of Tropical Medicine and Hygiene*, 64(1-2 Suppl), pp.12–7.

Van Tyne, D. et al., 2011. Identification and functional validation of the novel antimalarial resistance locus PF10_0355 in Plasmodium falciparum. *PLoS Genetics*, 7(4).

Vaughan, A.M. et al., 2009. TypeII Fatty Acid Synthesis is essential only for malaria parsaite late liver stage development. *Cellular Microbiology*, 11(3), pp.506–520.

Vial, H.J. & Ancelin, M.L., 1998. Malarial lipids. In I. Sherman, ed. *Malaria: Parasite Biology, Pathogenesis, and Protection*. American Society for Microbiology.

Vial, H.J. & Ben Mamoun, C., 2005. Plasmodium lipids: metabolism and function. In I. W. Sherman, ed. *Molecular Approaches to Malaria*. ASM Press, pp. 327–352.

de Vries, P. & Dien, T., 1996. Clinical pharmacology and therapeutic potential of artemisinin and its derivatives in the treatment of malaria. *Drugs*, 52(6), pp.818–836.

Waller, R.F. et al., 1998. Nuclear-encoded proteins target to the plastid in Toxoplasma gondii and Plasmodium falciparum. *PNAS*, 95, pp.12352–12357.

Watkins, P.A., 1997. Fatty acid activation. *Progress in Lipid Research*.

Wellems, T.E. & Plowe, C. V, 2001. Chloroquine-resistant malaria. *J Infect Dis*, 184, pp.770–776.

Wongsrichanalai, C. et al., 2002. Epidemiology of drug-resistant malaria. *Lancet Infectious Diseases*, 2(4), pp.209–218.

World Health Organization, 2011. *Global plan for artemisinin resistance containment*, Available at: http://www.who.int/malaria/publications/atoz/artemisinin_resistance_containment_2011.pdf.

World Health Organization, 2010. *Global Report on Antimalarial Drug Efficacy and Drug Resistance: 2000-2010*,

World Health Organization, 2015a. *Guidelines For The Treatment of Malaria, third edition*,

World Health Organization, 2015b. *World Malaria Report 2015*,

Yu, M. et al., 2008. The Fatty Acid Biosynthesis Enzyme FabI Plays a Key Role in the Development of Liver-Stage Malarial Parasites. *Cell Host and Microbe*, 4, pp.567–578.

Chapter 2:

***In vitro* selection of three independent artemisinin-resistant *P. falciparum* lines**

2.1 Attribution

AUTHORS:

Allison Demas[1], Wesley Wong[1], Angela Early[2], Seth Redmond[2], Selina Bopp[1], Daniel E. Neafsey[2], Sarah K. Volkman[1,2,3], Dyann F. Wirth[1,2]

[1] Harvard T.H. Chan School of Public Health, Boston, MA, USA.

[2] Broad Institute, Cambridge, MA, USA.

[3] Simmons College, Boston, MA USA

AUTHOR CONTRIBUTIONS:

A.D. performed drug resistance selections, phenotyping assays, PCR resequencing, and data analysis. W.W., A.E., and S.R. contributed to SNP calling and additional genetic analyses. S.B. assisted in data interpretation.

2.2 Introduction

Artemisinin combination therapies (or ACTs) are the current first-line treatment for malaria around the world. Drug resistance is one of the most pervasive challenges for malaria control, and the recent emergence and spread of artemisinin resistance in Southeast Asia is cause for serious concern (Noedl et al. 2008; Dondorp et al. 2009; Ashley et al. 2014). Identifying the genetic determinants of artemisinin resistance is crucial for understanding the emergence of this phenomenon and tracking the spread of these drug resistant parasites.

Clinical artemisinin resistance is defined by an increase in parasite clearance time, or a persistence of parasites in the blood by smear microscopy on day 3 following administration of ACT (World Health Organization 2010; Flegg et al. 2011; White 2011; Ashley et al. 2014). A parasite clearance half-life of >5 hours is considered to be resistant (Ashley et al. 2014). *In vitro* artemisinin resistance is defined by parasite survival following the $^{0\text{-}3h}$Ring Stage Survival Assay ($^{0\text{-}3h}$RSA) (Witkowski, Khim, et al. 2013; Witkowski, Amaratunga, et al. 2013). Parasite survival is determined by microscopy following 700nM DHA treatment of 0-3 hour rings; with survival > 1% considered resistant. A coordinated global effort is underway to contain the spread of artemisinin resistance, which would be devastating in the highly endemic countries of Africa (Dondorp & Ringwald 2013).

Efforts in the lab have focused on identifying a molecular marker for artemisinin resistance and determining the cellular mechanisms involved in resistance. In 2014, Ariey and colleagues published the result of a five-year *in vitro* selection experiment that generated artemisinin resistant parasites from a culture-adapted Tanzanian isolate (Ariey et al. 2014). After repeated selection with increasing concentrations of artemisinin, the parasites

developed resistance, evolving from an initial $^{0\text{-}3h}$RSA of less than 1% to a final $^{0\text{-}3h}$RSA ~14.1%. Whole genome sequencing of the resistant line identified multiple single nucleotide polymorphisms (SNPs) that differed from the parental strain. Upon comparison of these SNPs to those identified in resistant parasite isolates from SE Asia, mutations in the kelch13 locus (PF3D7_1343700) were found to be significantly associated with artemisinin resistance (as measured by *in vitro* $^{0\text{-}3h}$RSA). This publication established kelch13 propeller domain SNPs as molecular markers of artemisinin resistance.

The association of the kelch13 marker with artemisinin resistance was validated by genetic manipulation experiments in the lab. Ghorbal and colleagues demonstrated that introduction of the kelch13 C580Y mutation confers artemisinin resistance on an isogenic NF54 parasite background (Ghorbal et al. 2014). This was followed by a comprehensive study from Straimer and colleagues that sought to understand the specific contributions of individual kelch13 polymorphism to artemisinin resistance *in vitro* (Straimer et al. 2015). Straimer found that individual K13 mutations, when introduced onto an isogenic Dd2 background, conferred differing levels of resistance, as measured by $^{0\text{-}3h}$RSA. Furthermore, introduction of the same K13 mutation into different *P. falciparum* isolates conferred different levels of resistance. These data indicate that specific kelch13 mutations were functionally capable of conferring artemisinin resistance based upon *in vitro* survival phenotype; and that these mutations have differential impact. Importantly, genetic background and context matter.

It seems, however, that kelch13 mutations alone are not categorically indicative of artemisinin resistance in clinical isolates. Recent molecular genetic surveillance efforts have identified and characterized a diverse set of polymorphisms in the Pf kelch13 locus. In

Southeast Asia, 20 non-synonymous SNPs in the kelch13 propeller domain are associated with delayed parasite clearance (Ashley et al. 2014; Miotto et al. 2015; Takala-Harrison et al. 2015). Many additional kelch13 polymorphisms have been identified in malaria-endemic African countries (Ashley et al. 2014; Sibley 2015; Kamau et al. 2015; Taylor et al. 2015). The majority of these African isolates have not been phenotyped for associations with resistance, though delayed parasite clearance or clinical failure of ACTs have not been observed in these regions. A recent comprehensive molecular surveillance of diverse geographic clinical isolates from the MalariaGEN *Plasmodium falciparum* Community Project identified 155 total SNPs in kelch13, 46 of which were non-synonymous (Roberto Amato, Olivo Miotto, Charles Woodrow, Jacob Almagro-Garcia, Ipsita Sinha, Susana Campino, Daniel Mead, Eleanor Drury, Mihir Kekre, Mandy Sanders, Alfred Amambua-Ngwa, Chanaki Amaratunga, Lucas Amenga-Etego, Tim JC Anderson, Voahangy Andrianaranjak 2015). Approximately equal numbers of these non-synonymous SNPs were found in Southeast Asia and Africa, with some SNPs found in both populations. Though worrying, this pre-existing genetic diversity also suggests other genes may be involved in resistance or predispose parasites to kelch13-mediated resistance, and kelch13 propeller mutations in and of themselves are not a definitive resistance signature.

Additional work from our lab has identified Cambodian parasites with wildtype kelch13 alleles, but resistant $^{0\text{-}3h}$RSA phenotypes (Mukherjee et al, unpublished). Ashley et al reported similar findings, where parasites from patients with delayed clearance half-life did not have the associated kelch13 polymorphisms, while a small number of parasites had K13 propeller mutations but rapidly cleared in the patient (Ashley et al. 2014). Taken together, these findings present a complicated picture of artemisinin resistance. While K13 mutations

are sufficient to confer artemisinin resistance *in vitro*, additional as yet unidentified parasite factors may contribute to or modulate this resistance in the natural parasite population.

In 2011, prior to publication of the kelch13 resistance marker, we began an *in vitro* selection experiment to identify the genetic determinants of artemisinin resistance. This approach has previously been successful in generating drug resistant *P. falciparum* lines, and identifying either mechanisms of drug resistance or the target of the selection compound (Nzila & Mwai 2010; Witkowski et al. 2009; Lukens et al. 2014; Herman et al. 2015). Here we present the characterization of the three independently generated artemisinin-resistant parasite lines. This study identifies additional molecular markers of artemisinin resistance, increases our understanding of how this resistance is acquired, and sheds light on the molecular mechanisms of artemisinin resistance in the parasite.

2.3 Results

Selection of three independent artemisinin-resistant parasite lines. To increase our understanding of the molecular basis of artemisinin resistance, we implemented an *in vitro* resistance selection approach. We chose two different Senegalese field isolates as parental strains (Th032.09 and P19.04), which were adapted to *in vitro* growth and had slightly elevated EC_{50}s to artemisinin and its derivatives (Park et al. 2012). We started with four independent selections of each parental strain, each with approximately 10^9 parasites per flask. Using intermittent and step-wise *in vitro* selection methods, we pulsed the selections with steadily increasing concentrations of dihydroartemisinin (DHA), the active metabolite of artemisinin. Drug pressure started at 0.1μM DHA (approximately five times the EC_{50}), and increased by 0.1μM increments to 1.0μM. After four years, we have generated three

independent, artemisinin-resistant, selected lines (Figure 2.3.1, 2.3.2). Two selected lines are derived from the P19.04 parent (referred to as P19.04-A and P19.04-B), and one additional selected line is derived from the Th032.09 parent (named Th032.09-A). Each of these selected lines has a "sibling" no drug control that has been growing in culture for approximately the same number of parasite generations in the absence of drug.

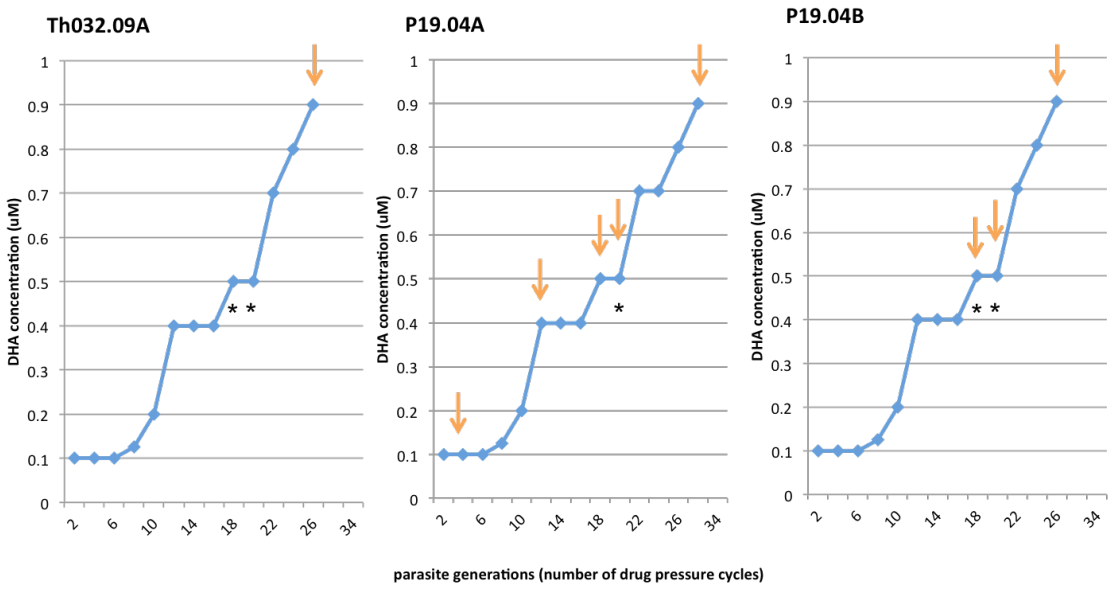

Figure 2.3.1. Three independent artemisinin-resistant lines were selected from two Senegalese field isolates. Using intermittent pulses of drug pressure and step-wise increases in drug concentration, these lines were selected over many parasite generations (1 generation = 2 days). Orange arrows indicate whole genome sequencing of end-point selected lines. Black asterisks indicate first appearance of Pf coronin (PF3D7_1251200) mutation.

Selected lines are resistant by $^{0\text{-}3h}$Ring Stage Survival Assay. Decreased artemisinin sensitivity was assessed using phenotypic assays, including the $^{0\text{-}3h}$RSA (Ring Stage Survival Assay) and 72-hour drug sensitivity assays with SYBR Green. Due to its known contribution to drug sensitivity and reported association with *in vitro* DHA resistance (Price et al. 2004;

Cui et al. 2012), *pfmdr1* copy number was also assessed in all of our cell lines. Selected lines P19.04-A, P19.04-B, and Th032.09-A all show a significant increase in their RSA survival percentage (6%, 7.9%, and 9.6%, respectively) as compared to their parents (Figure 2.3.2). Based upon an RSA > 1% being considered resistant (Witkowski, Khim, et al. 2013), these lines are all resistant to artemisinin, while their parental lines are sensitive. In contrast, these same lines show no change in their EC_{50} response to DHA, artemisinin, or other antimalarials in a classic 72-hour dose response assay (Figure 2.3.3). Furthermore, the selected lines do not have any variation in *pfmdr1* copy number (Figure 2.3.4).

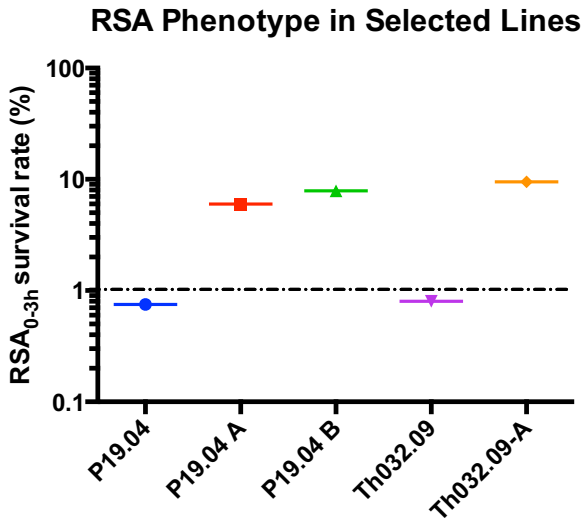

Figure 2.3.2. $^{0\text{-}3h}$RSA survival percentage was determined for selected lines P19.04-A, P19.04-B, and Th032.09-A, relative to the parental lines, P19.04 and Th032.09. Survival greater than 1% is considered resistant.

Figure 2.3.3. Selected lines P19.04-A, P19.04-B, and Th032.09-A show no change in EC_{50} in response to (A) artemisinin or its derivatives, or (B) unrelated antimalarials. Parasite drug sensitivity was measured by 72 hour *in vitro* assays with SYBR Green.

Figure 2.3.3 (continued).

A.

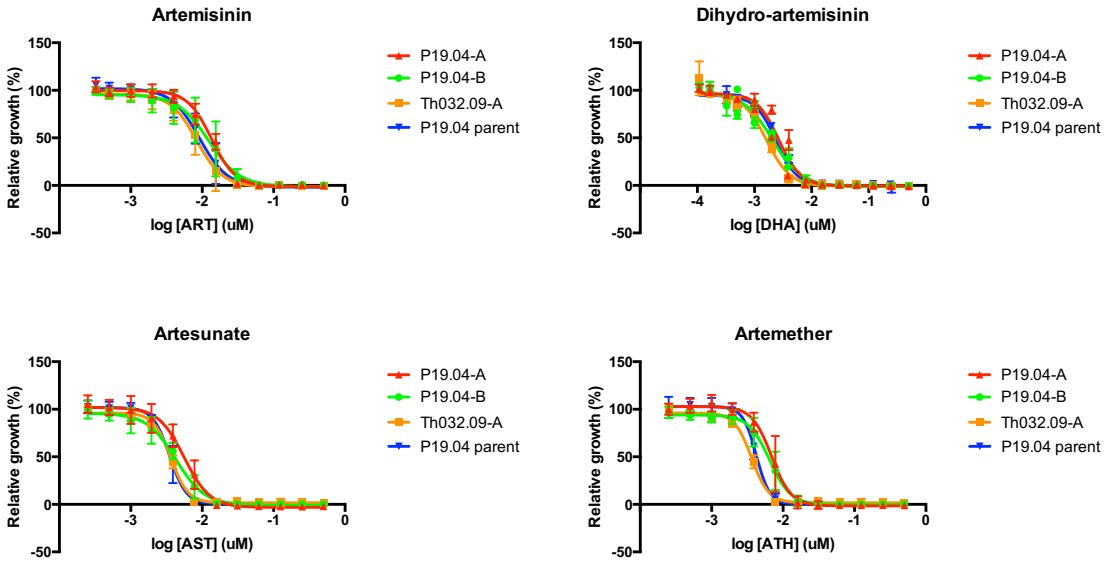

B.

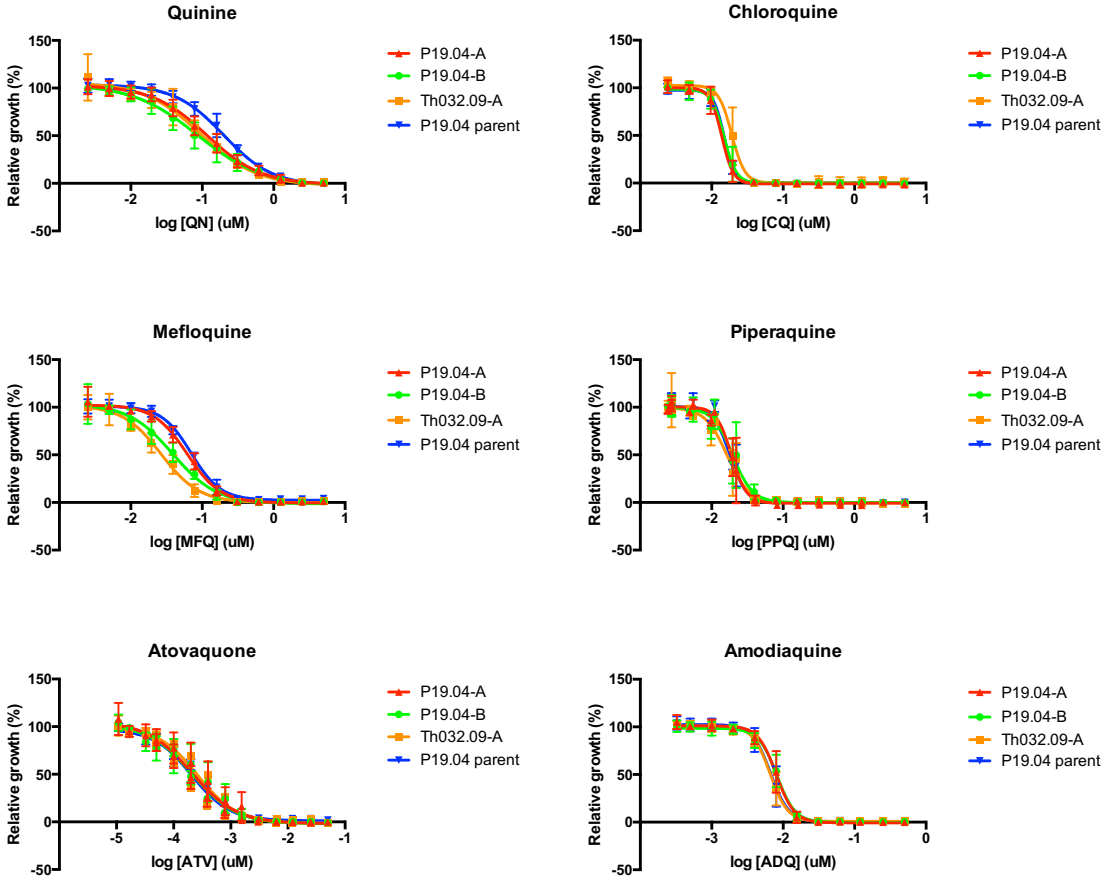

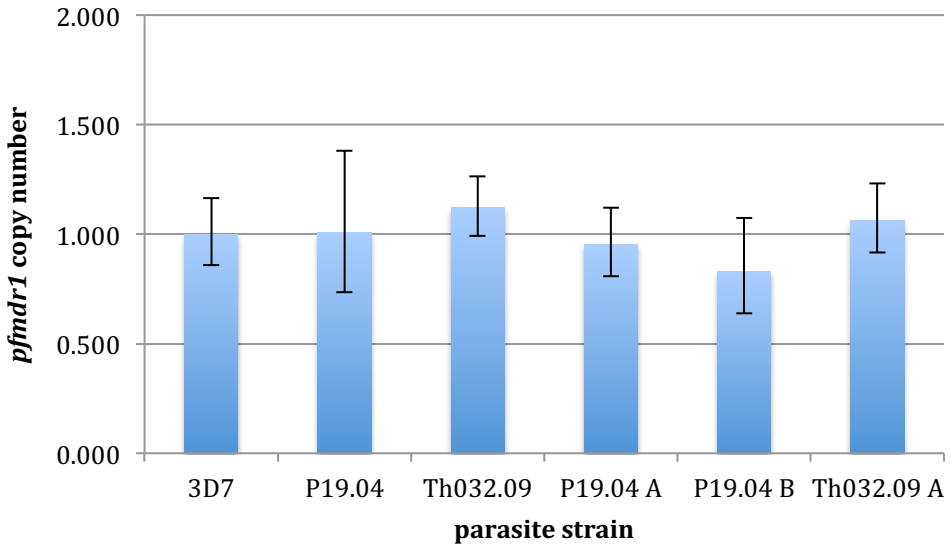

Figure 2.3.4. Quantitative Real time PCR was used to calculate *pfmdr1* copy number for the drug-selected lines. Parental lines, P19.04 and Th032.09, and reference strain, 3D7, were included as controls.

Whole genome sequencing of artemisinin-resistant selected lines. We performed whole genome sequencing to identify SNPs in our artemisinin-resistant selected lines, relative to their parental lines. We used the Illumina Next Gen sequencing platform at the Broad and GATK Unified Genotyper to call SNPs. We identified non-synonymous, coding SNPs that differed between the selected, drug-resistant "child" strains, as compared to the original parental lines and no-drug controls (Figure 2.3.5). SNPs found in the "no drug" controls, relative to the parental lines, were eliminated, as these were likely the result of genetic drift that occurred during the culturing process, and not associated specifically with artemisinin resistance. We further eliminated SNPs found in highly variable sub-telomeric regions, as well as SNPs for which there incorrect read alignment or insufficient read

coverage. This narrowed down the list of candidate genes to thirteen candidate SNPs in ten genes for further follow up (Table 2.3.1).

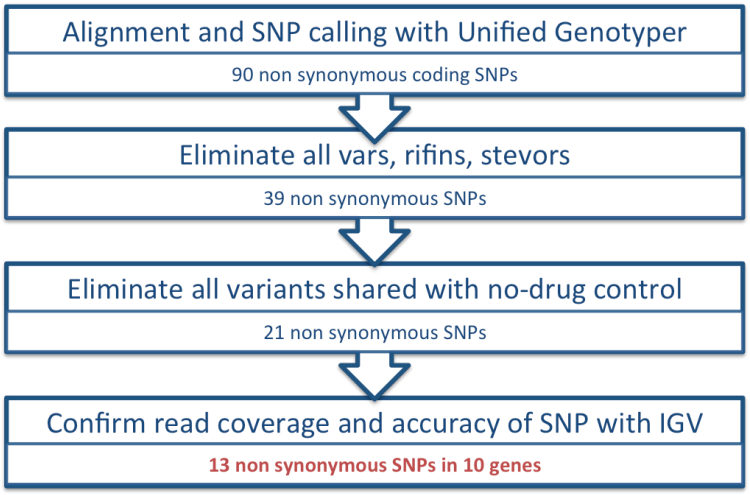

Figure 2.3.5. Flow chart of SNP calling and filtration process to identify candidate SNPs.

Chr	Location	Gene Name	Gene ID	aa change	Ref	Parent	Alt	P19.04-A	P19.04-B	Th032.09-A
2	394688	transporter putative	PF3D7_0209600	D1035N	C	C	T	C	T	C
5	1127588	minchromosome maintenance MCM complex putative MCM3	PF3D7_0527000	G187R	C	C	G	G	C	C
6	551338	AP-3 complex subunit beta, putative	PF3D7_0613500	G345D	C	C	T	T	T	C
7	1301194	transcription factor with AP2 domains ApiAP2	PF3D7_0730300	K1246E	A	A	G	G	A	A
11	836592	serine threonine protein kinase putative	PF3D7_1121900	A292E	G	G	T	G	G	T
11	1019374	autophagy-related protein 7, putative (ATG7)	PF3D7_1126100	N1041S	T	C	T	T	T	C
12	2092742	coronin	PF3D7_1251200	E107V	A	A	T	A	T	A
12	2092571	coronin	PF3D7_1251200	G50E	G	G	A	G	G	A
12	2092721	coronin	PF3D7_1251200	R100K	G	G	A	G	A	G
13	1016125	conserved Plasmodium membrane protein unknown function	PF3D7_1324300	M1060R	A	A	C	A	A	C
14	1355219	conserved Plasmodium protein unknown function	PF3D7_1433800	S1054F	G	G	A	G	A	G
14	901189	conserved Plasmodium protein unknown function	PF3D7_1422400	N268K	C	C/A	C	C	C	C
14	1356655	conserved Plasmodium protein unknown function	PF3D7_1433800	I575M	T	T	C	T	T	C

Table 2.3.1. List of SNPs identified in drug-selected lines. Thirteen nonsynonymous SNPs were identified in ten *P. falciparum* genes. Table shows chromosomal location of SNP ("Chr"), Position in the genome ("Location"), Gene name and ID, amino acid change ("aa change"), reference nucleic acid at that position in 3D7 ("ref"). parental allele ("parent", either Th032.09 or P19.04), alternate allele ("alt"), and the nucleic acid at that position in each of the child strains (P19.04-A, P19.04-B, Th032.09-A).

Candidate SNPs of interest. Of the SNPs identified by whole genome sequencing of the selection endpoints, none were initially identified in all three selected lines. Two SNPs were identified in two out of three selected lines: position 551338 of PF3D7_0613500 and position 1019374 of PF3D7_1126100 were each found in P19.04-A and P19.04B. Two additional loci had multiple SNPs in different selected lines: positions 1355219 and 1356655 of Pf3D7_1433800, and positions 2092571, 2092721, and 2092742 of PF3D7_1251200. Selected lines P19.04-B and Th032.09-A each had SNPs in these last two loci (PF3D7_1433800 and PF3D7_1251200), indicating that the same SNP independently arose on different parasite backgrounds. None of these SNPs have been identified in published studies of molecular markers of artemisinin resistance (Cheeseman et al. 2012; Takala-Harrison et al. 2013; Ariey et al. 2014; Miotto et al. 2015).

Candidate SNPs in the Pf coronin locus were independently acquired in all three selected lines. We performed additional whole-genome sequencing of earlier selection steps (red arrows in Figure 2.3.1). All SNPs were then validated by Sanger sequencing of 700-800bp PCR amplicons. Using these approaches, we were also able to determine when in the course of our resistance selection these SNPs first arose. Our most promising candidate SNPs are those found in the Pf coronin locus (PF3D7_1251200). The Pf coronin mutations first appear in the 9th step (18 parasite generations on drug) of the P19.04-B and Th032.09-A selections. Intriguingly, while not identified by the original WGS of the endpoint 14th step, the Pf coronin mutations do appear in the 10th step (20 parasite generations on drug) of the P19.04-A selection, and then are not found in subsequent selection steps. Additional follow up of other candidate hits and analysis of their chronological appearance is ongoing, however the independent evolution of the same set of SNPs in all three selections makes Pf coronin a promising candidate target.

Selected SNPs are located in the propeller domain of Pf coronin, a kelch13-related protein. Pf coronin is a member of the WD-40 superfamily of proteins, a superfamily characterized by β-propeller WD-40 repeats. There are 92 such WD-40 repeat-containing proteins encoded in the genome of *Plasmodium falciparum*. In other eukaryotes, these proteins have been implicated in diverse intracellular processes, including membrane trafficking, signaling, transcription, and as substrate adaptors for ubiquitin E3 ligases (Xavier et al. 2013). Pf coronin has been implicated in actin cytoskeleton remodeling and parasite motility (Tardieux et al. 1998; Olshina et al. 2015). Coronins are structurally related to kelch proteins, and have been shown to perform related intracellular functions (Hudson & Cooley 2013). Pf coronin has an N-terminal 7-bladed propeller domain composed of WD-40 repeats, similar to the C-terminal 6-bladed propeller domain found in kelch13 (Figure 2.3.6B)(Clemen et al. 2008; Ariey et al. 2014). The three SNPs identified in our resistance selections are located within this N-terminal propeller domain (Figure 2.3.6A). As kelch13 propeller domain mutations are associated with artemisinin resistance, it is tempting to speculate that the parallels in protein functionality and propeller-domain localization of the Pf coronin mutations suggest a similar intracellular mechanism of resistance may be at play.

A.

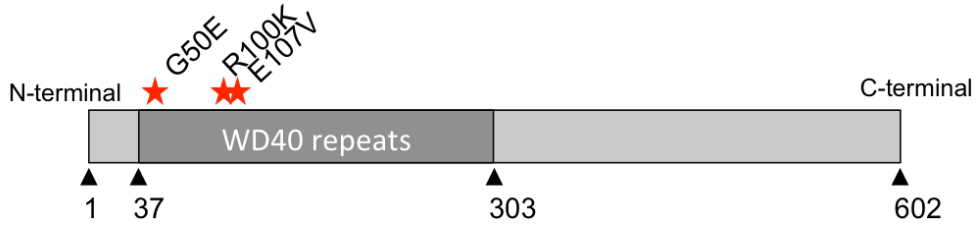

B.

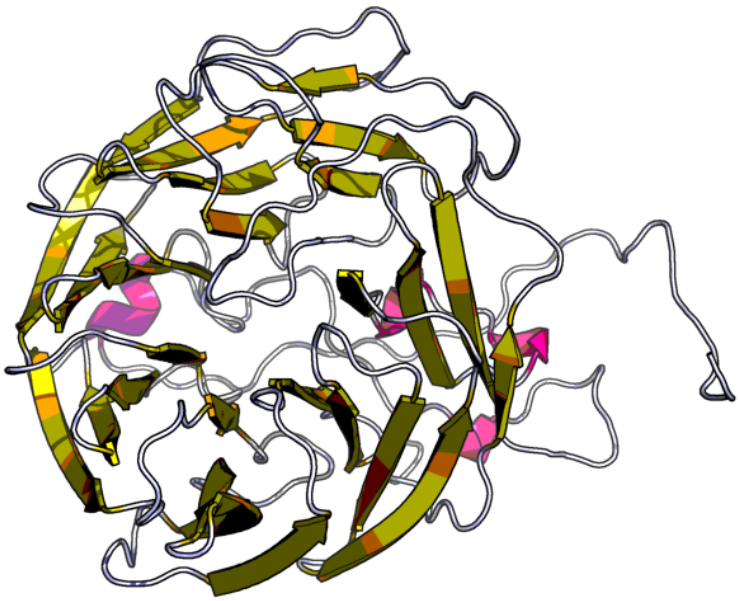

Figure 2.3.6. A. Protein domain configuration of Pf coronin (PF3D7_1251200) amino acid sequence. SNPs identified in our drug-selected lines (G50E, R100K, and E107V) are located in the N-terminal WD-40 propeller region. B. Ribbon diagram of a three-dimensional model of Pf coronin (PF3D7_1251200) showing the seven-bladed propeller. The Pf coronin model was generated by the Raptor X protein prediction server (Källberg et al. 2012).

2.4 Discussion

Emerging artemisinin resistance in Southeast Asia is an alarming public health crisis. Containing this resistance is crucial, as its spread would be devastating to worldwide malaria control efforts. Understanding the underlying mechanisms of artemisinin resistance and identifying molecular markers to track its emergence and spread in the field are important pubic health research priorities.

After approximately four years, we have successfully selected three independent, artemisinin-resistant lines from culture-adapted Senegalese parental strains. These three lines were all found to be phenotypically resistant as measured by $^{0\text{-}3h}$RSA after approximately 26 parasite generations under increasing concentrations of DHA drug pressure (Figure 2.3.1). Similar to the *in vitro* selected line generated by Ariey and colleagues, our parasites show no changes in EC_{50} to artemisinin or its derivatives (Figure 2.3.3) (Ariey et al. 2014). They also maintain a single copy of *pfmdr1*, a well-characterized drug resistance locus known to be amplified in other instances of antimalarial drug resistance (Figure 2.3.4)(Price et al. 2004).

Whole genome sequencing efforts identified multiple candidate SNPs in two out of three selected lines, the same SNP arising on each of the two parental background strains, and multiple candidate SNPs that hit the same gene (Table 2.3.1). None of our candidate SNPs have previously been identified in the literature. Though a non-propeller kelch13 mutation is fixed in our parental strains (K189T, fixed in Senegal), we did not select for any additional kelch13 mutations in these parasites. Nor do we see evidence for the SNPs previously identified as a resistance background signature common to resistant Cambodian parasites, namely mutations in apicoplast ribosomal protein S10 (*arps10*), multi-drug resistance

protein 2 (*mdr2*), ferredoxin (*fd*), and chloroquine resistance transporter (*pfcrt*) (Miotto et al. 2015). Our selected lines provide evidence that artemisinin resistance, based upon an RSA phenotype, can occur in the absence of known artemisinin resistance-associated SNPs, including kelch13. This suggests that the mechanism or mechanisms of artemisinin resistance are more complicated, and this work provides critical tools to identify other partners and understand how ART resistance occurs.

Our most promising target for follow up and functional validation is Pf coronin. Importantly, SNPs in this locus were found in both P19.04-B and Th032.09-A, arising independently on two different parasite backgrounds. Furthermore, despite not being detected at later selection steps, SNPs in Pf coronin were identified in the third selected line, P19.04-A, earlier in the selection process: the two endpoint mutations identified in the resistant P19.04-B line (R100K and E107V) also appear in the 10th step (20 parasite generations on drug) of the P19.04-A selection, and then are not found (positions were wildtype) in subsequent selection steps (Figure 2.3.1). P19.04-A was found to have a resistant RSA phenotype of ~5.5% immediately following the appearance of the Pf coronin SNPs (11th step), when the line had previously been sensitive to artemisinin by RSA (data not shown). This suggests that in the P19.04-A line, the coronin SNPs may have been a contributing factor in acquisition of resistance, rather than causative mutations. This mutation may also have an associated fitness cost to parasite growth in the absence of drug *in vitro*, and is thus lost over time. This suggests a complex, potentially multi-locus model of artemisinin resistance acquisition.

To investigate whether our candidate SNPs are associated with clinical artemisinin resistance, we plan to compare our sequenced lines to whole genome sequences of

Cambodian isolates (Miotto et al. 2015). While none of our 13 candidate SNPs was identified in the Cambodian set of 157 parasites, there are additional SNPs in the same genes. Investigating the associations between the resistance phenotypes observed in these Cambodian parasites (including clearance time and *in vitro* $^{0\text{-}3h}$RSA) and SNPs in our candidate genes will help confirm the role of our SNPs of interest with artemisinin resistance.

The mechanism of artemisinin resistance is not fully understood, and several studies have proposed putative mechanisms, many incorporating the previously proposed ideas of heme degradation for artemisinin activation, intracellular oxidant stress response pathways, and protein degradation pathways. Artemisinin itself is a pro-drug, requiring activation by heme or free Fe^{2+} (Klonis et al. 2013; Xie et al. 2015). Indeed, artemisinin treatment has been shown to affect hemoglobin catabolism in the parasite (Cobbold et al. 2016). The action of artemisinin within the cell implicates up-regulation of intracellular stress responses and anti-oxidant pathways as mechanisms of parasite resistance. Interestingly, the human homolog of Pf kelch13, keap1 (Kelch ECH associating protein 1), has been shown to be involved in mediation of such pathways in human cells (Itoh et al. 1999; Zhang & Hannink 2003), suggesting that kelch13 may be playing a similar role in *Plasmodium*.

With the results of their *in vitro* selection experiment, Ariey's group proposed a role for kelch13 in mediating oxidant stress in the parasite (Ariey et al. 2014). Mutant kelch13 allows for a more active response to the oxidative stress of artemisinin, rendering the parasites resistant. This proposed mechanism is supported by evidence that the human kelch13 homolog, keap1, interacts with Nrf2, a transcription factor known to activate cytoprotective anti-oxidant response in cells (Villeneuve et al. 2010). Building on these

ideas, work from Dogovski et al identified changes in the ubiquitin proteasome degradation pathway in resistant K13 mutant parasites from Cambodia (Dogovski et al. 2015). Resistant parasites show lower global levels of ubiquitinated proteins in response to artemisinin treatment, suggesting an enhanced cell stress response. A similar mechanism was proposed by Mok et al following their analysis of transcriptional profiles of SE Asian early ring stages (Mok et al. 2015). Looking at the resistant isolates, they identified increased expression of two *P. falciparum* protein chaperone subcomplexes involved in the unfolded protein response (UPR), Plasmodium reactive oxidative stress complex (PROSC) and TCP-1 ring complex (TRiC). Up-regulation of the UPR could be a cytoprotective response to oxidant damage of artemisinin, and the kelch13 homolog keap1 has also been implicated in regulation of this pathway in other cell types (Digaleh et al. 2013). An alternate mechanism, involving K13 binding of PI3K and altered levels of PI3P was proposed by Mbengue and colleagues (Mbengue et al. 2015). They demonstrate that kelch13 mutations lead to increased PI3K expression and thus increased intracellular PI3P, perhaps via AKT signaling in response to cellular stress. They propose this as a protective response to artemisinin pressure, and the AKT signaling pathway has indeed been implicated in previously mentioned stress response pathways, such as the Nrf2-keap1 axis (Tebay et al. 2015). The common themes of oxidative stress and protein turnover stress response pathways fit with well-characterized intracellular functions of kelch13. These proposed mechanisms are compelling and perhaps complementary, and further functional studies are needed to fully elucidate the functional role of kelch13, and potential interacting partners, in mediating artemisinin resistance.

To validate and better understand the functions of our candidate loci in mediating artemisinin resistance, perhaps in a complementary mechanism to those described above,

our next step is to introduce the mutations identified here (Table 2.3.1) and their corresponding wildtype alleles into isogenic parasite backgrounds. To do this, we will generate allelic replacements using the CRISPR-Cas9 system (Ghorbal et al. 2014; Wagner et al. 2014). The allele-swap experiment will allow us to replace the mutant copy in our selected lines with a sensitive wildtype allele, which we predict to result in drug sensitive parasites. For the inverse, sensitive, wildtype parasites will become drug resistant when we swap in the mutant allele. Our selected lines were generated on an African parasite background, and further characterization of the mechanism of artemisinin resistance in this population could have important implications for understanding and limiting the spread of resistance from SE Asia. Functional validation of specific candidate loci (either individually, or in combination) will increase our understanding of the mechanism of artemisinin resistance.

In conclusion, we have generated three independent artemisinin resistant lines. These selected lines lack kelch13 mutations yet exhibit artemisinin resistance based upon an RSA phenotype. Using a chemogenomics approach, we identified mutations in a kelch13-like protein, Pf coronin, in our selected lines. In future work, functional validation using a gene-editing approach will demonstrate the role of this locus in a mechanism of artemisinin resistance. However, identification of Pf coronin provides the first critical step of discovery of a potentially important locus involved in modulating resistance to artemisinin.

2.5 Materials and Methods

In vitro resistance selection

Culture adapted field isolates Th032.09 and P19.04 were maintained in culture in RPMI1640 media (Gibco) supplemented with 10% O+ serum. Long term *in vitro* resistance selection followed an "intermittent and stepwise" selection protocol, whereby approximately 10^9 parasites were pulsed with increasing concentrations of dihydroartemisinin (DHA), beginning at 0.1μM and increasing by increments of 0.1μM to 1.0μM at the final selection step. Parasites were pulsed on drug for 48hours (1 generation), then off drug for 48 hours. This was repeated until the culture was smear negative by Giemsa stained thin smear microscopy (usually 4-6 generations). Parasites were then allowed to recover off drug. This recovery took between 4-40 days, and "recovery time" for cultures was defined as time until smear negative culture reaches 1% parasitemia. Following successful recovery, parasites were pulsed again with the same concentration or a higher dose.

$^{0\text{-}3h}$RSA (Ring Stage Survival Assay)

The RSA was performed as described by Witkowski and colleagues (Witkowski, Amaratunga, et al. 2013; Witkowski, Khim, et al. 2013). Briefly, highly synchronized 0-3 hour post-invasion rings are exposed to 700nM DHA for 6 hours; the drug is subsequently washed out. 72 hours following initial drug treatment, parasitemia is counted by Giemsa-stained smear microscopy. The ring stage survival percentage is calculated as the fraction of surviving DHA-treated parasites over the DMSO-treated control of the same strain. An RSA survival percentage > 1% is considered to be resistant.

Drug sensitivity assays with SYBR Green I

Drug sensitivity assays were performed as described by Johnson and colleagues (Johnson et al. 2007). Briefly, parasites were grown at 0.8-1% parasitemia in 1% hematocrit in 100μL

total volume in 96 well plates. Parasite viability was determined by SYBR Green I staining of parasite DNA, following 72 hours in culture. Dose-response curves for standard antimalarials were generated from a 12-point dilution series of drugs, in triplicate, centered around expected EC_{50}s reported in the literature. 3-4 biological replicates were performed for each drug. A SpectraMax M5 (Molecular Devices) plate reader was used to measure fluorescence, and data was analyzed with GraphPad Prism (version 6). To determine the IC50, we used non-linear regression with the log(inhibitor) vs. response – variable slope (four parameters) curve-fitting equation.

Pfmdr1 copy number variation

Pfmdr1 copy number was determined by quantitative RT-PCR, following the method described by Ribacke and colleagues (Ribacke et al. 2007).

Next Gen sequencing

Parasite DNA was extracted from in vitro cultures using QIAamp DNA blood kits (Qiagen), per manufacturer's instructions. DNA was purified using ZymoKit DNA purification kit (Irvine, CA), per manufacturer's instructions. DNA samples were sequenced on the Illumina HiSeq 2500 at the Broad for an average read coverage of 60-100X. Reads were aligned to 3D7 reference strain and SNPs were called using GATK Unified Genotyper. Non-synonymous coding SNPs were then filtered according to the steps outlined in the Figure 2.3.5 flow chart.

Sanger sequencing.

Parasite DNA was extracted from in vitro cultures using QIAamp DNA blood kits (Qiagen), per manufacturer's instructions. Primers were designed to amplify candidate gene

sequences in 700-800bp overlapping amplicons, 3-4 amplicons per gene. PCR amplification was conducted as follows: 5 minutes at 95°C; followed by 40 cycles of 3 step amplification of 95°C for 30s, 58°C for 45s, 68°C for 30s; followed by final extension at 72°C for 7 m. DNA was purified using ZymoKit DNA purification kit (Irvine, CA), per manufacturer's instructions. Sanger sequencing for kelch13 (PF3D7_1343700) and Pf coronin (PF3D7_1251200) was performed by Macrogen USA (Cambridge, MA).

Primer target	Primer name	Sequence 5'-3'
PF3D7_1343700	kelch13 Fwd1	ATGGAAGGAGAAAAAGTAAAAACAAAAGC
PF3D7_1343700	kelch13 Rev1	ACG GTT TTC TAA TTC TTT GTA CAA TCG TAC
PF3D7_1343700	kelch13 Fwd2	GAA ACG GAA TTA AGT GAT GCT AGT GA
PF3D7_1343700	kelch13 Rev2	CCA GCA TTG TTG ACT AAT ATC TAA TAA TTC CA
PF3D7_1343700	kelch13 Fwd3	CAT TCC CAT TAG TAT TTT GTA TAG GTG GAT
PF3D7_1343700	kelch13 Rev3	TTA TAT ATT TGC TAT TAA AAC GGA GTG ACC AA
PF3D7_1251200	coronin fwd1	ATGTATAATGTTCCTTTAATCAAGA
PF3D7_1251200	coronin rev1	CTTTGGCATATTTATTTCAAAGG
PF3D7_1251200	coronin fwd2	GTGGTATAGCTTGTAGTGCT
PF3D7_1251200	coronin rev2	CTTTAAACTCCATAATTTCAATTCTC
PF3D7_1251200	coronin fwd3	AAGTTCTTTACAATGGGATATCG
PF3D7_1251200	coronin rev3	CTGTCTCATGACAGAACCCT
PF3D7_1251200	coronin fwd4	GATTTATATCCTCCTATTATTATGAG
PF3D7_1251200	coronin rev4	TACCGTTGCTGTACTTTTACAC

Table 2.5.1. PCR resequencing primers to amplify candidate genes PF3D7_1343700 and PF3D7_1251200.

Pf Coronin Protein Homology Modeling

Putative structure and ribbon diagram for Pf coronin (PF3D7_1251200) was generated using Raptor X protein prediction server (Källberg et al. 2012).

2.6 References

Ariey, F. et al., 2014. A molecular marker of artemisinin-resistant Plasmodium falciparum malaria. *Nature*, 505.

Ashley, E.A. et al., 2014. Spread of Artemisinin Resistance in Plasmodium falciparum Malaria. *New England Journal of Medicine*, 371(5), pp.411–423.

Cheeseman, I.H. et al., 2012. A major genome region underlying artemisinin resistance in malaria. *Science*, 336(79).

Clemen, C., Eichinger, L. & Rybakin, V. eds., 2008. The coronin family of proteins. In *Volume 48 of Subcellular Biochemistry*. Springer Science and Business Media.

Cobbold, S.A. et al., 2016. Metabolic Dysregulation Induced in Plasmodium falciparum by Dihydroartemisinin and Other Front-Line Antimalarial Drugs. *The Journal of Infectious Diseases*, 213.

Cui, L. et al., 2012. Mechanisms of in vitro resistance to dihydroartemisinin in Plasmodium falciparum. *Molecular Microbiology*, 86(1), pp.111–128.

Digaleh, H., Kiaei, M. & Khodagholi, F., 2013. Nrf2 and Nrf1 signaling and ER stress crosstalk: Implication for proteasomal degradation and autophagy. *Cellular and Molecular Life Sciences*, 70(24), pp.4681–4694.

Dogovski, C. et al., 2015. Targeting the Cell Stress Response of Plasmodium falciparum to Overcome Artemisinin Resistance. *PLoS Biology*, 13(4), pp.1–26.

Dondorp, A.M. et al., 2009. Artemisinin Resistance in Plasmodium falciparum Malaria. *New England Journal of Medicine*, 361(5), pp.455–467.

Dondorp, A.M. & Ringwald, P., 2013. Artemisinin resistance is a clear and present danger. *Trends in Parasitology*, 29(8), pp.359–360.

Flegg, J.A. et al., 2011. Standardizing the measurement of parasite clearance in falciparum malaria: the parasite clearance estimator. *Malaria Journal*, 10(1), p.339.

Ghorbal, M. et al., 2014. Genome editing in the human malaria parasite Plasmodium falciparum using the CRISPR-Cas9 system. *Nature biotechnology*, 32(8), pp.819–821.

Herman, J.D. et al., 2015. The cytoplasmic prolyl-tRNA synthetase of the malaria parasite is a dual-stage target of febrifugine and its analogs. *Science Translational Medicine*, 7(288), pp.1–9.

Hudson, A. & Cooley, L., 2013. Phylogenetic, Structural and Functional Relationships between WD-and Kelch-Repeat Proteins. In C. Clemen, L. Eichinger, & V. Rybakin, eds. *The Coronin Family of Proteins*.

Itoh, K. et al., 1999. Keap1 represses nuclear activation of antioxidant responsive elements by Nrf2 through binding to the amino-terminal Neh2 domain. *Genes and Development*, 13(1), pp.76–86.

Johnson, J.D. et al., 2007. Assessment and continued validation of the malaria SYBR Green I-

based fluorescence assay for use in malaria drug screening. *Antimicrobial Agents and Chemotherapy*, 51(6), pp.1926–1933.

Källberg, M. et al., 2012. Template-based protein structure modeling using the RaptorX web server. *Nature Protocols*, 7, pp.1511–1522.

Kamau, E. et al., 2015. K13-propeller polymorphisms in plasmodium falciparum parasites from sub-saharan Africa. *Journal of Infectious Diseases*, 211(8), pp.1352–1355.

Klonis, N., Creek, D.J. & Tilley, L., 2013. Iron and heme metabolism in Plasmodium falciparum and the mechanism of action of artemisinins. *Current Opinion in Microbiology*, 16(6), pp.722–727.

Lukens, A.K. et al., 2014. Harnessing evolutionary fitness in Plasmodium falciparum for drug discovery and suppressing resistance. *Proceedings of the National Academy of Sciences of the United States of America*, 111(2), pp.799–804.

Mbengue, A. et al., 2015. A molecular mechanism of artemisinin resistance in Plasmodium falciparum malaria. *Nature*, 520(7549), pp.683–687.

Miotto, O. et al., 2015. Genetic architecture of artemisinin-resistant Plasmodium falciparum. *Nature genetics*, 47(3), pp.226–34.

Mok, S. et al., 2015. Population transcriptomics of human malaria parasites reveals the mechanism of artemisinin resistance. *Science*, 347, pp.431–435.

Noedl, H. et al., 2008. Evidence of Artemisinin-resistant malaria in Western Cambodia. *New England Journal of Medicine*, 359(24), pp.2619–2620.

Nzila, A. & Mwai, L., 2010. In vitro selection of Plasmodium falciparum drug-resistant parasite lines. *The Journal of antimicrobial chemotherapy*, 65(3), pp.390–8.

Olshina, M.A. et al., 2015. Plasmodium falciparum coronin organizes arrays of parallel actin filaments potentially guiding directional motility in invasive malaria parasites. *Malaria journal*, 14(1), p.280.

Park, D.J. et al., 2012. Sequence-based association and selection scans identify drug resistance loci in the Plasmodium falciparum malaria parasite. *Proceedings of the National Academy of Sciences of the United States of America*, 109(32), pp.13052–7.

Price, R.N. et al., 2004. Mefloquine resistance in Plasmodium falciparum and increased pfmdr1 gene copy number. *Lancet*, 364, pp.438–447.

Ribacke, U. et al., 2007. Genome wide gene amplifications and deletions in Plasmodium falciparum. *Molecular and Biochemical Parasitology*, 155(1), pp.33–44.

Roberto Amato, Olivo Miotto, Charles Woodrow, Jacob Almagro-Garcia, Ipsita Sinha, Susana Campino, Daniel Mead, Eleanor Drury, Mihir Kekre, Mandy Sanders, Alfred Amambua-Ngwa, Chanaki Amaratunga, Lucas Amenga-Etego, Tim JC Anderson, Voahangy Andrianaranjak, M., 2015. Genomic epidemiology of the current wave of artemisinin resistant malaria. *bioRxiv*.

Sibley, C.H., 2015. Artemisinin resistance: The more we know, the more complicated it

appears. *Journal of Infectious Diseases*, 211(5), pp.667–669.

Straimer, J. et al., 2015. K13-propeller mutations confer artemisinin resistance in Plasmodium falciparum clinical isolates. *Science*, 347(6220).

Takala-Harrison, S. et al., 2013. Genetic loci associated with delayed clearance of Plasmodium falciparum following artemisinin treatment in Southeast Asia. *Proceedings of the National Academy of Sciences of the United States of America*, 110(1), pp.240–245.

Takala-Harrison, S. et al., 2015. Independent emergence of artemisinin resistance mutations among Plasmodium falciparum in Southeast Asia. *Journal of Infectious Diseases*, 211(5), pp.670–679.

Tardieux, I. et al., 1998. A Plasmodium falciparum novel gene encoding a coronin-like protein which associates with actin filaments. *FEBS letters*, 441(2), pp.251–6.

Taylor, S.M. et al., 2015. Absence of putative artemisinin resistance mutations among Plasmodium falciparum in sub-Saharan Africa: A molecular epidemiologic study. *Journal of Infectious Diseases*, 211(5), pp.680–688.

Tebay, L.E. et al., 2015. Mechanisms of activation of the transcription factor Nrf2 by redox stressors, nutrient cues, and energy status and the pathways through which it attenuates degenerative disease. *Free Radical Biology and Medicine*, 88, pp.108–146. Available at: http://dx.doi.org/10.1016/j.freeradbiomed.2015.06.021.

Villeneuve, N.F., Lau, A. & Zhang, D.D., 2010. Regulation of the Nrf2-Keap1 antioxidant response by the ubiquitin proteasome system: an insight into cullin-ring ubiquitin ligases. *Antioxidants & redox signaling*, 13(11), pp.1699–712. Available at: http://www.pubmedcentral.nih.gov/articlerender.fcgi?artid=2966484&tool=pmcentrez&rendertype=abstract.

Wagner, J.C. et al., 2014. Efficient CRISPR/Cas9-mediated genome editing in P. falciparum. *Nature Methods*, 11(9), pp.915–918.

White, N.J., 2011. The parasite clearance curve. *Malaria J*, 10, p.278.

Witkowski, B., Amaratunga, C., et al., 2013. Novel phenotypic assays for the detection of artemisinin-resistant Plasmodium falciparum malaria in Cambodia: In-vitro and ex-vivo drug-response studies. *The Lancet Infectious Diseases*, 13(12), pp.1043–1049.

Witkowski, B., Khim, N., et al., 2013. Reduced artemisinin susceptibility of plasmodium falciparum ring stages in western cambodia. *Antimicrobial Agents and Chemotherapy*, 57(2), pp.914–923.

Witkowski, B., Berry, A. & Benoit-Vical, F., 2009. Resistance to antimalarial compounds: Methods and applications. *Drug Resistance Updates*, 12(1-2), pp.42–50.

World Health Organization, 2010. *Global Report on Antimalarial Drug Efficacy and Drug Resistance: 2000-2010*,

Xavier, C. et al., 2013. Evolutionary and Functional Diversity of Coronin Proteins. In *Madame Curie Bioscience Database [Internet]*. Austin, TX: Landes Bioscience. Available at:

http://www.ncbi.nlm.nih.gov/books/NBK6170.

Xie, S.C. et al., 2015. Haemoglobin degradation underpins the sensitivity of early ring stage Plasmodium falciparum to artemisinins. , (December), pp.406–416.

Zhang, D.D. & Hannink, M., 2003. Distinct cysteine residues in Keap1 are required for Keap1-dependent ubiquitination of Nrf2 and for stabilization of Nrf2 by chemopreventive agents and oxidative stress. *Molecular and cellular biology*, 23(22), pp.8137–51.

Chapter 3:

Characterization of the Expanded *Plasmodium falciparum* Acyl Co-A Synthetase Gene Family

3.1 Attribution

AUTHORS:

Allison Demas[1], Selina Bopp[1], Pamela Magistrado[1], Sarah K. Volkman[1,2,4], Ulf Ribacke[3], Dyann F. Wirth[1,4]

[1] Harvard T.H. Chan School of Public Health, Boston, MA, USA.

[2] Simmons College, Boston, MA, USA

[3]Uppsala University, Uppsala, Sweden.

[4] Broad Institute, Cambridge, MA, USA.

AUTHOR CONTRIBUTIONS:

U.R. generated ACS DD tagged lines. U.R. and A.D. cloned ACS DD tagged lines. U.R., A.D., P.M., and S.B. confirmed integration by Southern blot. A.D., S.B., and P.M. generated anti-HA Western blots of tagged lines. S.B. conducted RT-PCR for ACS expression. A.D., S.B., and P.M. generated IFA images. S.B. and P.M. conducted fractionations for membrane associations. A.D. optimized and performed [^{3}H]-incorporation growth assays in normal and limited growth media conditions.

2.2 Introduction

Plasmodium falciparum occupies unique metabolic niches inside its human host. *P. falciparum* merozoites initially invade human hepatocytes, where they undergo exponential replication before rupturing the host cell and invading circulating red blood cells (RBCs). The parasite asexual replicative cycle, responsible for the symptoms of malaria disease, occurs within the parasitized RBC, which the parasite extensively remodels to meet its needs. In addition to other important nutrients, these eukaryotic parasites require fatty acids (FAs) for their growth and development. While liver stage *P. falciparum* parasites have active Type II (bacterial-like) fatty acid synthesis (FAS) for production of 10-14 carbon FAs in the apicoplast (Gardner et al. 2002; Waller et al. 1998; Shears et al. 2015), the intra-erythrocytic asexual stages do not actively synthesize FAs. These circulating parasites are instead reliant on scavenging from the host to meet their FA needs (Beaumelle & Vial 1988; Holz 1977).

Scavenging of FAs is mediated by enzymes belonging to the acyl CoA synthetase gene family. These enzymes activate free FAs, generating acyl-CoA molecules of various chain lengths that can then be transported into different downstream pathways. Intriguingly, while many eukaryotic organisms have 4-6 ACS enzymes (Watkins 2008), this gene family has expanded to thirteen genes in *P. falciparum* (Bethke et al. 2006). The expansion appears to be globally conserved across parasite isolates, and is not seen in the other four human-infecting *Plasmodium* species. Furthermore, members of the ACS gene family appear to be under recent positive selection in the parasite (Van Tyne et al. 2011). These two observations suggest that FA metabolism is an important metabolic pathway, and these processes may be essential for parasite growth. Their diversification in the parasite may be driven by the

diversity of the human host diet, whereby the expansion of distinct ACS isoforms allows the parasite to better scavenge a variety of fatty acids.

This chapter focuses on three of the expanded ACS paralogs, ACS1a, ACS4, and ACS5, and three conserved ACS orthologs, ACS9 (parent of the expanded family), ACS10, and ACS11. The PfACS9-11 orthologs share homology to ACS genes from other systems, including the characteristic ACS motif and AMP/ATP binding domains, and are predicted to perform canonical ACS functions (Black et al. 1997). The expanded ACS family members also share the characteristic ACS motifs and domains, as well as an N-terminal hydrophobic export sequence and a C-terminal lysine-enriched domain (LED) (Téllez et al. 2003). Their function in the cell is unknown. Our molecular and genetic characterization of several members of the *P. falciparum* ACS gene family will shed light on their function within the parasite, and may explain the functional significance of the expansion of ACS9.

3.3 Results

Generation of DD-tagged ACS lines. To characterize the different isoforms of the ACS gene family, we used the FKBP Destabilization Domain (DD) system to generate an inducible knockdown in a 3D7 lab strain background (Banaszynski et al. 2006; Armstrong & Goldberg 2007). In this system, the FKBP-DD and 3 hemagglutinin (HA) tags are introduced by homologous recombination at the 3' end of the endogenous locus to tag the gene of interest (Figure 3.3.1A). The FKBP-DD renders the protein product inherently unstable, and it will be degraded by the parasite proteasome unless the small molecule Shield1 is added to the culture media to stabilize it (Figure 3.3.1B). This effectively results in an inducible knockdown, where protein can be titrated out of the parasite through removal of Shield1,

giving us a tool to assess *in vitro* growth phenotypes of individual ACSs. The 3' 3x HA tag is a useful tool for tracking protein expression and localization. Integration of DD construct was confirmed by PCR and Southern blot.

A. B.

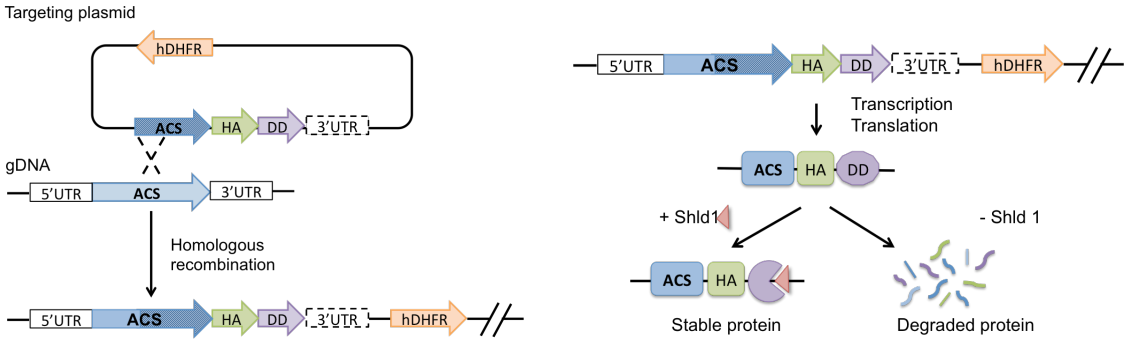

Figure 3.3.1. Generation of ACS inducible knockdown lines with the FKBP-DD system. A. Design of FKBP-DD constructs used to tag endogenous *P. falciparum* ACS genes. B. Schematic representation of the inducible knockdown regulated by Shield 1.

ACS Protein Levels and Localization. For initial characterization of the ACS gene family, we determined the transcript levels in our 3D7 lab strain, as well as protein expression profiles, and localization of ACS1a, ACS4, ACS5, ACS9, ACS10, and ACS11 using the HA-tagged DD transgenic lines. From the transcriptional profile shown in Figure 3.3.2, the ACSs are expressed to varying degrees. Many are lowly transcribed, relative to the seryl tRNA synthetase control, or a different endogenous housekeeping gene, beta-tubulin (not shown). Some, such as ACS2 and ACS6, are hardly expressed, while ACS5, ACS9, ACS10, and ACS11 are among the most abundantly expressed ACSs. In general, the conserved ACS family members (ACS9-12) appear more consistently highly expressed than the expanded family members, and most of the ACSs are expressed in the later stages of parasite development (30-48hpi).

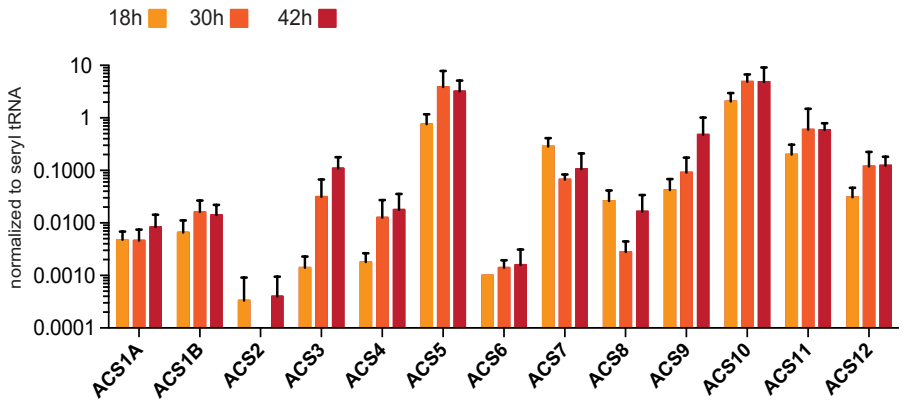

Figure 3.3.2. Transcriptional profile of ACS gene family was determined by real time PCR. Transcript levels normalized to seryl tRNA synthetase, a highly expressed *P. falciparum* gene. Transcript was measured at three stages in the intra-erythrocytic lifecycle: 18h late ring (yellow), 30h troph (orange), and 42 hour schizont (red).

Western blots of parasite lysate show similarly differential protein levels throughout the life cycle, with protein generally increasing at later stages of parasite development (Figure 3.3.3). Similar to their transcription profile, ACS4 and ACS5 show increasing abundance of protein in early trophs (30-36hpi) relative to the conserved ACSs, which are expressed later. Interestingly, protein abundance and transcript abundance of individual ACSs do not always correspond. For example, ACS9, ACS10, and ACS11 have highly abundant transcript (Figure 3.3.2) but relatively little protein by Western blot. Furthermore, ACS1a appears to have higher transcript levels in late stages, while the greatest protein expression is seen in early rings.

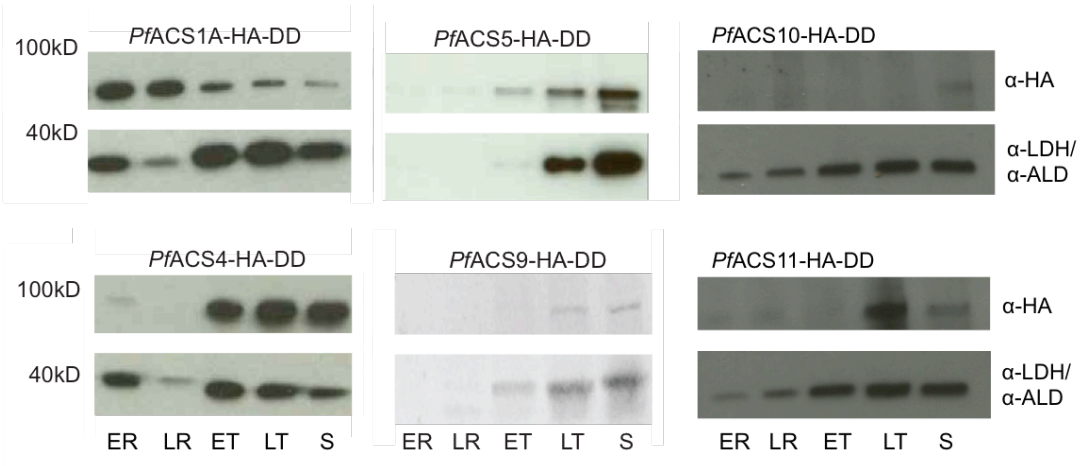

Figure 3.3.3. Anti-HA Western blots show timing of ACS protein expression. ACS1a, ACS4, ACS5, ACS9, ACS10, and ACS11 detected with anti-HA antibody, using anti-lactate dehydrogenase (LDH) and/or anti-Aldolase (ALD) as a loading control. Protein expression is measured throughout the intraerythrocytic life cycle stages: early ring (ER), late ring (LR), early trophozoite (ET), late trophozoite (LT), and schizont (S).

In addition to measuring expression of protein and transcript, we also looked at localization of these HA-tagged lines using immunofluorescence assays (IFAs). Again, we see different localization patterns in different ACS isoforms (Figure 3.3.4). ACS1a and ACS5 are exported outside the parasite, and associate with the host RBC. Both have somewhat punctate staining, and confocal images of ACS5 in particular show localization at the RBC membrane periphery. In contrast, ACS4 and ACS9 are localized within the parasite, though with the level of resolution here, it is not clear if ACS9 remains within the parasitophorous vacuole membrane (PVM) as well. We were unable to detect ACS10 or ACS11 by IFA, following several attempts and protocol modifications. This is likely due to the low expression of the protein, or perhaps the conformation of the HA tag is inaccessible to the anti-HA antibodies.

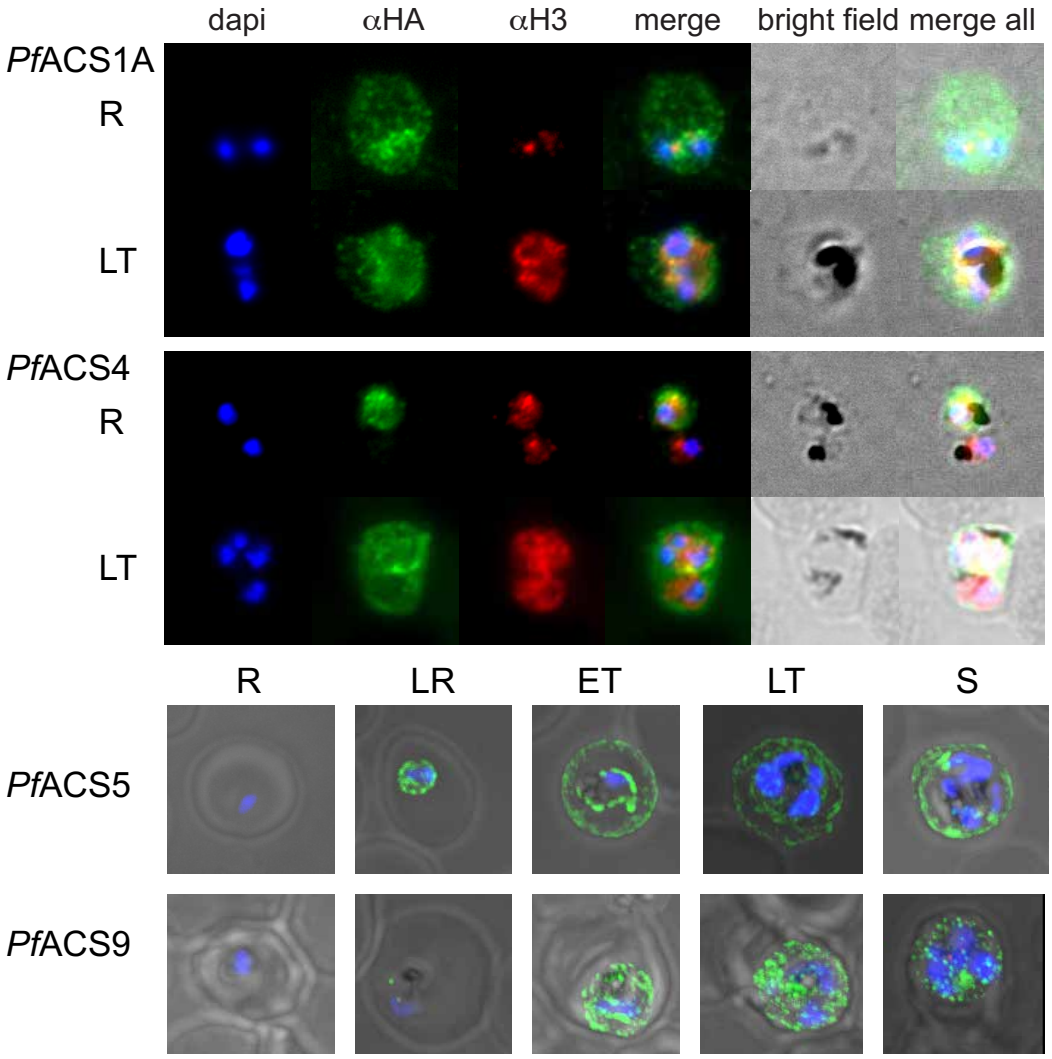

Figure 3.3.4. Immunofluorescence assays of HA-tagged ACS lines. Anti-HA marks individual ACS proteins, while dapi and anti-H3 are DNA and nuclear stains, respectively. ACS localization is measured throughout the following intraerythrocytic life cycle stages: ring (R), late ring (LR), early trophozoite (ET), late trophozoite (LT), and schizont (S).

To further understand ACS subcellular localization, we performed membrane fractionation assays using carbonate and urea with the HA-tagged DD lines (Figure 3.3.5). Cell membranes are disrupted using alkaline (carbonate) and acidic (urea) conditions to remove

membrane-associated and integral membrane proteins, respectively (Okamoto et al. 2001). While only ACS6 is predicted to have a transmembrane domain (PlasmoDB), we wanted to determine experimentally if any other ACSs are associated with membranes. With the exception of ACS9, all ACSs appear to be tightly associated with membranes, as evidenced by detection of the HA tag in the urea-extracted pellet.

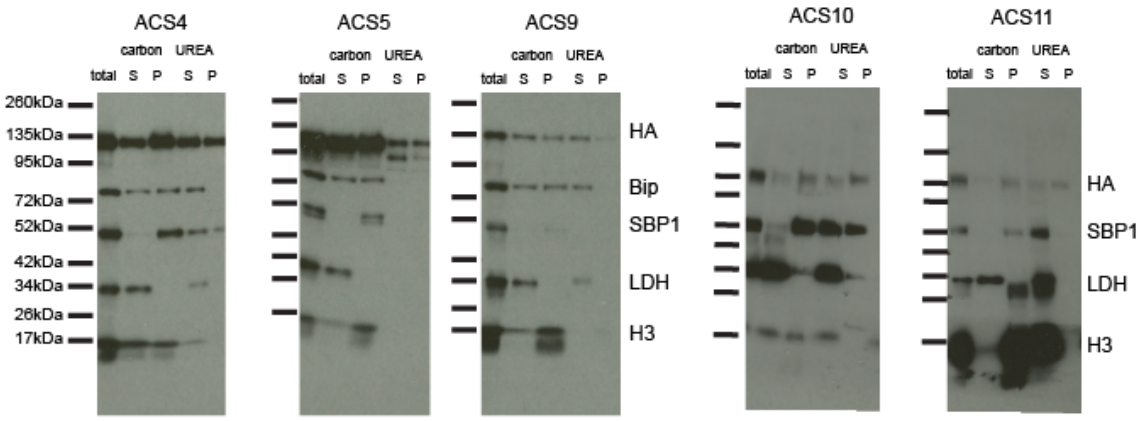

Figure 3.3.5. Membrane fractionation by carbonate and urea treatment. Tight membrane association is evident based on incomplete extraction of HA-tagged ACS from urea pellet (P). All ACS's are tightly membrane associated, except ACS9, which is extracted to the supernatant (S) by urea treatment. Additional well-characterized *Plasmodium* proteins (BiP, SBP1, LDH, and H3) are included as experimental controls.

Conditional knockdown of individual ACS proteins. By removing the small molecule Shield1 from the culture media, we were able to achieve approximately a 70% knockdown of ACS5 and ACS9 (Figure 3.3.6). Levels of knockdown appeared to be protein specific, as we were unable to knock down ACS1a, ACS4, ACS10, and ACS11 (data not shown). Maintaining DD lines without Shield1 into subsequent parasite growth cycles had no effect on knockdown (data not shown).

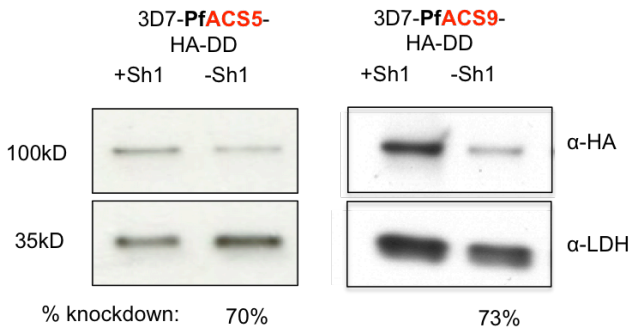

Figure 3.3.6. Anti-HA Western blot confirming knockdown of ACS5 and ACS9 protein levels in DD-tagged parasite lines with or without Shield1 (Sh1). Anti-LDH is a loading control. Knockdown was quantified relative to the LDH control by densitometry using ImageJ (Abràmoff et al. 2004).

Growth assays with ACS knockdown lines. To determine if ACS DD knockdown lines had a growth phenotype, we grew them for 72 hours in decreasing concentrations of the stabilizing molecule Shield 1. [^{3}H]-hypoxanthine incorporation assays were used to assess growth of the ACS DD knockdown lines. There was no growth defect observed in ACS5, ACS9, or ACS10 knockdown lines *in vitro* in the absence of Shield1 under normal growth conditions (Figure 3.3.7).

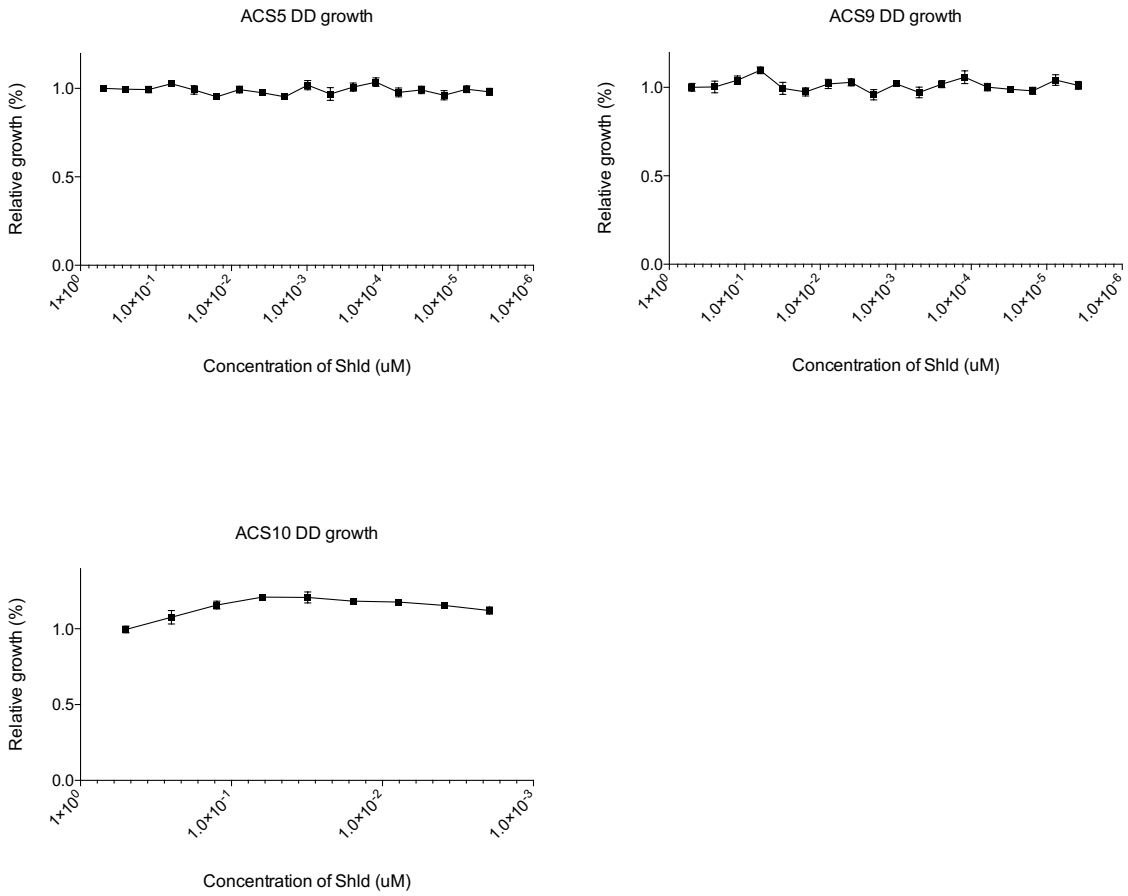

Figure 3.3.7. ACS knockdown lines had no growth defect in the absence of Shield1. [^{3}H]-hypoxanthine incorporation assays to assess growth of inducible knockdown lines without protein stabilizing small molecule Shield1.

To further test for growth phenotypes, we tried growing the knockdown lines in different combinations of minimal FAs known to support some parasite growth (Asahi et al. 2005; Mi-Ichi et al. 2006). As the ACSs are predicted to scavenge FAs and may have some specificity for FAs of different chain length (Black et al. 1997; Coleman et al. 2002; Shockey & Browse 2011; Beaumelle & Vial 1988), we hypothesized this would reveal some ACS-specific or ACS-associated FA growth requirements. However, there were no differences in the knockdown lines, relative to the control grown with Shield1 (Figure 3.3.8).

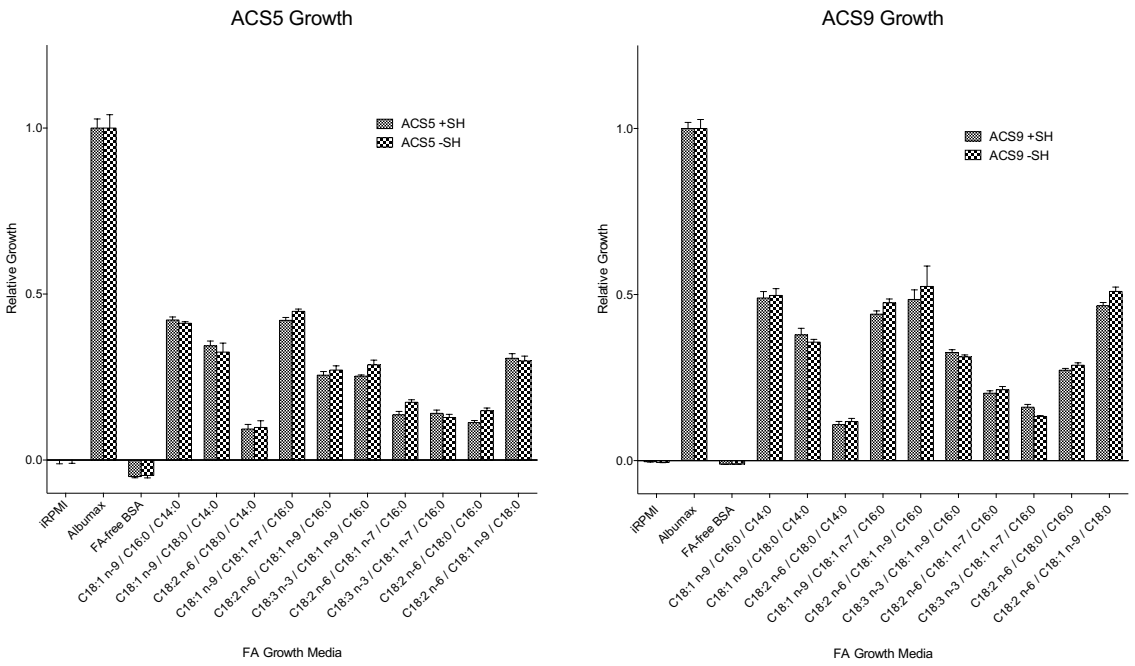

Figure 3.3.8. [^{3}H]-hypoxanthine incorporation assays to assess growth of inducible knockdown lines in different combinations of FAs. FA combinations were determined based on the work of (Asahi et al. 2005; Mi-Ichi et al. 2006).

To further explore potential growth phenotypes, we performed additional growth assays under limited glucose and restricted FAs (see more detailed explanation in Chapter 5). We predicted that excess of glucose and serum lipids in the normal growth condition (LeRoux et al. 2009) may be masking phenotypes of these FA metabolic genes, and limiting available nutrients would reveal their importance in sustaining parasite growth *in vitro*. These assays revealed a slight but consistent growth decrease in both the ACS5 and ACS9 knockdown parasites relative to the controls grown with Shield1 (Figure 3.3.9).

A. B.

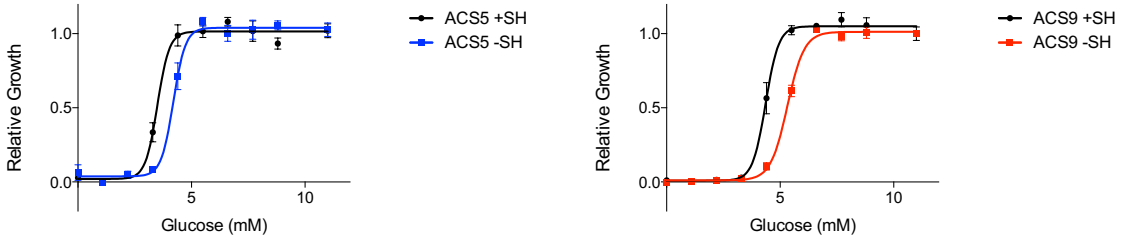

Figure 3.3.9. In the absence of Shield1, both ACS5 (A) and ACS9 (B) DD knockdown lines show sensitivity to limited glucose growth conditions. Parasite growth measured by [^{3}H]-incorporation assays in RPMI1640 with decreasing concentrations of glucose.

3.4 Discussion

The differential expression patterns and localization of the ACS isoforms suggest they may have distinct physiological roles in the cell. The majority of the ACS isoforms are expressed late in the parasite lifecycle, both in protein abundance and transcript. This matches well with previously reported data (PlasmoDB). There were some notable exceptions to the late stage expression. ACS4 and ACS5, both members of the expanded family, are expressed slightly earlier, peaking at approximately 30-36hpi. ACS1a shows late stage transcriptional expression, however the protein is most abundant in the ring stages. This may indicate that transcript is made and stored in the schizont stage so it is ready for early protein expression in the early ring stages. These earlier peaks in protein could signify distinct cellular functions from the other isoforms, and the lack of other ACS family members with similar expression profiles could indicate distinct, non-redundant physiological roles for these proteins.

Of note, we focused on the expression profile of the ACS family members in a 3D7 reference strain. Previous groups have described monoallelic expression or allelic exclusion of some ACS family members (Rovira-Graells et al. 2012). While previous results from our group determined that the expansion was globally conserved (Bethke et al. 2006), we have not specifically looked at expression of the different ACS isoforms in a globally representative set of parasites. In future work, measuring ACS expression in additional strains may help answer this question.

Export of certain ACS proteins into the RBC cytosol is an interesting phenomenon worth further investigation (Figure 3.3.4). ACS1a and ACS3 have previously been reported outside the parasite (Téllez et al. 2003; Matesanz et al. 1999) and our findings with ACS1a support this. The RBC peripheral localization of ACS5 is a novel finding, and its strong association with membranes suggest that it may be associated with the RBC membrane (Figures 3.3.4 and 3.3.5). This may hint at a role in FA uptake or vectorial acylation (Black & DiRusso 2003). It is interesting that not all members of the expanded family are exported outside the RBC, as they all share an N-terminal hydrophobic export sequence (Téllez et al. 2003). ACS9, parent of the expanded family, also contains the hydrophobic export sequence, however it appears to be localized within the parasite. It is unclear from this level of resolution if ACS9 is exported within the PVM. Though we were unable to detect the tagged ACS10 and ACS11, we would predict localization within the parasite as both genes lack an export sequence.

While we did not observe a growth defect in ACS DD knockdown lines in complete growth media, restriction of glucose revealed a slight growth defect in the ACS5 and ACS9 knockdown lines (Figure 3.3.9). This finding is intriguing, as it suggests a link between fatty acid and glucose metabolism. These pathways and the implication for energy metabolism in

the parasite will be further explored in the next chapter. The lack of growth phenotype under normal growth conditions suggests that individual ACS isoforms are not essential for *in vitro* growth. There may in fact be some redundancy, especially between members of the expanded family. However, the differential expression patterns and localization would argue for at least some specialization.

Our experiments with these transgenic lines were somewhat limited by the FKBP-DD-HA tagging system. Though localized to the C-terminus of the proteins, it is possible these tags interfered with protein expression, trafficking, or localization. Furthermore, the effectiveness of the HA tag seemed to be protein-specific, as it was not useful for tagging all proteins, and knockdown levels varied substantially. We were unable to characterize ACS10 and ACS11 localization by IFA, either due to the low level of protein expression, incorrect integration of the DD-HA tag, or inaccessibility of the tag to our antibodies.

Nevertheless, our results thus far support distinct physiological roles for different members of the ACS family within the cell. In particular, ACS5 has a distinct expression profile and subcellular localization, and ACS5 and ACS9 share an intriguing growth phenotype. We hypothesize that the expansion and recent positive selection of the PfACS gene family are the consequence of metabolic pressures driving parasite evolution, and further characterization of this family will shed light on the function of this expanded gene family.

3.5 Materials and Methods

Plasmids and constructs for DD parasites

FKBP DD parasites were generated by Ulf Ribacke, following the methods described by the Wandless and Goldberg labs (Banaszynski et al. 2006; Armstrong & Goldberg 2007). Plasmids were provided by Jeff Dvorin and Manoj Duraisingh (Dvorin et al. 2011).

Parasite culture and inducible knockdown of DD parasites

Parasites were maintained in vitro in the method of Trager and Jensen (Trager & Jensen 1976). Parasites were synchronized by 10-minute incubation in 5% sorbitol (Moll et al. 2008). Inducible knockdown of the FKBP-DD lines was achieved by washing highly synchronized early ring stage parasites in incomplete RPMI three times, then returning them to culture in complete RPMI media lacking Shield1.

Western blots

For all Western blots of HA-tagged ACS lines, 5-10mLs of 3-5% parsitemia culture was saponin lysed (0.025% w/v in PBS) and washed with PBS. Lysates were mixed with Laemmli sample buffer (BioRad) containing 1:20 beta-mercaptoethanol and boiled at 95°C for 10 minutes. Samples were run on Mini-PROTEAN TGX AnykD pre-cast gels (BioRad) in 1X Tris-glycine-SDS running buffer at approximately 100V for 1 hour. Gel was transferred to membrane using the iBlot 7-minute blotting system (ThermoFisher Scientific), set at program 3 for 8 minutes. Blots were probed in the following primary antibodies: rat anti-HA (Roche), diluted 1:1,000 in 3%BSA/PBST; Mouse anti-lactate dehydrogenase (LDH) diluted 1:20,000 in 3%BSA/PBST; or rabbit anti-aldolase (Abcam), diluted 1:5,000 in 3%BSA/PBST. Knockdown was quantified relative to the LDH control by densitometry using ImageJ (Abràmoff et al. 2004).

Real time PCR

Total RNA was extracted with Qiagen RNeasy mini columns (Qiagen Venlo, Limburg) according to manufacturer instructions, and DNAse-treated. First strand cDNA synthesis was performed using SuperScript III (Life Technologies) following manufacturer instructions. The absence of contaminating DNA and the success of the reverse transcriptase reaction were confirmed by comparing qPCR of Rt+ and Rt- with the control Seryl tRNA synthetase primer set in quadruplicate; samples were run on and ABI 7900 HT and Differences in expression levels were calculated using the ΔΔCt method with tRNA synthetase as a reference gene as described in the Applied Biosystems User Bulletin. cDNA concentrations were normalized to SerRS Ct values to minimize biases in PCR efficiency. PCR amplification was performed as follows: 15 minutes at 95 °C followed by 40 cycles of two-step amplification of 94 °C for 30 s and 52 °C for 30 s. 2.

ACS1aF	TGGTGGAAGGTTTAATGGAACG	forward
ACS1aR	ACCCAAACGTACATCCTCCA	reverse
ACS1bF	TTGGCTAGTTTCTGATTTGGGA	forward
ACS1bR	ACGTTCCAATATGCCTTCAACC	reverse
ACS2F	GCACGTAGAAATGAATTACCGC	forward
ACS2R	AGGACTCAAACGTATATCCTCCA	reverse
ACS3F	AGCAACTGATACACTGCCAA	forward
ACS3R	CTGAAATTATGGCTAGTGGACCA	reverse
ACS4F	GTGGAAGTAGCACGGGTAGT	forward
ACS4R	CTCCCTGAGTTATGTTCTTCTCT	reverse
ACS5F	CCGCTGATATGGCTTCTATGC	forward
ACS5R	TGAGCTAATAACCCTTCAACCA	reverse
ACS6F	AGGCATGCAATGAAGAAGAATCA	forward
ACS6R	GGCTTCAATACCTTTCCCTCC	reverse
ACS7F	GGTTGAAGGATTGTTGTGTCG	forward
ACS7R	AGGCACACAAACTAATGTCTTCT	reverse
ACS8F	TCGAACATGCTTATGGTGAACC	forward
ACS8R	ACCACTCATCATAGCTGCCA	reverse
ACS9F	TCGTGCATGTTAAGTGGTGT	forward
ACS9R	CTTGCCCTTCATCACCATTTT	reverse
ACS10F	TGACTGAATCTTTGGGTGCT	forward
ACS10R	GGTTGCATGTACTTGGTCCTC	reverse
ACS11F	AAAGGTGTTATGATTACGCACAA	forward
ACS11R	GAAGGTTGGTTTCAGTTCATTCA	reverse
ACS12F	ACTTTTCAGCTATCCCAACCA	forward
ACS12R	TGAGCTAACTTGATGACAGGC	reverse

Table 3.5.1 Primers used for RT PCR of ACS genes.

Immunofluorescence assays

100uL parasite culture (5% parasitemia, 4% hematocrit) is washed 1x in 500ul PBS, the resuspended in 500ul fix (4% paraformaldehyde/0.0075% glutaraldehyde in PBS). Incubate 30 mins at room temperature, rotating. Spin down and wash 1x 500ul PBS. Dilute pellet in 3mL PBS total volume (or adjust depending on initial parasitemia). 250ul cell suspension is deposited on Poly-L-lysine coverslip (BC biocoat Poly-L-Lysine cellware

354085) and allowed to settle for 30m. Coverslip was washed 2x in PBS, then permeabilized for 5m with 0.1% Triton-X 100 in PBS. Coverslips were washed 2X in PBS, then blocked in 3% BSA for 1 hour. Coverslips were incubated overnight, shaking at 4°C in primary antibody: rat anti-HA (Roche), diluted 1:1000 in 3% BSA/PBS. Coverslips were washed 3x in PBS, then incubated with secondary (1:2000 dilution of Alexa fluor 488 anti-rat (Abcam)) for 1 hour at room temperature. Coverslips were washed 3x in PBS, then mounted on glass slides with 2.5µl VectaShield liquid containing DAPI (Vector Laboratories H-1200). Microscopy for ACS1a and ACS4 IFAs was performed on a Nikon Eclipse TE300 microscope at HSPH. Microscopy for ACS5 and ACS9 IFAs was performed on a Zeiss LSM510 META 2-Photon confocal microscope at Boston Children's Hospital Imaging Center.

Membrane association

Late stage parasites were MACS purified and kept in PBS with protease inhibitor. For carbon extraction $3x10^6$ cells were incubated in 0.1M Na_2CO_3 (pH11) on ice for 30 minutes and then centrifuged at 100,000g for 1h at 4°C. The supernatant was taken off and mixed with 6x SDS buffer. The pellet was washed once with 0.1M Na_2CO_3 and then resuspended in 6x SDS buffer. For Urea extraction $3x10^6$ cells were incubated in 10mM Tris pH 8 (Trizma HCL), 8M Urea, 1mM EDTA for 1h at room temperature. Protein lysate was dialyzed over night against 10mM Tris pH 8, 0.1M Urea, 1mM EDTA. Urea protein lysate was then handled in the same way as the carbon extraction.

[^{3}H]-hypoxanthine incorporation assay

[^{3}H]-hypoxanthine incorporation assays were conducted following the method of Desjardins et al. (Desjardins et al. 1979). 3-4 biological replicates were performed for each condition. [^{3}H]-incorporation was measured on a TopCount NXT microplate scintillation

and luminescence counter (Packard Bioscience). To determine the IC50, we used non-linear regression with the log(inhibitor) vs. response – variable slope (four parameters) curve-fitting equation (Prism version 6.0).

3.6 References

Abràmoff, M.D., Magalhães, P.J. & Ram, S.J., 2004. Image processing with imageJ. *Biophotonics International*, 11(7), pp.36–41.

Armstrong, C.M. & Goldberg, D.E., 2007. An FKBP destabilization domain modulates protein levels in Plasmodium falciparum. *Nature methods*, 4(12), pp.1007–1009.

Asahi, H. et al., 2005. Investigating serum factors promoting erythrocytic growth of Plasmodium falciparum. *Experimental Parasitology*.

Banaszynski, L.A. et al., 2006. A Rapid, Reversible, and Tunable Method to Regulate Protein Function in Living Cells Using Synthetic Small Molecules. *Cell*, 126(5), pp.995–1004.

Beaumelle, B.D. & Vial, H.J., 1988. Acyl-CoA synthetase activity in Plasmodium knowlesi-infected erythrocytes displays peculiar substrate specificities. *Biochimica et Biophysica Acta*, 958, pp.1–9.

Bethke, L.L. et al., 2006. Duplication, gene conversion, and genetic diversity in the species-specific acyl-CoA synthetase gene family of Plasmodium falciparum. *Molecular and Biochemical Parasitology*.

Black, P.N. et al., 1997. Mutational analysis of a fatty acyl-coenzyme A synthetase signature motif identifies seven amino acid residues that modulate fatty acid substrate specificity. *The Journal of Biological Chemistry*, 272(8), pp.4896–4903.

Black, P.N. & DiRusso, C.C., 2003. Transmembrane movement of exogenous long-chain fatty acids: proteins, enzymes, and vectorial esterification. *Microbiology and Molecular Biology Reviews*, 67(3).

Coleman, R. et al., 2002. Do Long-Chain Acyl-CoA Synthetases Regulate Fatty Acid Entry into Synthetic Versus Degradative Pathways? *The Journal of Nutrition*, 132, pp.2123–2126.

Desjardins, R. et al., 1979. Quantitative assessment of antimalarial activity in vitro by a semiautomated microdilution technique. *Antimicrobial Agents and Chemotherapy*,

16(6).

Dvorin, J.D. et al., 2011. A Plant-like kinases in Plasmodium falciparum regulates parasite egress from erythrocytes. *Science*, 328(5980), pp.910–912.

Gardner, M.J. et al., 2002. Genome sequence of the human malaria parasite Plasmodium falciparum. *Nature*, 419.

Holz, G.G., 1977. Lipids and the malarial parasite. *Bulletin of the World Health Organization*, 55(2-3), pp.237–248.

LeRoux, M., Lakshmanan, V. & Daily, J.P., 2009. Plasmodium falciparum biology: analysis of in vitro versus in vivo growth conditions. *Trends in Parasitology*, 25(10), pp.474–481.

Matesanz, F., Dura, I. & Alcina, A., 1999. The Cloning and Expression of Pf acs1 , a Plasmodium falciparum Fatty Acyl Coenzyme A Synthetase-1 Targeted to the Host Erythrocyte Cytoplasm.

Mi-Ichi, F., Kita, K. & Mitamura, T., 2006. Intraerythrocytic Plasmodium falciparum utilize a broad range of serum-derived fatty acids with limited modification for their growth. *Parasitology*, 133, pp.399–410.

Moll, K. et al., 2008. *Methods In Malaria Research 5th edition*,

Okamoto, T. et al., 2001. Analysis of the association of proteins with membranes. *Current protocols in cell biology*, Chapter 5, p.Unit 5.4.

Rovira-Graells, N. et al., 2012. Transcriptional variation in the malaria parasite Plasmodium falciparum. *Genome Research*, 22, pp.925–938.

Shears, M.J., Botté, C.Y. & McFadden, G.I., 2015. Fatty acid metabolism in the Plasmodium apicoplast: Drugs, doubts and knockouts. *Molecular and Biochemical Parasitology*, 199(1-2), pp.34–50. Available at: http://dx.doi.org/10.1016/j.molbiopara.2015.03.004.

Shockey, J. & Browse, J., 2011. Genome-level and biochemical diversity of the acyl-activating

enzyme superfamily in plants. *The Plant Journal*, 66, pp.143–160.

Téllez, M.D.M., Matesanz, F. & Alcina, A., 2003. The C-terminal domain of the Plasmodium falciparum acyl-CoA synthetases PfACS1 and PfACS3 functions as ligand for ankyrin. *Molecular and Biochemical Parasitology*, 129(2), pp.191–198.

Trager, W. & Jensen, J.B., 1976. Human Malaria Parasites in Continuous Culture. *Science*, 193(4254), pp.673–675.

Van Tyne, D. et al., 2011. Identification and functional validation of the novel antimalarial resistance locus PF10_0355 in Plasmodium falciparum. *PLoS Genetics*, 7(4).

Waller, R.F. et al., 1998. Nuclear-encoded proteins target to the plastid in Toxoplasma gondii and Plasmodium falciparum. *PNAS*, 95, pp.12352–12357.

Watkins, P.A., 2008. Very-long-chain Acyl-CoA Synthetases. *The Journal of Biological Chemistry*, 283(4), pp.1773–1777.

Chapter 4:

The role of Acyl CoA Synthetases in *Plasmodium falciparum* fatty acid metabolism.

4.1 Attribution

AUTHORS:

Allison Demas[1], Selina Bopp[1], Erik Allman[2], Nathan Hicks[1], Ulf Ribacke[3], Sarah K. Volkman[1,4,5], Manuel Llinás[2], Dyann F. Wirth[1,5]

[1] Harvard T.H. Chan School of Public Health, Boston, MA, USA.

[2] Pennsylvania State University, University Park, PA, USA.

[3] Uppsala University, Uppsala, Sweden.

[4] Simmons College, Boston, MA USA

[5] Broad Institute, Cambridge, MA, USA.

AUTHOR CONTRIBUTIONS:

S.B. and N.H. generated the ACS CRISPR-Cas9 knockout lines. S.B. confirmed knockouts with Southern blot, PCR, and RT-PCR. S.B. conducted parasite growth assays with FACS, while A.D. conducted [^{3}H]-hypoxanthine incorporation growth assays. A.D. prepared parasites and performed metabolite extractions for GC-FID and LC-MS/MS. E.A. ran LC-MS/MS, and E.A. and A.D. performed analysis of LC-MS/MS data.

4.2 Introduction

Fatty acids (FAs) are essential for *Plasmodium falciparum* growth. Though the parasite has the ability to synthesize fatty acids *de novo*, these apicoplast-localized pathways are only active during sexual and liver stages of development (Shears et al. 2015). During the asexual erythrocytic stage, the parasite relies on scavenging from the human host to meet its substantial fatty acid requirements (Holz 1977; Beaumelle & Vial 1988). Scavenged fatty acids are activated through the addition of an acyl CoA molecule by the Acyl CoA Synthetase (ACS) family of enzymes. These fatty acids can then be modified through elongation and desaturation pathways, and supply many downstream metabolic pathways, such as *de novo* lipid biosynthesis for parasite membranes.

In *P. falciparum* the ACS gene family has expanded from four conserved homologs common to all Plasmodium species, to thirteen distinct isoforms (Bethke et al. 2006). In this chapter, we expand on our previous characterization of the ACS family, and explore their specific contributions to downstream metabolic pathways. Using the CRISPR-Cas9 gene editing system to genetically disrupt individual ACS genes, we are able to assess their specific roles in parasite growth, and fatty acid and lipid metabolism. Of particular interest is ACS5, a member of the expanded family. We have previously shown that ACS5 is exported outside the parasite and strongly associates with host red blood cell membrane (Figures 3.3.3 and 3.3.4). Unlike the late stage expression of other members of the ACS family, ACS5 is expressed in trophozoite stages, 30-36 hours post-invasion. In addition, a slight growth defect was observed for ACS5 knockdown parasites under restricted media growth conditions, suggesting this ACS enzyme might play an important, though not essential, role in supporting *in vitro* growth (Figures 3.3.8).

In this chapter, we generated and characterized four individual ACS knockout (KO) lines, confirming a clear growth phenotype for the ACS5 KO in an isogenic background. We then used gas chromatography (GC) and liquid chromatography-mass spectrometry (LC-MS) approaches to explore this growth defect and the functional role of ACS5 in the parasite. Using these approaches, we increased our understanding of the role of ACS5 in supplying FAs to downstream metabolic pathways, including FA desaturation and elongation pathways, and lipid biosynthesis. Our ongoing studies of this expanded gene family will help us to better understand the functional significance of their expansion and selection in *P. falciparum* parasites.

4.3 Results

CRISPR-Cas9 knockout of ACS5, ACS8, ACS9, and ACS12. We used the CRISPR-Cas9 system to generate knockouts of ACS5, ACS8, ACS9, and ACS12, following the methodology described by (Ghorbal et al. 2014). These knockouts have been confirmed using PCR (data not shown), Southern blot (Figure 4.3.1), and RT-PCR of cDNA (Figure 4.3.2). These methods confirmed loss of gene expression and correct integration of the human DHFR (hDHFR) selectable marker at the endogenous locus, though some residual transcript expression was observed for ACS8 trophozoites and ACS12 rings (Figure 4.3.2). Real time PCR of ACS expression in individual KO lines revealed there was little compensatory expression of alternate ACSs in the individual KOs (Figure 4.3.2). There may be a slight increase in ACS1a expression in the ACS8 KO line, however this appears to be the only potential example for compensatory expression.

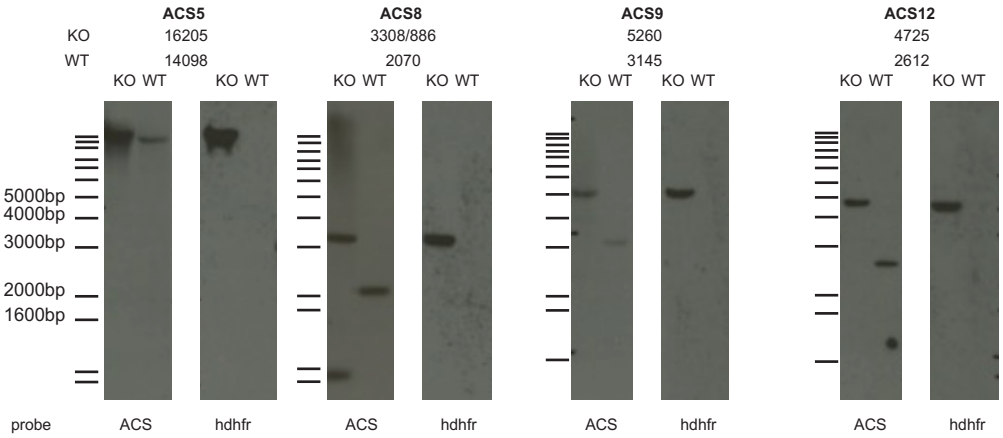

Figure 4.3.1. Southern blot confirmation of individual ACS knockout lines, determined by gene specific probe and integration of hdhfr cassette. Expected band sizes for integrated knockout ("KO") and wildtype ("WT") are shown above each blot.

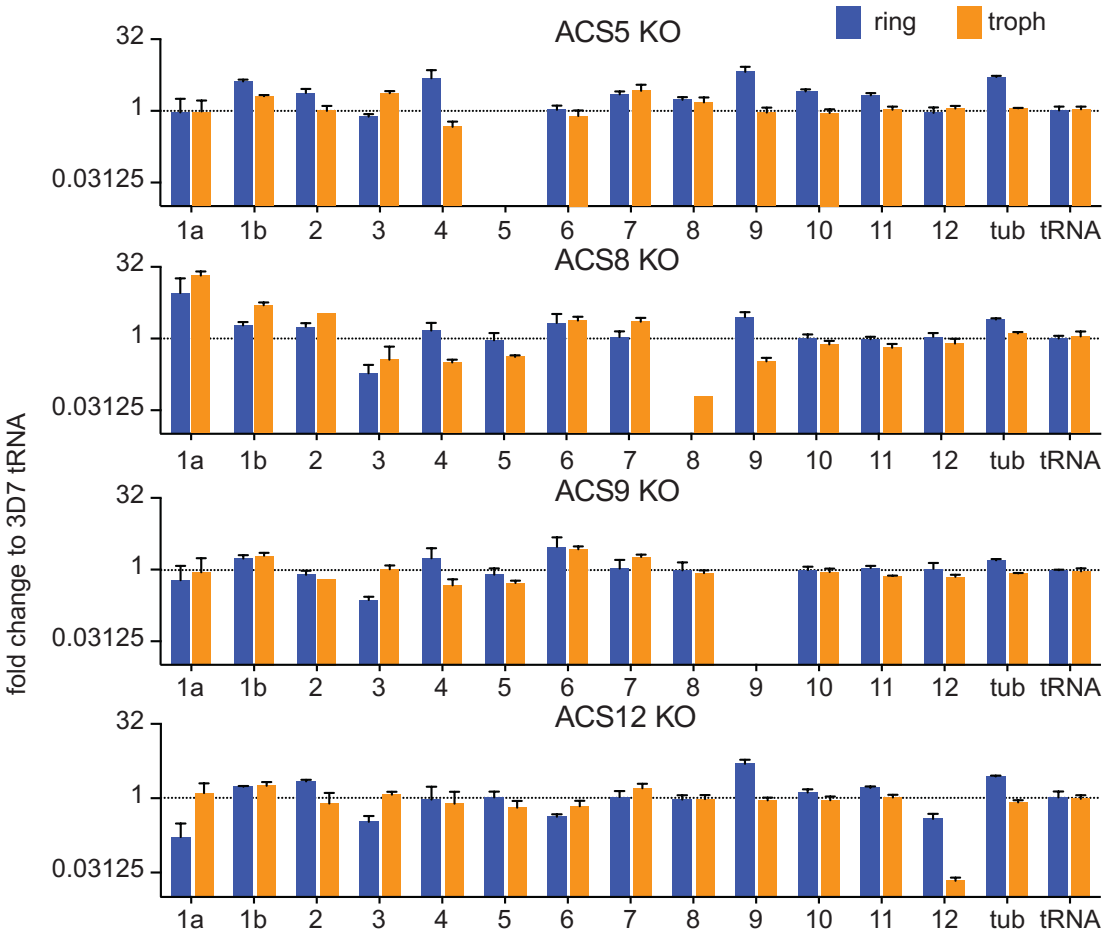

Figure 4.3.2. RT-PCR for ACS gene family expression in individual ACS knockout lines. Expression level expressed as fold change relative to seryl tRNA synthetase control gene expression in 3D7. Expression was measured at two stages in the lifecycle, ring and trophozoite ("troph").

CRISPR-Cas9 knockout of ACS5 results in a growth defect *in vitro*. We characterized the growth of the knockout parasites in normal and limited nutrient conditions. The ACS5 KO line has a pronounced growth defect (Figure 4.3.3), and *in vitro* growth is further reduced by restricted glucose and glutamine (45%) and limited free fatty acids (30uM each C16:0 and C18:1) (Figures 4.3.3 and 4.3.4). This finding is in line with the growth defect observed previously in the ACS5 DD knockdown line (Figure 3.3.8). This further establishes the link

between FA and glucose metabolism for supporting parasite growth. The ACS8, 9, and 12 KO lines all grow similarly to the 3D7 parent in normal and restricted growth media (Figure 4.3.3). Though when growth was measured using [^{3}H]-hypoxanthine incorporation, the ACS8 and ACS12 knockouts have slightly intermediate phenotypes in restricted growth media, with a potential slight growth inhibition relative to the 3D7 parental strain, while ACS9 grows as well or better than the parent (Figure 4.3.4).

ACS enzymes are known to have different substrate specificities, so we predicted that the growth of the ACS KO lines would be affected differently by RPMI supplemented with specific combinations of FAs. These different combinations of FAs could then be used to make predictions about substrate specificity of individual ACSs. Using [^{3}H]-hypoxanthine incorporation assays, we assessed growth of our ACS knockout lines in serum-free RPMI supplemented with different combinations of FAs (Figure 4.3.5). Results for basic FA requirements were similar to those described in more detail in Chapter 5 (Figure 5.3.2). Though parasite growth overall was reduced relative to the albumax control, combinations of FAs containing C16:0 and C18:1 were best able to support parasite growth *in vitro*, and C18:1 alone was sufficient to sustain growth. There were no significant differences in growth of the ACS knockout lines in different FA combinations, though the ACS8 knockout grew slightly better overall.

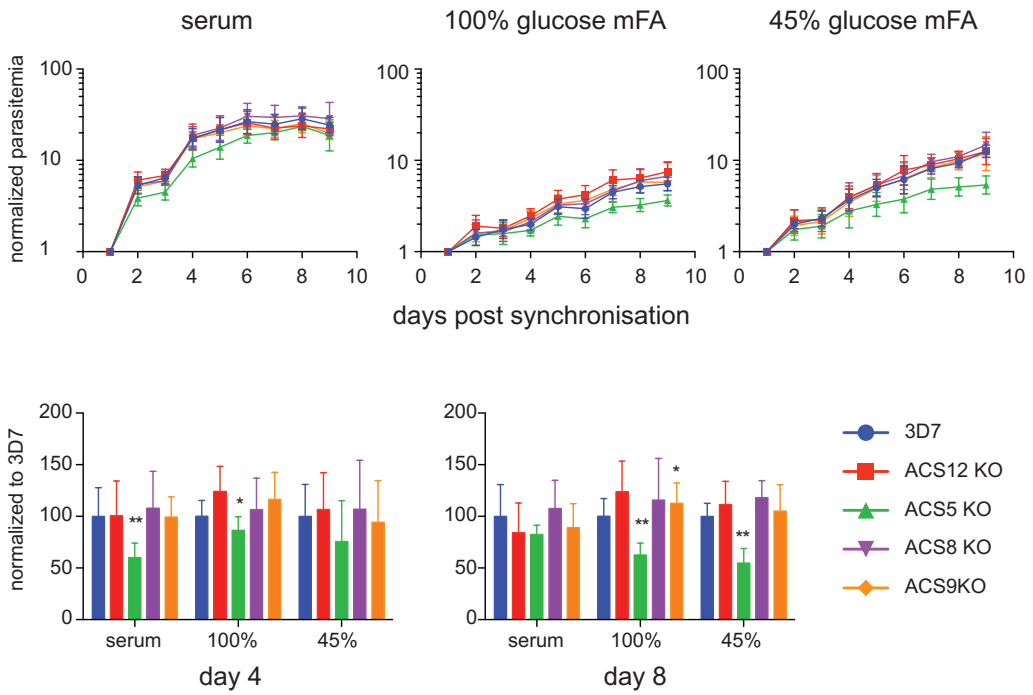

Figure 4.3.3. Growth of of ACS knockout lines over several cycles. Parasites were grown in RPMI1640 media supplemented with serum ("serum" condition) or minimal FAs ("100%" condition), or 45% limited glucose and glutamine RPMI media, supplemented with minimal FAs ("45%" condition). Parasitemia was determined by SYBR Green I staining of DNA as measured by FACS. Statistical significance determined using one-way ANOVA in Prism v 6.0 (* = $p<0.05$; ** = $p<0.005$).

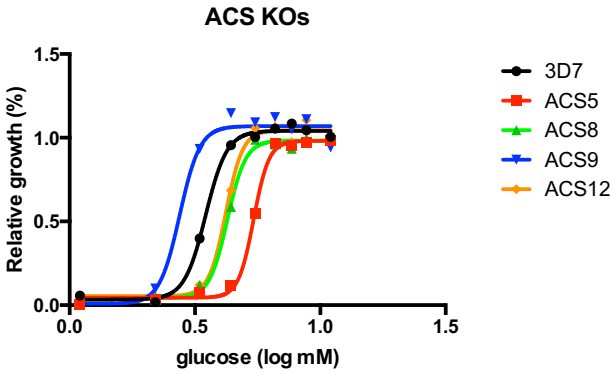

Figure 4.3.4. [^{3}H]-hypoxanthine incorporation assays were used to assess growth of ACS knockouts in limited glucose conditions.

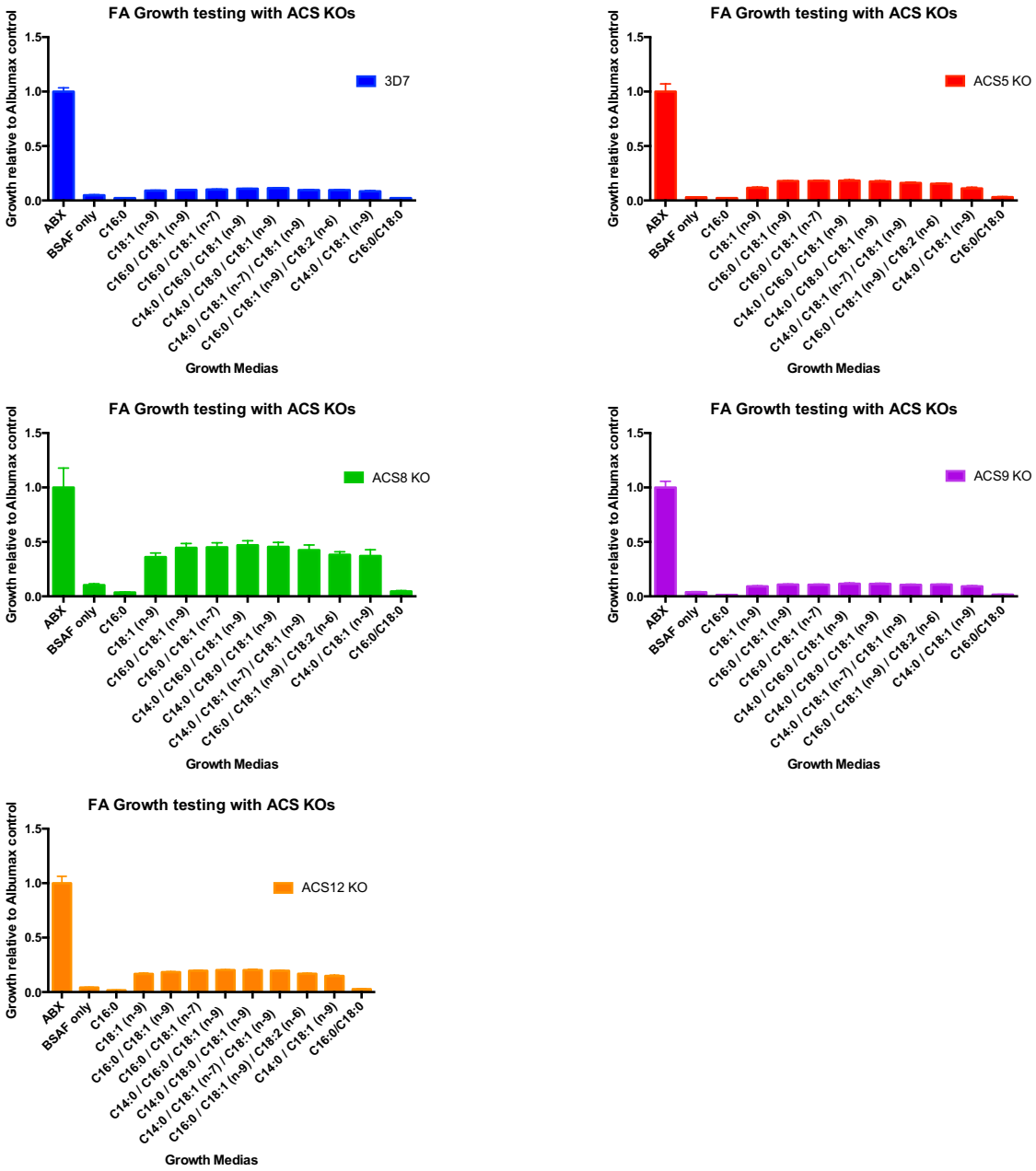

Figure 4.3.5. Growth of ACS KO lines in different FA combinations. One cycle (96 hour) [^{3}H]-hypoxanthine incorporation assays demonstrate that palmitic and oleic acid are necessary and sufficient to support parasite growth in vitro. ACS knockout lines grow similarly in different combinations of fatty acids. Raw scintillation counts are normalized relative to the albumax ("ABX") positive growth control.

ACS5 knockout lines show significant reductions in oleic and linoleic acid. ACSs mediate FA activation, and, similar to other eukaryotes, *Plasmodium knowlesi* ACS have been shown to exercise chain-length-dependent substrate preferences (Beaumelle & Vial 1988). We hypothesized that *P. falciparum* ACSs will function similarly, leading to changes in the intracellular fatty acid profile of our knockouts. To test this, we profiled the FA species present in our different ACS knockout lines using gas chromatography with a flame ionization detector (GC-FID). This gas chromatography method is highly sensitive for hydrophobic molecules, and allows us to detect specific known FA acid species in our cells. Enriched infected RBCs were normalized by cell count and profiled for relative abundance of 45 different FA species. The most significant differences were between infected and uninfected cells. The profiles of all ACS knockout lines examined (ACS5, ACS8, and ACS9 knockouts) were overall very similar to the 3D7 parental line (Figure 4.3.6A). Focusing on the ACS5 knockout in relation to 3D7, we see statistically significant differences in the FA profile (Figure 4.3.6B). Unsaturated FA species C18:1n-9c (oleic acid) and C18:2n-6cc (linoleic acid) are significantly reduced in the ACS5 knockout. This is accompanied by a slight, though not significant, enrichment of saturated C18:0 (stearic acid). There is also a slight increase in the long chain polyunsaturated FA species C20:4n-6c (arachidonic acid).

A.

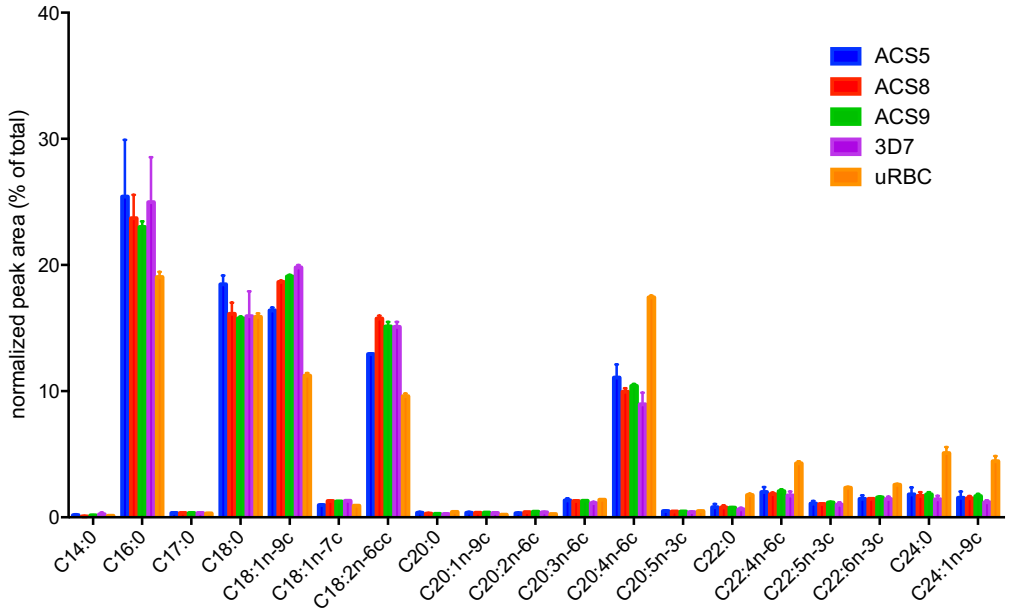

B.

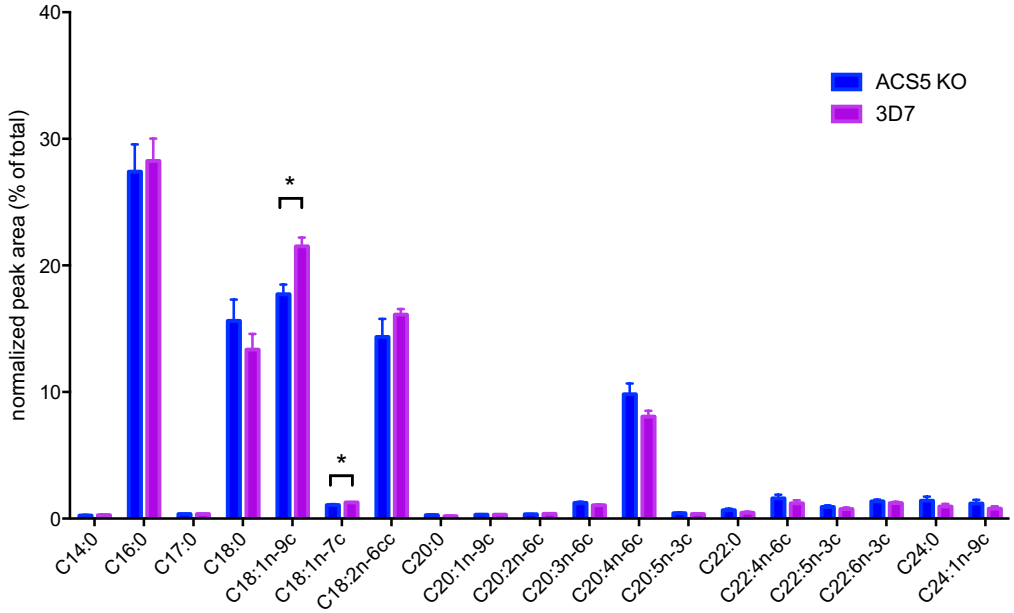

Figure 4.3.6. Fatty acid profile of *P. falciparum*-infected enriched red blood cells. A. FA profiles of enriched parasitized red blood cells of 3D7 or ACS KO lines are compared to uninfected RBC controls. B. FA profile of ACS5 KO line as compared to 3D7 parental strain. Statistical significance determined using unpaired t-test in Prism v6.0 (* = $p < 0.05$).

4.4 Discussion

In this chapter, we continued our study of the ACS gene family, using CRISPR-Cas9 knockouts of individual ACS isoforms to interrogate their function in the cell. Our previous findings had suggested that, based on different localization and expression patterns, the ACSs may be playing different roles in FA metabolism in the cell. Of particular interest was the ACS5 isoform, one of the most highly expressed ACSs, which showed a slightly early pattern of transcript and protein expression, with a greater abundance of protein in the trophozoite stages (30-36hpi) relative to the other ACSs. ACS5 was also shown exported outside the parasite into the host cell RBC to associate with its membrane. The differential expression and localization patterns of the ACSs suggest they may be playing different roles in the cell. In this chapter, we generated and used KO lines of individual ACSs in an attempt to better understand their role in intracellular growth and FA metabolism.

Of the four KO lines we looked at, only ACS5 showed significantly perturbed growth (Figure 4.3.3). ACS8 and ACS12 KO lines grow as well as the 3D7 parental line, with a slight sensitivity to glucose restriction, while ACS9 grows as well or better than the 3D7 parent. The ACS5 KO growth defect was exacerbated by restriction of fatty acids and glucose in our limited growth media (Figure 4.3.4). This growth defect was similar to the one observed previously with the DD knockdown line (Figure 3.3.9). Together with our previous data, this points to an important role for ACS5 in intracellular metabolic processes necessary for *P. falciparum* in vitro growth, and further establishes the connection between fatty acid metabolism and glucose metabolism in the cell.

ACS's activate free FAs, and they have been shown to have specific substrate preferences in other organisms, including *Plasmodium knowlesi* and the related Apicomplexan parasite,

Cryptosporidium parvum (Black et al. 1997; Coleman et al. 2002; Shockey & Browse 2011; Beaumelle & Vial 1988; Guo et al. 2014). These substrate preferences are mediated by the conserved fatty acyl CoA synthetase region of the protein (Black et al. 1997). Though this motif is conserved in the *P. falciparum* ACSs, there are slight amino acid differences that could indicate different substrate specificity (Bethke et al. 2006; Téllez et al. 2003). We hypothesized that ACS FA substrate specificities would affect the ability of the KOs to grow in RPMI1640 media supplemented with specific combinations of FAs. However, as seen in Figure 4.3.5, different combinations of FAs did not result in differential growth for the KOs. This finding suggests that there is some functional redundancy or broad range substrate specificity for the ACS family. Alternatively, it is possible that the loss of specific FA substrates caused by the KO has no measureable impact on overall *in vitro* growth phenotypes measured here, but instead results in other changes to intracellular metabolism.

We next addressed the question of ACS FA substrate specificity using a different approach. To determine if knockout of any particular ACS isoform resulted in a global change of the fatty acid pool in the parasite, we profiled fatty acids with GC-FID. Overall, there were few differences observed in the four knockout lines, relative to 3D7 (Figure 4.3.6). This further supports the argument that the ACSs have some redundant function and overlapping substrate specificity, whereby loss of a specific ACS can be compensated for by another isoform. Such compensation, however, was not reflected in the expression profiles of the ACS transcripts (Figure 4.3.2).

There were some changes observed in the ACS5 knockout, however (Figure 4.3.6B). Loss of ACS5 resulted in slight but significant decreases in unsaturated fatty acids C18:1n-9c (oleic

acid) and C18:2n-6cc (linoleic acid). This suggests that ACS5 is involved in either: 1) uptake and activation of these specific fatty acids; 2) channeling of saturated fatty acids into the parasite's desaturation pathways; or 3) channeling these specific unsaturated fatty acids into lipid biosynthesis pathways. The slight increase in saturated C18:0 observed in the ACS5 knockout provides some support for ACS5 playing a role in supplying the parasite's desaturation pathways. Loss of this activity in the knockout results in decreases in the associated unsaturated species, and a slight build up of the saturated C18:0 species.

We next proposed a metabolomics approach to better understand the role of the PfACS enzymes in mediating fatty acid activation and incorporation into lipid biosynthesis and utilization pathways. We used LC-MS/MS to generate a comprehensive dataset of hydrophobic lipid species and hydrophilic metabolites in the parasite. At this time, however, we have only the results of one biological replicate, comparing the ACS5 KO to its 3D7 parent, at 30-36 hours post invasion (hpi) and 36-42hpi. While the standard deviation (SD) between sample technical replicates was low, additional biological replicates are needed to confirm these findings. Preliminary analysis of metabolites in the ACS5 KO lines revealed differences in both neutral lipid species and phospholipid species, including phosphatidylethanolamine and phosphatidylcholine (Appendix, Figures 7.1.1, 7.1.2, 7.1.3, and Table 7.1.1). Other significant differences were observed in the hydrophilic metabolites, with notable reductions in TCA metabolites in the ACS5 KO, including succinate, α-ketoglutarate, and glutamate (Appendix Figures 7.1.1 and 7.1.4, Table 7.1.2). These significant decreases in TCA metabolites are particularly interesting, and could explain how the ACS5 KO is sensitive to starvation conditions, relative to the 3D7 parent. ACS5 KO-induced deficiencies in TCA function could make these parasites unable to respond to changes in available carbon sources.

Our next steps will be to confirm these LC-MS/MS preliminary findings with two additional biological replicates. We will then explore complementary approaches to validate the findings. Thin layer chromatography (TLC) experiments are currently underway to measure incorporation of ^{14}C palmitate into parasite lipids. Comparing the ACS5 KO to 3D7 with this approach will identify any significant differences in neutral lipids, phospholipids, and free FAs, and validate the LC-MS/MS lipid findings. We are also currently using Seahorse Bioanalyzer to thoroughly assess glycolytic and mitochondrial metabolism of the ACS KO lines, and their utilization of different carbon substrates. This technology will allow us to determine the effects of the TCA deficiencies identified by LC-MS/MS on mitochondrial respiration in the ACS5 KO.

In conclusion, in this chapter we continued our investigation of the ACS family, using KO lines to functionally characterize a subset of these enzymes. The growth defect identified in the ACS5 KO line suggests that this gene may play an important role in *P. falciparum in vitro* growth. The sensitivity of the ACS5 KO to glucose restriction, not FA restriction, suggests that ACS5 plays an important role in *P. falciparum* central carbon metabolism. Our initial metabolic profiling with LC-MS/MS suggests the knockout of ACS5 causes significant perturbations in key metabolic pathways. This work is ongoing, and additional experiments described above will allow us to confirm these findings. Our continued study of the expanded ACS gene family in *P. falciparum* will elucidate their intracellular roles in FA and carbon metabolism, and the functional significance of the expansion and selection of this gene family.

4.5 Materials and Methods

Parasite culture

Parasites were maintained in culture using the methods described by Trager & Jenson (Trager & Jensen 1976). Parasites were grown in RPMI1640 (Gibco) supplemented with 10% O+ serum, unless otherwise stated for specific growth assays. ACS knockout parasites were grown with 2.5ul WR per 10mL media. Minimal glucose / minimal fatty acid media was prepared as follows: RPMI1640 media (Gibco) was mixed with RPMI1640 lacking glucose and L-glutamine (US Biologicals) at 45%, 50%, or 100%. Media was supplemented with 60uM fatty acid free BSA (Sigma) and 30uM each palmitic and oleic acids (Sigma). Parasites were confirmed to be mycoplasma-free using the e-Myco plus PCR kit (Boca Scientific) per manufacturer's instructions.

CRISPR/Cas9 knockout lines

CRISPR/Cas9 knockouts of ACS genes on a 3D7 background were generated by Selina Bopp and Nathan Hicks, following the method described in (Ghorbal et al. 2014) and using plasmids generously provided by Jose-Juan Lopez-Rubio.

Real time PCR

Total RNA was extracted with Qiagen RNeasy mini columns (Qiagen Venlo, Limburg) according to manufacturer instructions, and DNAse-treated. First strand cDNA synthesis was performed using SuperScript III (Life Technologies) following manufacturer instructions. The absence of contaminating DNA and the success of the reverse transcriptase reaction were confirmed by comparing qPCR of Rt+ and Rt- with the control Seryl tRNA synthetase primer set in quadruplicate; samples were run on and ABI 7900 HT. Differences in expression levels were calculated using the ΔΔCt method with tRNA

synthetase as a reference gene as described in the Applied Biosystems User Bulletin. cDNA concentrations were normalized to SerRS Ct values to minimize biases in PCR efficiency. PCR amplification was performed as follows: 15 minutes at 95 °C followed by 40 cycles of two-step amplification of 94 °C for 30 s and 52 °C for 30 s. 2.

ACS1aF	TGGTGGAAGGTTTAATGGAACG	forward
ACS1aR	ACCCAAACGTACATCCTCCA	reverse
ACS1bF	TTGGCTAGTTTCTGATTTGGGA	forward
ACS1bR	ACGTTCCAATATGCCTTCAACC	reverse
ACS2F	GCACGTAGAAATGAATTACCGC	forward
ACS2R	AGGACTCAAACGTATATCCTCCA	reverse
ACS3F	AGCAACTGATACACTGCCAA	forward
ACS3R	CTGAAATTATGGCTAGTGGACCA	reverse
ACS4F	GTGGAAGTAGCACGGGTAGT	forward
ACS4R	CTCCCTGAGTTATGTTCTTCTCT	reverse
ACS5F	CCGCTGATATGGCTTCTATGC	forward
ACS5R	TGAGCTAATAACCCTTCAACCA	reverse
ACS6F	AGGCATGCAATGAAGAAGAATCA	forward
ACS6R	GGCTTCAATACCTTTCCCTCC	reverse
ACS7F	GGTTGAAGGATTGTTGTGTCG	forward
ACS7R	AGGCACACAAACTAATGTCTTCT	reverse
ACS8F	TCGAACATGCTTATGGTGAACC	forward
ACS8R	ACCACTCATCATAGCTGCCA	reverse
ACS9F	TCGTGCATGTTAAGTGGTGT	forward
ACS9R	CTTGCCCTTCATCACCATTTT	reverse
ACS10F	TGACTGAATCTTTGGGTGCT	forward
ACS10R	GGTTGCATGTACTTGGTCCTC	reverse
ACS11F	AAAGGTGTTATGATTACGCACAA	forward
ACS11R	GAAGGTTGGTTTCAGTTCATTCA	reverse
ACS12F	ACTTTTCAGCTATCCCAACCA	forward
ACS12R	TGAGCTAACTTGATGACAGGC	reverse

Table 4.5.1. Real time PCR primers used to measure transcript expression of PfACS genes.

FACS with SYBR Green

Parasites were stained in 10x SYBR green I in 1x PBS for 30 min in the dark at 37C. The staining solution was removed and cells were resuspended in 5 times the volume of the initial volume of PBS. FACS data acquisition was performed on a MACSQuant VYB (Milteni Biotec) with a 488nm laser and a 525nm filter and analyzed with FlowJo 2. RBCs were gated on the forward light scatter (FSC) and side scatter (SSC) and infected RBCs were detected in channel B1. At least 100,000 events were analyzed per sample.

[^{3}H]-hypoxanthine incorporation assays

This assay was conducted following the method of Desjardins (Desjardins et al. 1979). Fatty acid combinations for growth assays were chosen based on the work of Asahi and Mi-Ichi (Asahi et al. 2005; Mi-Ichi et al. 2006). Growth assays were performed in 3-4 biological replicates, with 3-6 technical replicates per assay. [^{3}H]-incorporation was measured on a TopCount NXT microplate scintillation and luminescence counter (Packard Bioscience). Parasite growth curves were generated in Prism (version 6.0) using non-linear regression and the curve fitting equation, log(inhibitor) vs response – variable slope, four parameters.

GC-FID

Parasite-infected RBCs were enriched by Vario MACS magnet purification with25CS or 25LD columns (Miltenyi Biotec). Cell counts were determined by hemocytometer, and 10^8 cells/sample were submitted for GC-FID. Sample extraction, chromatography, and data analysis was performed by Matthew Lopes and Jeremy Furtado in the Nutrition Department GC-FID core facility (Harvard T.H. Chan School of Public Health, Boston, MA). Briefly, total lipids are extracted from erythrocyte into isopropanol and hexane containing 50 mg 2.6-di-tert-butyl-p-cresol as an antioxidant (Lillington et al. 1981). Fatty acids are transmethylated

with methanol and sulfuric acid as described by Zock et al. (Zock et al. 1996; Zock et al. 1997). After esterification, samples are evaporated, and the fatty acid methyl esters are redissolved in iso-octane. Fatty acids are separated using a Hewlett-Packard Model (now Agilent) GC 6890 FID gas chromatograph with 7673 Autosampler injector (Palo Alto, CA), splitless injection port at 240°C, and a constant flow hydrogen carrier gas at 1.3 ml/min. 1 μl of sample is injected into a fused silica capillary cis/trans column SP2560, 100 meters X 250 μm internal diameters X .20 μm film (Supelco, Belefonte, PA), and run through a temperature program of 90 to 170°C at 10°C/min, 170°C for 5 minutes, 170 to 175°C at 5°C/min, 175 to 185°C at 2°C/min, 185 to 190°C at 1°C/min, 190 to 210 at 5°C/min, 210 °C for 5 minutes, 210 to 250°C at 5°C/min, 250°C for 10 minutes. Peak retention times are identified by injecting known standards with purity ranges above 99 percent (NuCheck Prep, Elysium, MN), using Agilent Technologies ChemStation A.08.03 software for analysis. A total of 45 fatty acids can be identified with this methodology.

4.6 References

Asahi, H. et al., 2005. Investigating serum factors promoting erythrocytic growth of Plasmodium falciparum. *Experimental Parasitology*.

Beaumelle, B.D. & Vial, H.J., 1988. Acyl-CoA synthetase activity in Plasmodium knowlesi-infected erythrocytes displays peculiar substrate specificities. *Biochimica et Biophysica Acta*, 958, pp.1–9.

Bethke, L.L. et al., 2006. Duplication, gene conversion, and genetic diversity in the species-specific acyl-CoA synthetase gene family of Plasmodium falciparum. *Molecular and Biochemical Parasitology*.

Black, P.N. et al., 1997. Mutational analysis of a fatty acyl-coenzyme A synthetase signature motif identifies seven amino acid residues that modulate fatty acid substrate specificity. *The Journal of Biological Chemistry*, 272(8), pp.4896–4903.

Coleman, R. et al., 2002. Do Long-Chain Acyl-CoA Synthetases Regulate Fatty Acid Entry into Synthetic Versus Degradative Pathways? *The Journal of Nutrition*, 132, pp.2123–2126.

Desjardins, R. et al., 1979. Quantitative assessment of antimalarial activity in vitro by a semiautomated microdilution technique. *Antimicrobial Agents and Chemotherapy*, 16(6).

Ghorbal, M. et al., 2014. Genome editing in the human malaria parasite Plasmodium falciparum using the CRISPR-Cas9 system. *Nature biotechnology*, 32(8), pp.819–821.

Guo, F. et al., 2014. Amelioration of cryptosporidium parvum infection in vitro and in vivo by targeting parasite fatty acyl-coenzyme a synthetases. *Journal of Infectious Diseases*, 209(8), pp.1279–1287.

Holz, G.G., 1977. Lipids and the malarial parasite. *Bulletin of the World Health Organization*, 55(2-3), pp.237–248.

Lillington, J.M., Trafford, D.J.H. & Makin, H.L.J., 1981. A rapid and simple method for the esterification of fatty acids and steroid carboxylic acids prior to gas-liquid chromatography. *Clinica Chimica Acta*, 111(1), pp.91–98.

Mi-Ichi, F., Kita, K. & Mitamura, T., 2006. Intraerythrocytic Plasmodium falciparum utilize a broad range of serum-derived fatty acids with limited modification for their growth. *Parasitology*, 133, pp.399–410.

Shears, M.J., Botté, C.Y. & McFadden, G.I., 2015. Fatty acid metabolism in the Plasmodium apicoplast: Drugs, doubts and knockouts. *Molecular and Biochemical Parasitology*, 199(1-2), pp.34–50. Available at: http://dx.doi.org/10.1016/j.molbiopara.2015.03.004.

Shockey, J. & Browse, J., 2011. Genome-level and biochemical diversity of the acyl-activating enzyme superfamily in plants. *The Plant Journal*, 66, pp.143–160.

Téllez, M.D.M., Matesanz, F. & Alcina, A., 2003. The C-terminal domain of the Plasmodium falciparum acyl-CoA synthetases PfACS1 and PfACS3 functions as ligand for ankyrin. *Molecular and Biochemical Parasitology*, 129(2), pp.191–198.

Trager, W. & Jensen, J.B., 1976. Human Malaria Parasites in Continuous Culture. *Science*, 193(4254), pp.673–675.

Zock, P.L. et al., 1997. Fatty acids in serum cholesteryl esters as quantitative biomarkers of dietary intake in humans. *American journal of epidemiology*, 145(12), pp.1114–1122.

Zock, P.L., Gerritsen, J. & Katan, M.B., 1996. Partial conservation of the sn-2 position of

dietary triglycerides in fasting plasma lipids in humans. *European journal of clinical investigation*, 26(2), pp.141–150.

Chapter 5:

Fatty acids in *P. falciparum* growth and metabolism.

5.1 Attribution

AUTHORS:

Allison Demas[1], Erik Allman[2], Selina Bopp[1], Sarah K. Volkman[1,3,4], Manuel Llinás[2], Dyann F. Wirth[1,4]

[1] Harvard T.H. Chan School of Public Health, Boston, MA, USA.

[2] Pennsylvania State University, University Park, PA, USA.

[3]Simmons College, Boston, MA USA

[4]Broad Institute, Cambridge, MA, USA.

AUTHOR CONTRIBUTIONS:

A.D. performed all [^{3}H]-hypoxanthine growth assays. A.D. performed [^{3}H]-palmitate fatty acid oxidation assays and Seahorse experiments. A.D. prepared parasite metabolite extracts for metabolite profiling by GC-FID and LC-MS/MS. E.A. completed metabolite extractions and ran LC-MS/MS. E.A. performed analysis of LC-MS/MS data, with input from A.D.

5.2 Introduction

Plasmodium falciparum has highly specialized minimalist metabolic pathways, which allow it to navigate different host environments. Increased understanding of the biochemical and metabolic pathways that enable parasite survival in the host cell is needed to discover potential metabolic chokepoints and opportunities for chemotherapeutic intervention.

During the asexual stages the parasite meets most of its energy demands via glycolysis, whereby glucose is broken down to lactate to generate ATP (MacRae et al. 2013; Jensen et al. 1983). A functional Tricarboxylic Acid (TCA) cycle is also active during the asexual stages, fueled primarily by glutamine and, to a lesser extent, glucose (MacRae et al. 2013). The TCA cycle is not essential for asexual stage growth *in vitro* (Ke et al. 2015), though it may offer the parasite metabolic flexibility in meeting its energy demands throughout the lifecycle (Cobbold et al. 2013). Mitochondrial energy metabolism appears to be more important during the sexual stages, where glucose drives TCA activity essential for parasite development (MacRae et al. 2013; Ke et al. 2015). In addition to being developmentally regulated (Cobbold et al. 2013) there is some evidence that these pathways are responsive to nutrient availability (Botté et al. 2013; Ke et al. 2015). Given the excess of sugars, amino acids, and lipids in standard *in vitro* culture conditions (LeRoux et al. 2009) it seems likely that some of the dynamic capabilities of parasite metabolism, both in terms of flux and substrate utilization, could be masked *in vitro*.

In addition to glucose-derived acetyl CoA, other eukaryotes catabolize amino acids or FAs to provide carbon chains for the TCA cycle (Watkins 1997). While the parasite shows no evidence of amino acid catabolism as a source of carbon for the TCA cycle (Gardner et al. 2002; Seeber et al. 2008; Polonais & Soldati-Favre 2010), the possibility of a fatty acid

catabolism pathway remains an intriguing possibility. In other eukaryotes, fatty acids feed into oxidation pathways to generate acetyl CoA that drives the TCA cycle. These pathways are especially active in low glucose environments or cells with high ATP demands (Watkins 1997).

Use of fatty acids as an alternate source of acetyl CoA has not yet been demonstrated experimentally in the parasite. The canonical FA oxidation (FAO) pathway is not strongly conserved in *P. falciparum*. Only two of the five canonical FAO enzymes are annotated, though the pathway is believed to be present in the related Apicomplexan, *Toxoplasma gondii* (Gardner et al. 2002; Possenti et al. 2013). We used bioinformatics approaches to identify candidate genes encoding enzymes of the putative FAO pathway in *P. falciparum* (Table 5.2.1).

FA Oxidation Enzyme	**Gene ID**	**PlasmoDB annotation**
Carnitine acyl transferase	not found	not found
Acyl CoA dehydrogenase	PF3D7_1135900	3-oxo-5-alpha-steroid 4-dehydrogenase, putative
Enoyl CoA hydratase	PF3D7_1017200	enoyl coA hydratase-related protein, putative
Enoyl CoA hydratase	PF3D7_1425200	enoyl coA hydratase, putative
3-Hydroxy acyl CoA dehydrogenase	PF3D7_0422000	steroid dehydrogenase, putative
Acetyl CoA acyltransferase	PF3D7_1450900	acetyl-CoA acetyltransferase, putative

Table 5.2.1. Putative FA Oxidation enzymes as identified by BLAST and PlasmoDB annotation.

In this chapter, we sought to increase our understanding of parasite nutrient requirements for growth, and the metabolic changes that occur under starvation conditions. To answer these questions and characterize parasite response to starvation, we used biochemical

approaches, including LC-MS/MS metabolomics, radiolabeled FA incorporation methods, and Seahorse Bioanalyzer technology. Our interrogation of parasite metabolic pathways supports the hypothesis that a functional FAO pathway exists in the parasite, and we present multiple lines of evidence for FAO in *P. falciparum*. To our knowledge, this is the first reported experimental evidence for this pathway in Plasmodium, or other Apicomplexans.

5.3 Results

Parasite growth in different lipid and carbon sources. Our previous results indicated that ACS5 KO lines were more sensitive to glucose and glutamine depletion in the context of limited FAs (Figure 4.3.4). This led us to hypothesize that there is a link between glucose and FA metabolism. To determine the effects of limited nutrients on parasite survival, we first sought to understand the baseline FA profile of 3D7 lab strain parasites, and the effects of different lipid and carbon sources on parasite growth.

During the asexual stages, *P. falciparum* scavenges diverse species of FAs from the host serum to support its growth (Mi-Ichi et al. 2006). *P. falciparum* uses these exogenous FAs in de novo lipid biosynthesis pathways, while also scavenging from human serum and modifying host RBC lipid species (Holz 1977; Vial et al. 2003; Vial & Ben Mamoun 2005). To determine the diversity and relative abundance of FA species present in our 3D7 lab strain, we used gas chromatography with a flame ionization detector (GC-FID). This gas chromatography method is highly sensitive for hydrophobic molecules and allows us to detect specific known FA acid species in our cells. Enriched infected RBCs were normalized by cell count and profiled for relative abundance of 45 standard FA species. The FA profiles

of enriched 3D7 parasite-infected RBCs and uninfected RBCs (uRBCs) were similar (Figure 5.3.1). There were, however, notable differences in the relative quantities of certain fatty acids. While infected and uninfected cells had similar abundance of saturated C18:0, there were significant increases in C16:0, C18:1 n-9c, and C18:2 n-6c in the parasite. In contrast, there were higher concentrations of long chain saturated and unsaturated FAs in the uninfected RBC.

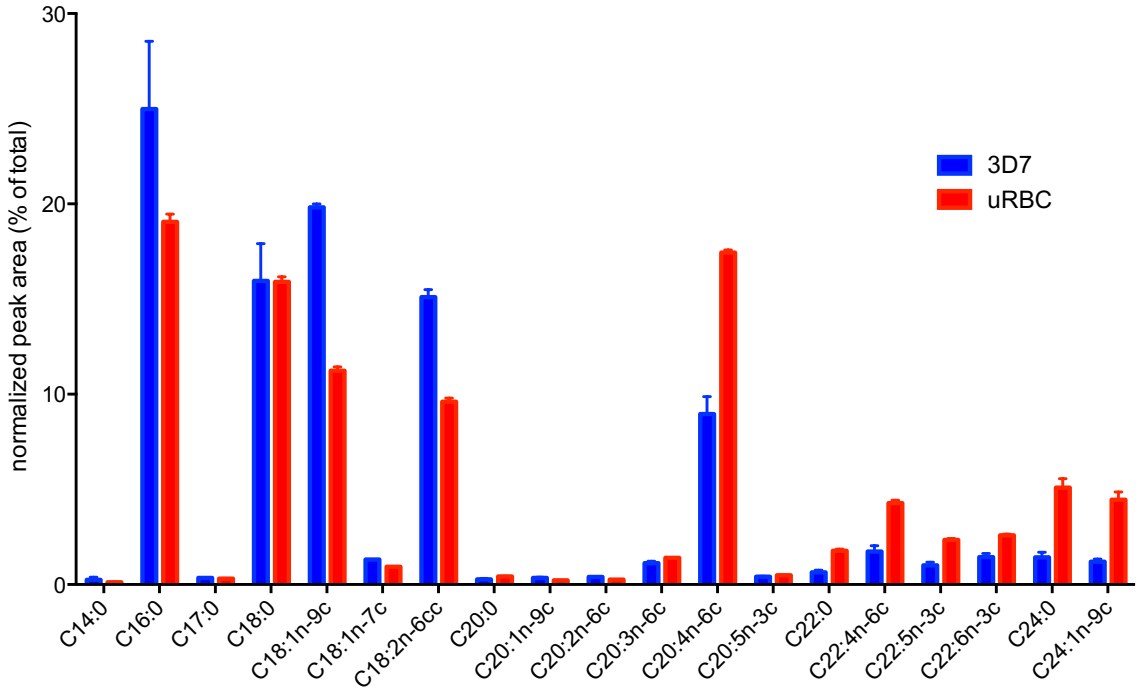

Figure 5.3.1. GC-FID detection of fatty acids in 3D7 lab strain, compared to uninfected RBC control.

In vitro growth conditions contain an excess of glucose, amino acids, and lipids that do not reflect baseline nutrient concentrations found in human blood (LeRoux et al. 2009). As standard *in vitro* growth conditions are not physiological, we sought to limit both available sugar sources, as well as FAs. Work from others had established palmitic acid (C16:0) and oleic acid (C18:1) as the most important FAs for sustaining parasite growth (Mi-Ichi et al.

2006; Asahi et al. 2005). Using [^{3}H]-hypoxanthine incorporation assays to assess parasite growth in serum-free RPMI supplemented with different combinations of FAs, we were able to replicate this finding and demonstrate that other combinations of saturated and unsaturated FAs could also support parasite growth (Figure 5.3.2). In contrast to previous findings (Asahi et al. 2005), we found that C18:1 alone was sufficient for sustaining parasite growth (Figure 5.3.2B). FA supplementation was required for parasite growth, as demonstrated by the lack of growth in the BSAF condition, which contained only FA-free bovine serum albumin (BSA) and lacked all other FAs or serum components.

To further restrict parasite growth media, we titrated the C16:0 and C18:1 paired FAs to establish the minimal FA substrate required to support parasite growth (Figure 5.3.3A). 50% inhibition of parasite growth was achieved at approximately 6.8μM each of C16:0 and C18:1. In the context of these minimal FAs (C16:0 and C18:1, each at 30μM), we further titrated down glucose to establish a similar "IC50" (Figure 5.3.3B). The 50% inhibition of parasite growth was achieved at approximately 40% of normal glucose levels (or an average of 4.4mM; normal glucose in culture medium is 11mM).

A.

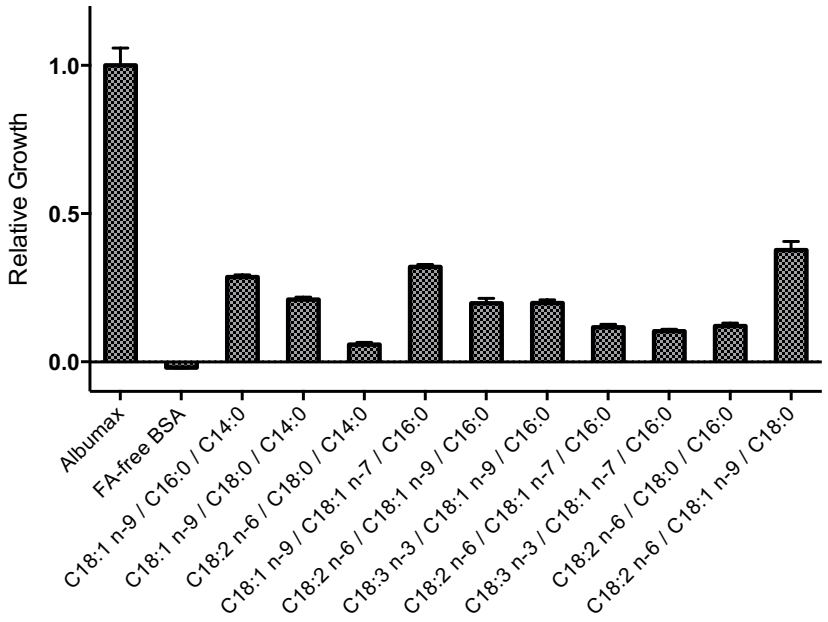

B.

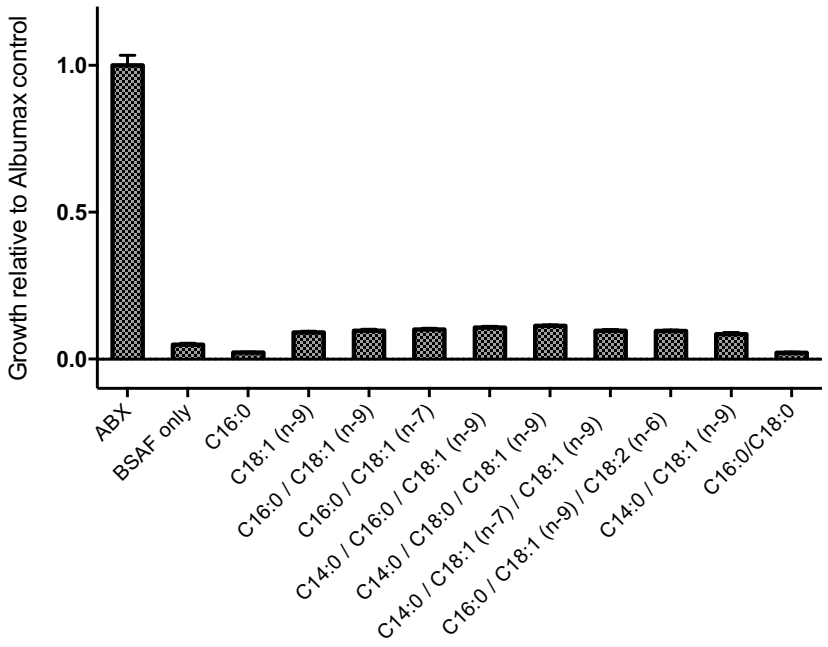

Figure 5.3.2. Two cycle (A) and one cycle (B) [^{3}H]-hypoxanthine incorporation assays in RPMI supplemented with BSAF and different combinations of saturated and unsaturated FAs. Growth for different conditions is expressed relative to parasite growth in albumax ("ABX").

A. B.

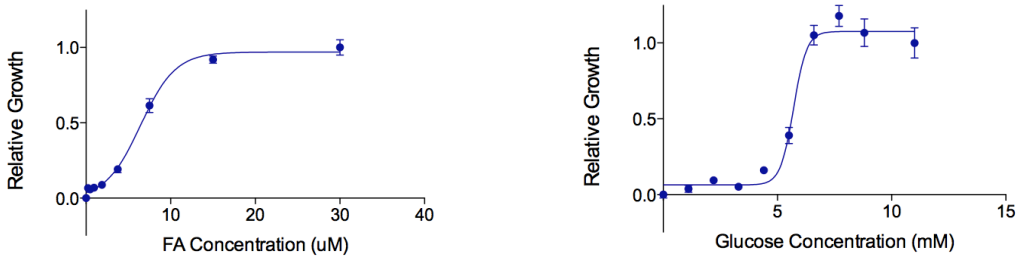

Figure 5.3.3. Defining minimal growth media *in vitro*. A. 3D7 parasites were grown in serial dilutions of C16 and C18:1 "minimal fatty acids" with standard concentration of glucose. 50% inhibition of parasite growth was achieved at approximately 6.8μM each of C16:0 and C18:1. B. 3D7 parasites grown 30uM minimal fatty acids and serial dilution of glucose, in the absence of glutamine. 50% inhibition of parasite growth was achieved at approximately 4.4mM glucose.

Metabolic profile of starved parasites using LC-MS/MS.

To determine the effects of this starvation on the *P. falciparum* metabolome, we generated a comprehensive LC-MS/MS data set comparing parasites grown under normal *in vitro* growth conditions (RPMI1640 supplemented with albumax or minimal FAs) to those grown under starvation conditions (limited glucose and glutamine, and minimal FAs). We extracted both hydrophilic and hydrophobic metabolites from MACS-enriched parasite samples. Targeted metabolite profiling was performed using a standards library (~300 metabolites) for three biological replicates, each with 2-3 technical replicates. In the starvation condition, there were significant reductions in the metabolites of the glycolytic and pentose phosphate pathways (Table 5.3.1 and Figure 5.3.4). These differences were confirmed with partial least-squares discriminant analysis (Appendix Figure 7.2.1 and 7.2.2).

	Peaks(mz/rt)	p.value	-log10(p)	FDR
1	3-phosphoglycerate	0.0001838	3.7357	0.011084
2	Pyroglutamic acid	0.00019277	3.715	0.011084
3	glutamate	0.00048836	3.3113	0.016293
4	ADP-D-glucose	0.0005667	3.2466	0.016293
5	dGDP	0.00084935	3.0709	0.019535
6	glutamine	0.0012354	2.9082	0.023678
7	Sedoheptoluse bisphosphate	0.0016669	2.7781	0.027384
8	UDP-N-acetyl-glucosamine	0.0021311	2.6714	0.030634
9	6-phospho-D-gluconate	0.0024225	2.6157	0.03082
10	acetyl-aspartate	0.00268	2.5719	0.03082
11	D-gluconate	0.0030642	2.5137	0.032035
12	D-glyceraldehdye-3-phosphate	0.0033618	2.4734	0.032218
13	tyrosine	0.003736	2.4276	0.032744
14	D-glucono-lactone-6-phosphate	0.0040698	2.3904	0.032744
15	phosphoenolpyruvate	0.004271	2.3695	0.032744
16	ADP	0.0047294	2.3252	0.033799
17	3-phospho-serine	0.005224	2.282	0.033799
18	alanine	0.0052903	2.2765	0.033799
19	2-dehydro-D-gluconate	0.0056784	2.2458	0.034369
20	histidine	0.0064754	2.1887	0.037234
21	sn-glycerol-3-phosphate	0.0073955	2.131	0.040499
22	quinolinate	0.007857	2.1047	0.041071
23	Inositol	0.0092509	2.0338	0.046255

Table 5.3.1. List of metabolites that differed between parasites in starvation versus normal growth conditions (n=3, $p<0.01$).

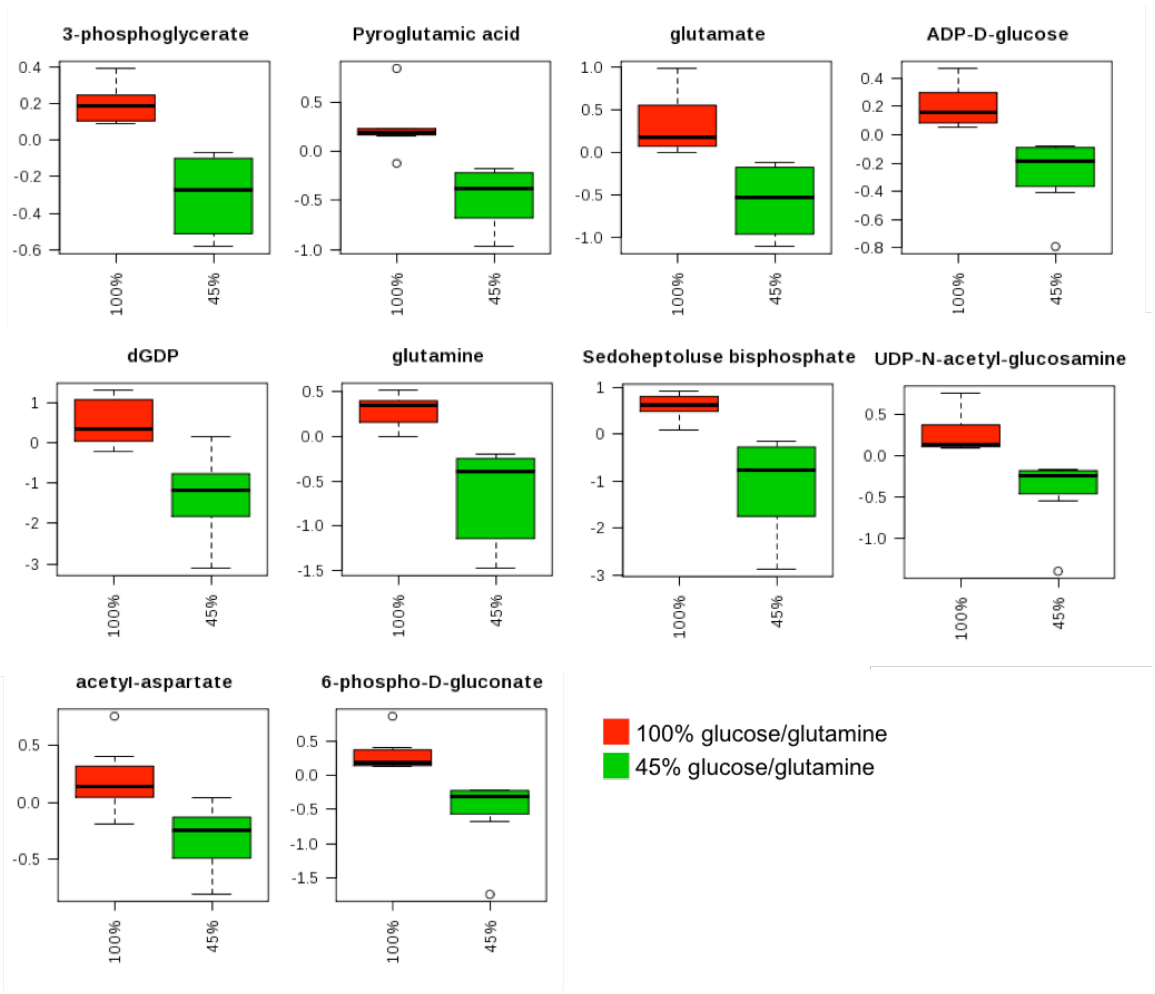

Figure 5.3.4. Top ten metabolites that differ between 45% and 100% glucose/glutamine conditions.

Analysis of metabolites by pathway shows significant decreases across glycolytic, pentose phosphate, and TCA metabolism (Figure 5.3.5). Interestingly, the parasite maintained similar levels of fumarate under starvation conditions (Figure 5.3.5B). Given that parasites continue to progress through the intra-erythrocytic developmental cycle and actively replicate under starvation conditions, we hypothesized they might become reliant on alternative carbon sources for energy.

A.

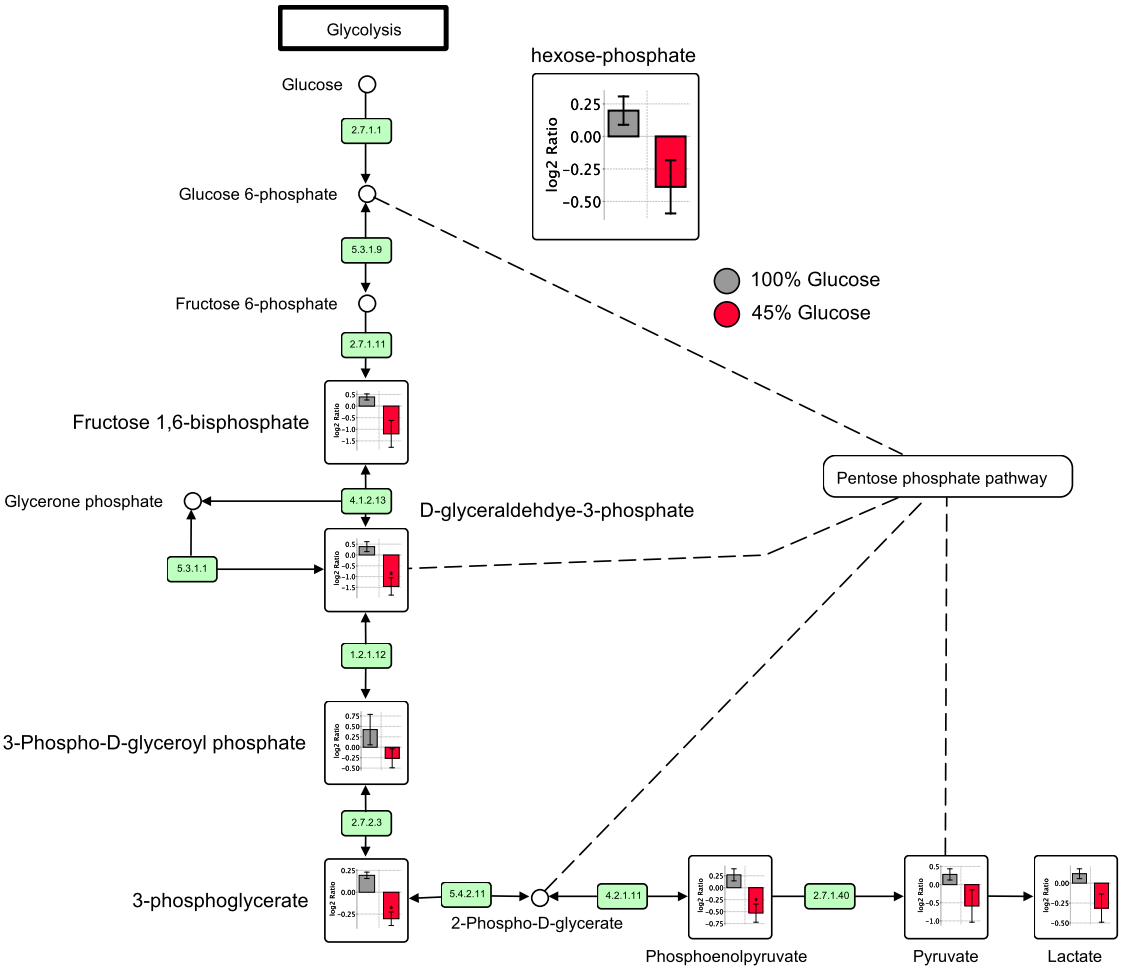

Figure 5.3.5. Pathway analysis by Metaboanalyst highlights differences in (A) glycolytic and pentose phosphate pathway intermediates and (B) TCA cycle intermediates.

B.

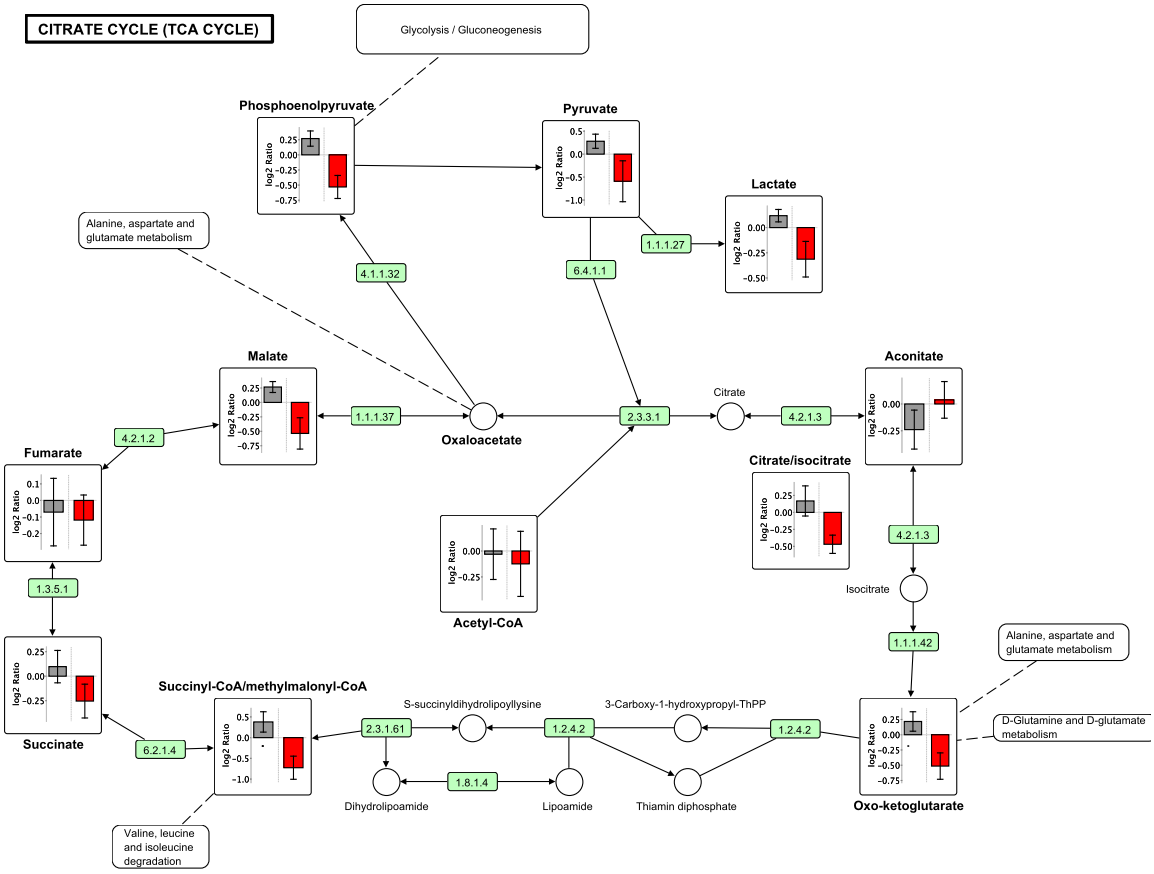

Figure 5.3.5 (continued). Pathway analysis by Metaboanalyst highlights differences in (A) glycolytic and pentose phosphate pathway intermediates and (B) TCA cycle intermediates.

^{3}H palmitate assays for measuring parasite fatty acid oxidation. Given the evidence of a connection between FA and glucose metabolism (Figure 4.3.4) and evidence of significant reductions in metabolic pathways in starved parasites, we decided to directly test if FAO was possible as an alternate energy source in the parasite. We adapted and optimized a mammalian protocol for measuring FAO using a ^{3}H-labeled palmitate substrate (Moon & Rhead 1987). Given a labeled FA substrate, FAO activity is measure through release of $^{3}H_20$

into the culture media. An increase in $^{3}H_20$ would indicate increased FAO activity. Using this method, we were successfully able to measure FAO in both 3D7 and Dd2 parasites starved for glucose (Figure 5.3.6A and D). Activity was 10-20 fold higher in 45% glucose starved 3D7 parasites, relative to uRBC controls. Interestingly, parasites in full and half glucose ("100% G mFA" and "50% G mFA") still showed increased FAO relative to uRBCs, though not as much as the fully starved parasites. To confirm the activity was specific to the parasite, and not a function of the host RBC, we used Saponin to lyse the host cell and isolate the parasites. Saponin-lysed free parasites also exhibited FAO activity (Figure 5.3.6B). Starved parasites were able to oxidize a desaturated [^{3}H]-oleic acid substrate as well, though less $^{3}H_20$ was produced relative to the [^{3}H]-palmitic acid substrate (Figure 5.3.6C).

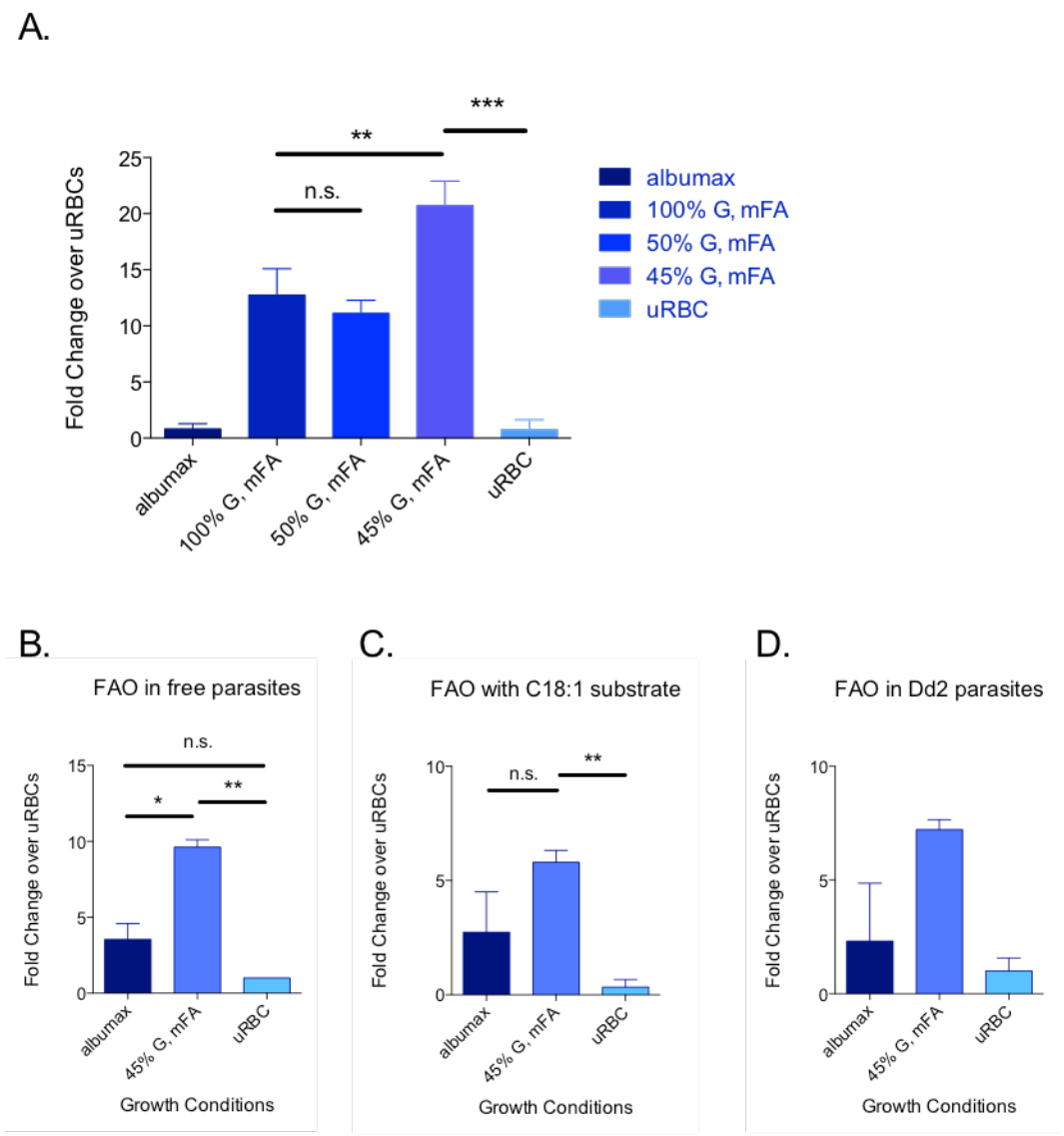

Figure 5.3.6. ^{3}H palmitate assay demonstrates FAO in 3D7 parasites. Parasites were grown in RPMI supplemented with albumax, 45% glucose supplemented with minimal FAs ("45% G, mFA"), 50% glucose supplemented with minimal FAs ("50%G mFA"), or 100% glucose supplemented with minimal FAs ("100%G mFA"). Activity measured in parasite samples was compared uninfected RBCs ("uRBC"). (A) FAO activity in glucose-deprived 3D7 parasites. (B) FAO activity in saponin-treated free parasites. (C) FAO activity with ^{3}H C18:1 substrate. (D) FAO activity in Dd2 parasites with ^{3}H palmitate substrate.

Seahorse Flux Bioanalyzer confirms FAO activity in *P. falciparum*. Seahorse Bioanalyzer uses fluorescent sensors to measure changes in pH (extracellular acidification) or oxygen consumption of cells. Each cell plate has four injection ports to allow timed injection of specific substrates or compounds while the machine measures real time metabolic flux. We optimized Seahorse Bioanalyzer protocols for measuring FA oxidation in *P. falciparum* to validate the fatty acid oxidation phenotype and better understand parasite FA metabolism as it occurs in real time. In the absence of any glucose or glutamine in the system, the measured oxygen consumption rate (OCR) in response to a FA substrate is indicative of FAO activity (Seahorse Biosciences). Initial results show an increase in oxygen consumption OCR in parasites in response to a palmitate substrate (Figure 5.37). Parasites given minimal FAs from time 0 show elevated baseline oxygen consumption, in comparison to lack of OCR in BSA-treated control parasites.

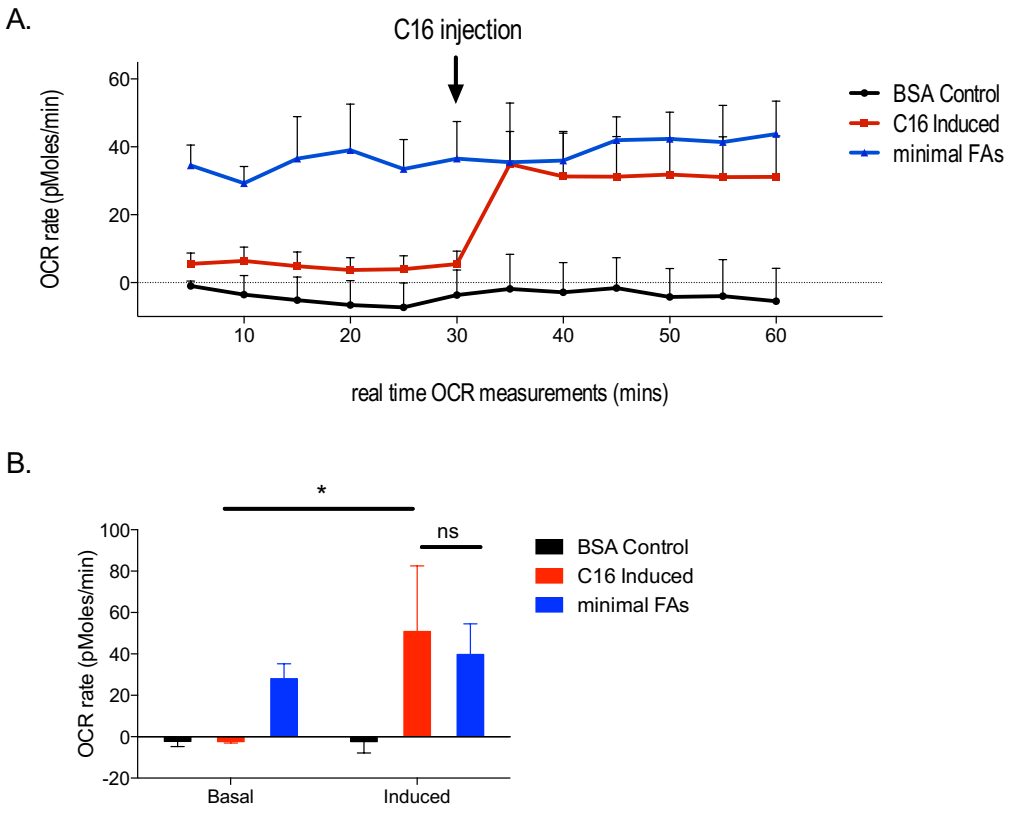

Figure 5.3.7. Oxygen consumption is increased in parasites in response to FA substrate. (A) Real time measurements of OCR in starved 3D7 parasites in response to FAs. (B) Injection of C16 significantly induces mitochondrial respiration in starved 3D7 parasites (red bar). Basal respiration was calculated as an average of the two initial OCR readings (5-10 mins). Induced OCR was calculated as an average of two readings immediately following injection of substrate (35-40 mins).

5.4 Discussion

Previous studies have made great progress towards understanding *P. falciparum* energy metabolism *in vitro* (Olszewski & Llinas 2011; MacRae et al. 2013; Oppenheim et al. 2014; Cobbold et al. 2013; Ke et al. 2015). Careful mapping of metabolic enzymes and substrate preferences has raised the hypothesis that, in addition to metabolic changes during their lifecycle, parasites may undergo more immediate metabolic switches in response to

available nutrients. Here we have presented evidence that *P. falciparum* can respond to starvation conditions by using available FAs as a carbon source.

We first set out to further define the *in vitro* growth conditions of *P. falciparum*, including the FA profile, and minimum FA and glucose growth requirements of our 3D7 lab strain. In general, the FA profile of 3D7-infected RBCs resembled that of uninfected RBCs (Figure 5.3.1). We found significant increases in C16:0, C18:1 n-9c, and C18:2 n-6c in the parasite. In contrast, there were higher concentrations of long chain saturated and unsaturated FAs in the uninfected RBC. These findings are similar to the published FA profile of *P. falciparum*-infected RBCs (Cobbold et al. 2013). Having established the baseline FA profile using GC-FID, we restricted both diversity and concentration of FAs available to the parasite (Figure 5.3.2), as well as glucose (Figure 5.3.3) to establish the absolute minimal requirements for *P. falciparum* growth *in vitro*. We then used parasites grown in these minimal conditions to assess parasite metabolism under the stress of restricted nutrients.

We generated a comprehensive data set of metabolic profiles of starved parasites (limited glucose/glutamine and restricted FAs). In general, overall metabolism is reduced in starvation conditions. The glycolytic and pentose phosphate pathways in particular show significant reductions in metabolites (Table 5.3.1). Of note, fumarate levels remained unchanged, suggesting this metabolite is essential or independently regulated (Figure 5.3.5B). This finding is intriguing, given that previous efforts to genetically disrupt fumarate dehydrogenase and malate quinone oxidoreductase were unsuccessful (Ke et al. 2015). While previous studies have shown that the TCA cycle is not essential for asexual growth (MacRae et al. 2013), our findings suggest that some metabolic intermediates (fumarate and malate) may be necessary for maintaining asexual growth.

The previously observed sensitivity of ACS5 knockout lines to glucose depletion led us to suspect a link between glucose and FA metabolism (Figure 4.3.4). Following up on this initial observation, we were able to show evidence of FA oxidation in *P. falciparum* 3D7 strain using two different methodologies (Figures 5.3.6 and 5.3.7). *Plasmodium* parasites are not predicted to oxidize FA species as an alternate carbon source, so these findings are paradigm-shifting (Oppenheim et al. 2014; Ralph et al. 2004; Olszewski & Llinas 2011; Gardner et al. 2002). Our results indicate that this is a parasite-specific phenomenon, not reliant on host RBC enzymes (Figure 5.3.6). Both 3D7 and Dd2 lab strains were able to oxidize either ^{3}H palmitic or ^{3}H oleic acid, further supporting the activity of a FA oxidation pathway, rather than the activity of desaturase enzymes, for example. Relatively less $^{3}H_2O$ was produced from the ^{3}H oleic acid substrate, however, suggesting that palmitic acid may be the preferred substrate for this pathway.

Given our evidence of a FAO pathway, the significant reductions in major carbon metabolism pathways could be indicative of a metabolic switch, whereby reductions in available glucose and glutamine prompt the parasite to burn other substrates for energy, such as FAs. Previous studies have shown that parasites "switch" or alter their metabolic states or substrate preferences in response to limited nutrient conditions *in vitro* (Botté et al. 2013; Ke et al. 2015) or their developmental cycle (Cobbold et al. 2013). Some studies have identified transcriptional changes in TCA-associated *P. falciparum* genes in response to glucose deprivation *in vitro* (Fang et al. 2004); and a 2007 study of *ex vivo P. falciparum* gene expression characterized three metabolically distinct transcriptional profiles (Daily et al. 2007). Of particular interest, the authors described two contrasting metabolic profiles: 1) an actively glycolytic state, and 2) a starvation profile, characterized by increased

mitochondrial function, FA metabolism, and glycerol metabolism. They suggest these two profiles could represent a transcriptional switch, where parasites alter their metabolism in response to host conditions and nutrient availability.

Metabolic flexibility, such as the ability to modify glycolytic or mitochondrial energy flux or substrate utilization would be particularly advantageous for navigating the unique and dynamic host environments the parasite encounters during its complex lifecycle. For example, during the later stages of parasite asexual development, mature forms sequester in the microvasculature (Miller et al. 2002; Chen et al. 2000). This sequestration phenomenon is believed to cause localized depletion of glucose, resulting in a hypoglycemic microenvironment for the developing parasite (Planche & Krishna 2006). Additionally, severe malaria disease in humans is associated with hypoglycemia, where fasting blood glucose levels can drop as low as 2.75mM (Taylor et al. 1988; Planche & Krishna 2006; White et al. 1983; White et al. 1987). Anopheles hemolymph is known to have much lower glucose than human serum, perhaps explaining the metabolic differences between asexual and sexual parasite stages (MacRae et al. 2013; LeRoux et al. 2009). Together, these observations argue that metabolic flexibility in general, and use of alternate carbon sources such as FAs, in particular, could be necessary for parasite survival in the dynamic environment of multiple hosts.

The next logical hypothesis to test was the incorporation of FAO acetyl CoA end product into TCA metabolic intermediates. We labeled our 45% glucose/glutamine starved 3D7 parasites with ^{13}C-palmitate for the full duration of starvation (2.5 cycles) or a shorter 2 or 4 hour "pulse" immediately before extraction. Unfortunately, we were unable to detect any FAO intermediates, and thus could not determine any labeling into these metabolites. We

next looked downstream to the TCA metabolites, where we would expect to see ^{13}C labeling if the acetyl CoA generated from FAO of ^{13}C-palmitate fed into the TCA cycle. Efforts to detect ^{13}C labeling here were unsuccessful. Given the results of these experiments, our evidence suggests that while palmitate can be oxidized via a FAO pathway, the resulting acetyl CoA does not feed into the TCA cycle. There are alternate methods we can use to further explore oxidation of palmitate, such as $^{14}CO_2$ trapping from a ^{14}C palmitate substrate (Huynh et al. 2014). We are planning to explore this additional method to confirm that oxidized palmitate is not used to supply the TCA cycle in *Plasmodium*.

Our next steps will be to confirm the enzymes responsible for this metabolic activity. While only two of the five canonical FAO enzymes are annotated in the *P. falciparum* genome, further analysis of functional domains suggests that the other members of the pathway may be present as well (Table 5.2.1). Interestingly, no putative carnitine acyl transferase was identified in our search. This enzyme is the first step in FAO, and facilitates transfer of FAs across the mitochondrial membrane (Kerner & Hoppel 2000). However, metabolic profiling with LC-MS/MS identified palmitoyl acyl-carnitine species, the product of this enzymatic reaction, suggesting that the parasite can indeed generate or acquire these necessary metabolites (unpublished observations, A.D., E.A., and J.D.H). Going forward, we are interested in confirming these other putative enzymes. We are currently cloning CRISPR-Cas9 knockout constructs for the first two enzymes in the FAO pathway.

The disconnect between our FAO observation and the lack of continuity into the TCA cycle raises a number of interesting questions as to the purpose of the FAO pathway in *Plasmodium*. In other organisms, non-mitochondrial non-ATP-generating FAO pathways are localized in the peroxisome (Schrader et al. 2016). The primary purpose of these pathways

is to break down long chain FAs into shorter chain FA substrates. A similar phenomenon could be occurring in our *P. falciparum* parasites. Ongoing functional analysis of the enzymes involved in the observed FAO activity will increase our understanding of these metabolic pathways.

5.5 Materials and Methods

Parasite culture conditions: starvation conditions

Lab isolate 3D7 was maintained in culture by the methods of Trager and Jensen (Trager & Jensen 1976). Parasites were synchronized using 5% Sorbitol (Moll et al. 2008). Synchronized parasites were put on minimal glucose and fatty acids as 6-12hpi rings, and maintained in these conditions for either 24 or 120hours (0.5 or 2.5 cycles, respectively). Minimal glucose / minimal fatty acid media was prepared as follows: RPMI1640 media (Gibco) was mixed with RPMI1640 lacking glucose and L-glutamine (US Biologicals) at 45%, 50%, or 100%. Media was supplemented with 60uM fatty acid free BSA (Sigma) and 30uM each palmitic (C16:0) and oleic acids (C18:1) (Sigma). Free parasites were obtained by RBC lysis from 0.01% saponin in PBS solution. Parasites were confirmed to be mycoplasma-free using the e-Myco plus PCR kit (Boca Scientific) per manufacturer's instructions.

GC-FID

Parasite-infected RBCs were enriched by Vario MACS magnet purification with25CS or 25LD columns (Miltenyi Biotec). Cell counts were determined by hemocytometer, and 10^8 cells/sample were submitted for GC-FID. Sample extraction, chromatography, and data analysis was performed by Matthew Lopes and Jeremy Furtado in the Nutrition Department GC-FID core facility (Harvard T.H. Chan School of Public Health, Boston, MA). Briefly, total

lipids are extracted from erythrocyte into isopropanol and hexane containing 50 mg 2.6-di-tert-butyl-p-cresol as an antioxidant (Lillington et al. 1981). Fatty acids are transmethylated with methanol and sulfuric acid as described by Zock et al. (Zock et al. 1996; Zock et al. 1997). After esterification, samples are evaporated, and the fatty acid methyl esters are redissolved in iso-octane. Fatty acids are separated using a Hewlett-Packard Model (now Agilent) GC 6890 FID gas chromatograph with 7673 Autosampler injector (Palo Alto, CA), splitless injection port at 240°C, and a constant flow hydrogen carrier gas at 1.3 ml/min. 1 μl of sample is injected into a fused silica capillary cis/trans column SP2560, 100 meters X 250 μm internal diameters X .20 μm film (Supelco, Belefonte, PA), and run through a temperature program of 90 to 170°C at 10°C/min, 170°C for 5 minutes, 170 to 175°C at 5°C/min, 175 to 185°C at 2°C/min, 185 to 190°C at 1°C/min, 190 to 210 at 5°C/min, 210 °C for 5 minutes, 210 to 250°C at 5°C/min, 250°C for 10 minutes. Peak retention times are identified by injecting known standards with purity ranges above 99 percent (NuCheck Prep, Elysium, MN), using Agilent Technologies ChemStation A.08.03 software for analysis. A total of 45 fatty acids can be identified with this methodology.

[^{3}H]-hypoxanthine incorporation assay

This assay was conducted following the method of Desjardins (Desjardins et al. 1979). Fatty acid combinations for growth assays were chosen based on the work of Asahi and Mi-Ichi (Asahi et al. 2005; Mi-Ichi et al. 2006). [^{3}H] incorporation was measured on a TopCount NXT microplate scintillation and luminescence counter (Packard Bioscience). Parasite growth curves were generated in Prism (version 6.0) using non-linear regression and the curve fitting equation, log(inhibitor) vs response – variable slope, four parameters.

LC-MS/MS sample preparation and extraction

Methods adapted from Simon Cobbold and Ian Lewis (Cobbold et al. 2013). Parasite-infected RBCs were enriched by Vario MACS magnet purification with25CS or 25LD columns (Miltenyi Biotec). Parasites were counted by hemocytometer, and approximately 10^7-10^8 cells were used per sample. Cell pellets were washed 3x in cold PBS before extractions. Hydrophilic metabolites were extracted by the addition of 1mL 90% HPLC grade methanol (90 methanol:10 water, containing 5uM +5 Aspartate internal standard), followed by immediate vortex. Samples were spun down (3500g for 2m), and the supernatant transferred to a new tube. Extraction was repeated, and a final clarifying spin (10m at 13000rpm) removes any cell debris. Combined supernatants were dried down under N_2 gas and stored at -80°C. Hydrophobic extractions were performed by the addition of 50:50 HPLC grade methanol:water (containing 0.05M HCl and 5uM +5 Aspartate internal standard) followed by the addition of 0.5mL chloroform. The samples are vortexed, then spun down (13000rpm for 2m). The chloroform layer was transferred to a glass vial and chloroform extraction is repeated. Combined chloroform extractions are dried down under N_2 gas and stored at -80°C.

LC-MS/MS analytical methods

Hydrophilic samples

Samples were resuspended in HPLC grade water to a concentration of $1x10^5$-$1x10^6$ cells per microliter. A pooled QC sample was generated for each run to identify instrument drift, samples were randomized, and 10uL was injected for analysis. Positive ion LCMS was performed through the Penn State metabolomics core facility. Chromatographic separation (225uL/min flow rate) was achieved using a Prominence 20 UFLCXR system with a Waters BEH C18 column (1.7 uM, 100 x 2mm) maintained at 55 C. Solvent A is water with 0.1%

formic acid and solvent B is acetonitrile with 0.1% formic acid. The gradients are – 0 min = 3%B, 10 min = 45%, 12 min = 75%B, 18-21 min = 3% B with data acquisition stopping at 20 minutes. The eluate was delivered into a 5600 (QTOF) TripleTOF using a Duospray™ ion source. A scan range of m/z = 50-1250 was used for the study of small molecule metabolites. The mass spectrometer was operated in IDA (Information Dependent Acquisition) mode with a 100 ms survey scan from 50-1250 m/z, and up to 10 MS/MS product ion scans (100 ms) per duty cycle using a collision energy of 50V with a 20V spread.

Hydrophobic samples

Samples were resuspended in a 1/1/0.3 chloroform/methanol/water solution to 6.3 x 10^4 cells/uL. A pooled QC sample was generated for each run to identify instrument drift, samples were randomized, and 10uL was injected for analysis. Negative ion LCMS was performed using the method described in (Kamphorst et al. 2011; Cobbold et al. 2013). Chromatographic separation was achieved using a Phenomenex Luna C8 RP column (3 uM x 100A, 150 x 2 mm) with the negative ion solvents described above. The gradient was linear – 0-20 min = 80-99% B, 20-40 min = 99% B, 40-41 min = 99%-80% B , and 41-50 min = 80%B. The eluate was delivered into a Thermo Exactive Plus Orbitrap using a ESI-ion source. The scan range was adjusted to m/z = 125-400 from 0-20 min and m/z 300-575 from 20-50 min for the study of both short and long chain fatty acids. Other parameters include 140,000 resolving power at m/z 200, ACG = $3x10^6$, and a maximum injection time of 100 mS.

LC-MS/MS analysis

Thermo Fisher .raw files were converted to .mzXML and analyzed as described in (Lu et al. 2010; Kamphorst et al. 2011). Metabolite identification was confirmed using an in-house generated knowns list, consisting of m/z and RT for pure standard compounds (292 total)

run on the same analytical platform. Stable isotope labeled compounds were extracted using the RT for the unlabeled standard using the isotope extraction function of the open-source program "Metabolomics Analysis and Vizualization Engine". Isotope enrichment was determined by comparing the observed M+1/M and M+2/M ratios to the calculated theoretical $M = (1\text{-}0.011)^N$, $M+1 = N(0.011)(1\text{-}0.011)^{N-1}$, and $M+2 = (N(N\text{-}1)/2)(0.011^2)(1\text{-}0.011)^{N-2}$ metabolites fractions, where N is the number of carbons and 1.1% is the natural abundance of ^{13}C. Extracted ion chromatogram (EIC) peak areas were exported as .csv files for further data processing (background subtraction and normalization), visualization, and statistical analysis.

^{3}H fatty acid oxidation assay with palmitic acid and oleic acid

Fatty acid oxidation was measured by conversion of ^{3}H-palmitic or ^{3}H-oleic acid (Perkin Elmer) to $^3H_20$, using a method adapted from Moon and Rhead (Moon & Rhead 1987). Briefly, parasites were starved in 45%, 50%, or 100% glucose and minimal fatty acid conditions for 2.5 cycles. For intact parasitized RBC assays, parasites were purified by Vario MACS magnet purification with25CS or 25LD columns (Miltenyi Biotec) as 30-36hpi trophs. For free parasite assays, parasites were saponin lysed (0.01% saponin in PBS) as 36-42hpi schizonts. Following 45 minutes of equilibration in fatty acid free, minimal glucose loading media (40% glucose RPMI, 1% BSAF, 50uM Carnitine), parasites were incubated with ^{3}H fatty acid label for 18 hours (intact RBCs) or 2 hours (free parasites). Media supernatants were harvested and fatty acids were extracted per protocol and read on a Beckman LS 6500 multi purpose scintillation counter (Beckman Coulter). All data points were normalized to a ^{3}H labeled blank to account for hydrolysis of labeled fatty acid during the assay.

Seahorse bioanalyzer fatty acid oxidation assay

Seahorse protocol for *P. falciparum* parasites was adapted with permission from Tomoyo Kato (unpublished). Parasites were starved for 24hours or 2.5 cycles prior to assay. 36-42hour trophs were lysed with 0.01% saponin and washed 3x with PBS. Cell counts were determined by hemocytometer, and cells were plates at 10 million cells per well. Cell plate wells were coated with Cell Tak (Corning) at a concentration of 5.9µg/well. Fatty acid oxidation assay was conducted following manufacturer's protocol, with some modification. KHB media (111mM NaCl, 4.7mM KCl, 2mM $MgSO_4$, 1.2mM Na_2HPO_4, 2.5mM Glucose; pH 7.4) was supplemented with 50uM L-Carnitine (Sigma). Baseline fatty acid oxidation was established by supplementing KHB assay medium with 200uM palmitic and oleic acid (Sigma), 200uM BSA-palmitate conjugate (Seahorse Biosciences), or 200uM BSA control (Seahorse Biosciences).

5.6 References

Asahi, H. et al., 2005. Investigating serum factors promoting erythrocytic growth of Plasmodium falciparum. *Experimental Parasitology*.

Botté, C.Y. et al., 2013. Atypical lipid composition in the purified relict plastid (apicoplast) of malaria parasites. *PNAS*, 110(18), pp.7506–7511.

Chen, Q., Schlichtherle, M. & Wahlgren, M., 2000. Molecular aspects severe malaria. *Clinical Microbiology Reviews*, 13(3), pp.439–450.

Cobbold, S.A. et al., 2013. Kinetic Flux Profiling Elucidates Two Independent Acetyl-CoA Biosynthetic Pathways in Plasmodium falciparum. *Journal of Biological Chemistry*, 288(51), pp.36338–36350.

Daily, J.P. et al., 2007. Distinct physiological states of Plasmodium falciparum in malaria-infected patients. *Nature*, 450(7172), pp.1091–1095.

Desjardins, R. et al., 1979. Quantitative assessment of antimalarial activity in vitro by a semiautomated microdilution technique. *Antimicrobial Agents and Chemotherapy*, 16(6).

Fang, J. et al., 2004. Ambient glucose concentration and gene expression in Plasmodium falciparum. *Molecular and Biochemical Parasitology*, 133(1), pp.125–129.

Gardner, M.J. et al., 2002. Genome sequence of the human malaria parasite Plasmodium falciparum. *Nature*, 419.

Holz, G.G., 1977. Lipids and the malarial parasite. *Bulletin of the World Health Organization*, 55(2-3), pp.237–248.

Huynh, F.K. et al., 2014. Measurement of fatty acid oxidation rates in animal tissues and cell lines. *Methods in Enzymology*, 542, pp.391–405.

Jensen, M., Conley, M. & Helstowski, L., 1983. Culture of Plasmodium falciparum: the role of pH, glucose, and lactate. *Journal of Parasitology*, 69(3), pp.1060–7.

Kamphorst, J.J. et al., 2011. Liquid Chromatography-High Resolution Mass Spectrometry Analysis of Fatty Acid Metabolism. *Analytical Chemistry*, 83.

Ke, H. et al., 2015. Genetic Investigation of Tricarboxylic Acid Metabolism during the Plasmodium falciparum Life Cycle. *Cell Reports*, 11(1), pp.164–174.

Kerner, J. & Hoppel, C., 2000. Fatty acid import into mitochondria. *Biochimica et Biophysica Acta - Molecular and Cell Biology of Lipids*, 1486(1), pp.1–17.

LeRoux, M., Lakshmanan, V. & Daily, J.P., 2009. Plasmodium falciparum biology: analysis of in vitro versus in vivo growth conditions. *Trends in Parasitology*, 25(10), pp.474–481.

Lu, W. et al., 2010. Metabolomic analysis via reversed-phase ion-pairing liquid chromatography coupled to a stand alone orbitrap mass spectrometer. *Analytical Chemistry*, 82(8), pp.3212–3221.

MacRae, J.I. et al., 2013. Mitochondrial metabolism of sexual and asexual blood stages of the malaria parasite Plasmodium falciparum. *BMC Biology*, 11(67).

Mi-Ichi, F., Kita, K. & Mitamura, T., 2006. Intraerythrocytic Plasmodium falciparum utilize a broad range of serum-derived fatty acids with limited modification for their growth. *Parasitology*, 133, pp.399–410.

Miller, L.H. et al., 2002. The pathogenic basis of malaria. *Nature*, 415.

Moll, K. et al., 2008. *Methods In Malaria Research 5th edition*,

Moon, A. & Rhead, W.J., 1987. Complementation analysis of fatty acid oxidation disorders. *The Journal of Clinical Investigation*, 79(1), pp.59–64.

Olszewski, K.L. & Llinas, M., 2011. Central carbon metabolism of Plasmodium parasites. *Molecular and Biochemical Parasitology*, 175, pp.95–103.

Oppenheim, R.D. et al., 2014. BCKDH: The Missing Link in Apicomplexan Mitochondrial Metabolism Is Required for Full Virulence of Toxoplasma gondii and Plasmodium berghei. *PLoS Pathogens*, 10(7).

Planche, T. & Krishna, S., 2006. Severe malaria: metabolic complications. *Current Molecular Medicine*, 6(2), pp.141–153.

Polonais, V. & Soldati-Favre, D., 2010. Versatility in the acquisition of energy and carbon sources by the Apicomplexa. *Biology of the cell*, 102(8), pp.435–445.

Possenti, A. et al., 2013. Global proteomic analysis of the oocyst/sporozoite of Toxoplasma gondii reveals commitment to a host-independent lifestyle. *BMC genomics*, 14(1), p.183.

Ralph, S.A. et al., 2004. Tropical infectious diseases: metabolic maps and functions of the Plasmodium falciparum apicoplast. *Nature Reviews Microbiology*, 2(3), pp.203–216.

Schrader, M. et al., 2016. Metabolic Interplay between Peroxisomes and Other Subcellular Organelles Including Mitochondria and the Endoplasmic Reticulum. *Frontiers in Cell and Developmental Biology*, 3.

Seeber, F., Limenitakis, J. & Soldati-Favre, D., 2008. Apicomplexan mitochondrial metabolism: a story of gains, losses and retentions. *Trends in Parasitology*, 24(10), pp.468–478.

Taylor, T.E. et al., 1988. Blood glucose levels in Malawian children before and during the administration of intravenous quinine for severe falciparum malaria. *New England Journal of Medicine*, 319(16), pp.1040–1047.

Trager, W. & Jensen, J.B., 1976. Human Malaria Parasites in Continuous Culture. *Science*, 193(4254), pp.673–675.

Vial, H.J. et al., 2003. Phospholipids in parasitic protozoa. *Molecular and Biochemical Parasitology*, 126, pp.143–154.

Vial, H.J. & Ben Mamoun, C., 2005. Plasmodium lipids: metabolism and function. In I. W. Sherman, ed. *Molecular Approaches to Malaria*. ASM Press, pp. 327–352.

Watkins, P.A., 1997. Fatty acid activation. *Progress in Lipid Research*.

White, N.J. et al., 1987. Hypoglycemia in African children with severe malaria. *The Lancet*, 329(8535), pp.708–711.

White, N.J. et al., 1983. Severe hypoglycemia and hyperinsulinemia in falciparum malaria. *New England Journal of Medicine*, 309(2), pp.61–66.

Chapter 6: Conclusions and Future Directions

Despite recent advances in malaria control, the ambitious goal of eradication remains elusive in many endemic regions of the world (World Health Organization 2015). The recent emergence and spread of artemisinin resistance in Southeast Asia threatens these gains (Noedl et al. 2008; Dondorp & Ringwald 2013). *P. falciparum* malaria parasite research is of increased importance to support public health policy decisions and identify potential new drug targets to continue the fight against this pathogen.

In this dissertation, I presented findings from two distinct projects, linked by a common theme of selective pressures acting on *P. falciparum* malaria parasites. Artemisinin drug pressure applied *in vitro* selects for resistant parasites, and characterization of these mutants lines allows us to make predictions about the natural evolution of resistance observed in the clinical setting in Southeast Asia. In contrast, the ACS gene family was previously found to be under selection in *P. falciparum*, suggesting that particular alleles may confer a selective advantage to the parasite. Using molecular genetic and biochemical approaches, we sought to better understand the role of these proteins in parasite metabolism, and the functional significance of their expansion and selection.

In Chapter 2, I described the findings of a four-year *in vitro* drug resistance selection experiment. Through intermittent and stepwise selection methods, we have generated three artemisinin resistant lines on a Senegalese parasite background. These lines are significantly resistant by the standard measure of *in vitro* artemisinin resistance, the $^{0\text{-}3h}$RSA (Witkowski et al. 2013). Whole genome sequencing of the resistant lines revealed thirteen

non-synonymous mutations in ten genes. Polymorphisms in one candidate gene, Pf coronin, a kelch13-like gene, were found in all three selected lines.

Importantly, none of our three selected lines have mutations in the previously reported kelch13 locus (Ariey et al. 2014). SNPs in kelch13 are associated with both clinical and *in vitro* artemisinin resistance (Ariey et al. 2014). The first reports of this resistance marker were followed up in the laboratory, where introduction of mutant kelch13 into an isogenic NF54 background was sufficient to confer artemisinin resistance (Ghorbal et al. 2014). Subsequent surveillance efforts identified 46 non-synonymous mutations in kelch13 in natural parasite populations in Southeast Asia and Africa (Roberto Amato, Olivo Miotto, Charles Woodrow, Jacob Almagro-Garcia, Ipsita Sinha, Susana Campino, Daniel Mead, Eleanor Drury, Mihir Kekre, Mandy Sanders, Alfred Amambua-Ngwa, Chanaki Amaratunga, Lucas Amenga-Etego, Tim JC Anderson, Voahangy Andrianaranjak 2015). However, it is clear that this underlying genetic diversity is not associated with resistance in all cases. Furthermore, recent reports have described artemisinin sensitive parasites with mutant kelch13 as well as artemisinin resistance parasites with wildtype kelch13 alelles (Ashley et al. 2014; Mukherjee et al, unpublished). Taken together, these findings suggest that while mutations in kelch13 are clearly associated with artemisinin resistance and are sufficient to confer resistance in an *in vitro* setting, this is not the whole story.

Thorough investigation of the contribution of individual kelch13 mutations from Straimer and colleagues demonstrated that individual mutations confer different levels of resistance, and one single mutation can confer different levels of resistance on different background parasite strains (Straimer et al. 2015). These important observations suggest that parasite background is very important for determining artemisinin resistance. There are likely

additional as yet unidentified parasite factors that modulate or otherwise contribute to acquisition of resistance.

Interestingly, while SNPs in the Pfcoronin locus were identified in all three selected lines, the SNPs identified in the P19.04-A line appeared earlier in the course of selection (the 10th step), and then disappeared in subsequent stages. This suggests that there may be a fitness disadvantage to this particular mutation, and other compensatory mutations may be necessary to support parasite growth. In future work, we plan to conduct additional WGS of earlier selection steps to thoroughly investigate the sequential acquisition of resistance-associated mutations.

The candidate SNPs identified in our *in vitro* selection experiment are an important contribution to our understanding of artemisinin resistance. In future work, we will leverage available whole genome sequence and phenotype data from Southeast Asian parasite isolates to look for associations between SNPs in our candidate genes and resistance phenotypes. We are also planning to validate the contribution of our individual candidate SNPs to artemisinin resistance by generating allelic replacement parasites in the lab. We predict that we will be able to restore artemisinin sensitivity to our selected lines by swapping in wildtype alleles in place of the mutations we identified. The reverse experiment, replacing wildtype alleles with resistance-associated mutants in an isogenic background, would be expected to confer resistance. These experiments will validate our candidate SNPs, and the allelic replacement transgenic parasites will be an important tool for further investigation of artemisinin resistance mechanism.

Identifying the important genetic markers and their gene products is the first step to understanding the mechanisms of artemisinin resistance in *P. falciparum*. Several groups have proposed different mechanisms of resistance (Dogovski et al. 2015; Ariey et al. 2014; Mbengue et al. 2015; Mok et al. 2015). The common theme of oxidative stress and the unfolded protein response emerges from these studies, though further work is needed to fully understand the intracellular pathways involved. Characterization of our candidate SNPs will add to this growing literature and further elucidate the mechanism of artemisinin resistance.

In Chapter 3 and subsequent chapters, I turn to the story of the *P. falciparum* ACSs, and present the findings from our efforts to understand the functional significance of the expansion and selection of this metabolic gene family. Our initial findings in Chapter 2 suggest distinct roles for the ACSs in *P. falciparum* FA metabolism. We characterized the transcript and protein expression of individual ACSs throughout the lifecycle, as well as the localization of HA-tagged ACSs within the infected RBC. We identified differential localization and expression patterns for members of this expanded gene family. Notably, ACS5 was found to be expressed slightly earlier in the intra-erythrocytic developmental cycle, and was exported outside the parasite to associate with the host RBC membrane. Using the FKBP-DD inducible knockdown system, we identified a slight growth defect in the ACS5 knockdown when grown in limited glucose growth media. These findings suggest that ACS5 plays an important role in supporting *P. falciparum* growth *in vitro*, and that ACS5 may play a role in central carbon metabolism in the cell.

In Chapter 4, we continued our investigation of the expanded ACS gene family, using CRISPR-Cas9 knockouts of individual ACSs for clear phenotypes on an isogenic background.

In this chapter, we confirmed the ACS5 growth defect identified in Chapter 3, though none of the other ACS KOs we tested had a growth defect. We used GC-FID to profile the FA content of the KO parasite lines, and identified significant reductions in mono- and poly-unsaturated FAs in the ACS5 KO. These findings are interesting, and suggest that ACS5 might play a role in desaturation pathways, or uptake and activation of these specific FAs.

Given the phenotypes observed with the ACS5 KO, we are currently conducting a thorough characterization of its metabolome using LC-MS/MS. With this approach, we have identified some significant differences between the ACS5 KO and its 3D7 parent, including some significant differences in TCA metabolites that may explain the glucose sensitivity growth phenotype of this line. At this time, these experiments have only been performed once, and additional biological replicates are needed to confirm the findings.

Increased understanding of the metabolic pathways perturbed by the ACS knockouts will shed light on the function of the individual ACS isoforms. Together with our growth data and descriptive characterization of different ACSs, we aim to fully understand the role of these individual enzymes in *P. falciparum* metabolism.

In the fifth and final chapter, I took a step back to build on some of our previous observations of FA metabolism in the parasite and understand how these pathways function under starvation conditions in the cell. Throughout its complex lifecycle, *P. falciparum* navigates two very different host environments (human and mosquito) and must rely on scavenging available nutrients to meet its metabolic needs. Even within the human host, the parasite encounters dramatic changes in available nutrients, depending on host cell type (hepatocyte vs RBC) or tissue localization (liver or microvasculature) (LeRoux

et al. 2009). Metabolic flexibility, including adaptive changes in substrate preference and flux, would be key to dealing with these changing environments.

In this chapter, we characterized the FA profile of our 3D7 reference strain. We then defined minimal FA and glucose conditions, and measured the growth of the parasite under these restrictions. Using LC-MS/MS, we profiled hydrophilic metabolites of the starved parasites, and found significant decreases in metabolites of the glycolysis and pentose phosphate pathways. Our previous finding that ACS5 KOs are sensitive to glucose restriction led us to the hypothesis that, as in many eukaryotes, FAs are connected to central carbon metabolism in *P. falciparum*. Using two different methodologies, we were able to demonstrate a functional FAO pathway in the parasite. Interestingly, the end products of FAO do not appear to feed into the TCA cycle, as incubation with ^{13}C-palmitate did not result in detectable labeling of TCA intermediates. This finding suggests that *P. falciparum* uses FAO for another purpose, perhaps to break down long chain FAs as seen in the peroxisomes of other eukaryotes (Schrader et al. 2016).

In our next steps, we plan to follow up on these findings using additional approaches to confirm FAO, and using CRISPR-Cas9 genetic disruption techniques to perturb the pathway. We plan to adapt $^{14}CO_2$ trapping methods to measure FAO in *P. falciparum*. Such methods will confirm the finding that FAO in the parasite is disconnected from the TCA cycle. Additionally, we will knock out putative enzymes of the FAO pathway in *P. falciparum.* We expect these knockouts to disrupt the measured FAO activity, confirming their putative biochemical function in this pathway.

The findings presented here, as well as our proposed future work, provide additional evidence for metabolic flexibility in *P. falciparum* parasites. We characterized the metabolome of starved parasites, showing significant reductions in glycolytic pathways, the primary energy source for asexual intra-erythrocytic stages (Jensen et al. 1983). We conclusively demonstrate the activity of a FAO pathway in the parasite, despite previous reports that this pathway was non-existent in *P. falciparum*. Finally, we were unable to establish a connection between the observed FAO activity and the TCA cycle. Future experiments will continue to explore the role of this pathway in parasite metabolism.

In conclusion, selection is an important phenomenon in biological organisms. In this dissertation, we explored selection in two ways. In the first example, we used artificial selection to explore the genetic determinants of *in vitro* artemisinin resistance. Second, we investigated members of the ACS gene family known to be under recent positive selection in the parasite, to determine their functional role in promoting parasite growth. These results extend our fundamental knowledge of *P. falciparum* parasite biology and metabolism, as well as the consequences of interventions (such as drug treatment) on parasite survival.

References

Ariey, F. et al., 2014. A molecular marker of artemisinin-resistant Plasmodium falciparum malaria. *Nature*, 505.

Ashley, E.A. et al., 2014. Spread of Artemisinin Resistance in Plasmodium falciparum Malaria. *New England Journal of Medicine*, 371(5), pp.411–423.

Dogovski, C. et al., 2015. Targeting the Cell Stress Response of Plasmodium falciparum to Overcome Artemisinin Resistance. *PLoS Biology*, 13(4), pp.1–26.

Dondorp, A.M. & Ringwald, P., 2013. Artemisinin resistance is a clear and present danger. *Trends in Parasitology*, 29(8), pp.359–360.

Ghorbal, M. et al., 2014. Genome editing in the human malaria parasite Plasmodium falciparum using the CRISPR-Cas9 system. *Nature biotechnology*, 32(8), pp.819–821.

Jensen, M., Conley, M. & Helstowski, L., 1983. Culture of Plasmodium falciparum: the role of pH, glucose, and lactate. *Journal of Parasitology*, 69(3), pp.1060–7.

LeRoux, M., Lakshmanan, V. & Daily, J.P., 2009. Plasmodium falciparum biology: analysis of in vitro versus in vivo growth conditions. *Trends in Parasitology*, 25(10), pp.474–481.

Mbengue, A. et al., 2015. A molecular mechanism of artemisinin resistance in Plasmodium falciparum malaria. *Nature*, 520(7549), pp.683–687.

Mok, S. et al., 2015. Population transcriptomics of human malaria parasites reveals the mechanism of artemisinin resistance. *Science*, 347, pp.431–435.

Noedl, H. et al., 2008. Evidence of Artemisinin-resistant malaria in Western Cambodia. *New England Journal of Medicine*, 359(24), pp.2619–2620.

Roberto Amato, Olivo Miotto, Charles Woodrow, Jacob Almagro-Garcia, Ipsita Sinha, Susana Campino, Daniel Mead, Eleanor Drury, Mihir Kekre, Mandy Sanders, Alfred Amambua-Ngwa, Chanaki Amaratunga, Lucas Amenga-Etego, Tim JC Anderson, Voahangy Andrianaranjak, M., 2015. Genomic epidemiology of the current wave of artemisinin

resistant malaria. *bioRxiv*.

Schrader, M. et al., 2016. Metabolic Interplay between Peroxisomes and Other Subcellular Organelles Including Mitochondria and the Endoplasmic Reticulum. *Frontiers in Cell and Developmental Biology*, 3.

Straimer, J. et al., 2015. K13-propeller mutations confer artemisinin resistance in Plasmodium falciparum clinical isolates. *Science*, 347(6220).

Witkowski, B. et al., 2013. Novel phenotypic assays for the detection of artemisinin-resistant Plasmodium falciparum malaria in Cambodia: In-vitro and ex-vivo drug-response studies. *The Lancet Infectious Diseases*, 13(12), pp.1043–1049.

World Health Organization, 2015. *World Malaria Report 2015*,

Ariey, F. et al., 2014. A molecular marker of artemisinin-resistant Plasmodium falciparum malaria. *Nature*, 505.

Ashley, E.A. et al., 2014. Spread of Artemisinin Resistance in Plasmodium falciparum Malaria. *New England Journal of Medicine*, 371(5), pp.411–423.

Dogovski, C. et al., 2015. Targeting the Cell Stress Response of Plasmodium falciparum to Overcome Artemisinin Resistance. *PLoS Biology*, 13(4), pp.1–26.

Dondorp, A.M. & Ringwald, P., 2013. Artemisinin resistance is a clear and present danger. *Trends in Parasitology*, 29(8), pp.359–360.

Ghorbal, M. et al., 2014. Genome editing in the human malaria parasite Plasmodium falciparum using the CRISPR-Cas9 system. *Nature biotechnology*, 32(8), pp.819–821.

Jensen, M., Conley, M. & Helstowski, L., 1983. Culture of Plasmodium falciparum: the role of pH, glucose, and lactate. *Journal of Parasitology*, 69(3), pp.1060–7.

LeRoux, M., Lakshmanan, V. & Daily, J.P., 2009. Plasmodium falciparum biology: analysis of in vitro versus in vivo growth conditions. *Trends in Parasitology*, 25(10), pp.474–481.

Mbengue, A. et al., 2015. A molecular mechanism of artemisinin resistance in Plasmodium

falciparum malaria. *Nature*, 520(7549), pp.683–687.

Mok, S. et al., 2015. Population transcriptomics of human malaria parasites reveals the mechanism of artemisinin resistance. *Science*, 347, pp.431–435.

Noedl, H. et al., 2008. Evidence of Artemisinin-resistant malaria in Western Cambodia. *New England Journal of Medicine*, 359(24), pp.2619–2620.

Roberto Amato, Olivo Miotto, Charles Woodrow, Jacob Almagro-Garcia, Ipsita Sinha, Susana Campino, Daniel Mead, Eleanor Drury, Mihir Kekre, Mandy Sanders, Alfred Amambua-Ngwa, Chanaki Amaratunga, Lucas Amenga-Etego, Tim JC Anderson, Voahangy Andrianaranjak, M., 2015. Genomic epidemiology of the current wave of artemisinin resistant malaria. *bioRxiv*.

Schrader, M. et al., 2016. Metabolic Interplay between Peroxisomes and Other Subcellular Organelles Including Mitochondria and the Endoplasmic Reticulum. *Frontiers in Cell and Developmental Biology*, 3.

Straimer, J. et al., 2015. K13-propeller mutations confer artemisinin resistance in Plasmodium falciparum clinical isolates. *Science*, 347(6220).

Witkowski, B. et al., 2013. Novel phenotypic assays for the detection of artemisinin-resistant Plasmodium falciparum malaria in Cambodia: In-vitro and ex-vivo drug-response studies. *The Lancet Infectious Diseases*, 13(12), pp.1043–1049.

World Health Organization, 2015. *World Malaria Report 2015*,

Chapter 7: Appendix

7.1 Supplemental material for Chapter 4

LC-MS/MS analysis of metabolites in ACS5 knockout and 3D7 parent. Given the growth defect and differences observed with GC-FID, we used LC-MS/MS to profile the metabolites of the ACS5 KO to further understand the mechanism behind its growth phenotype. Our GC profile of FAs revealed an altered FA pool in the ACS5 KO. Such changes could impact the neutral lipid and phospholipid content of the cell. Hydrophilic and hydrophobic metabolite extracts were prepared from enriched parasitized RBCs of the ACS5 KO and the 3D7 parental strain at 30-36 hours post invasion and 36-42 hours post invasion. These samples were subjected to LC-MS/MS. It is important to note that this dataset was obtained from 1 biological replicate, with 2 technical replicates of each strain at the 30-36 hour timepoint, and 3 technical replicates of each strain at the 36-42 hour timepoint.

The overall dataset reveals several striking differences between the ACS5 KO and its parental line (Figure 7.1.1). We focus here on the lipid data obtained from positive ion mode (Figure 7.1.1A), as well as the targeted hydrophilic metabolite data set (Figure 7.1.1B). Linear regression of the ACS5 KO versus 3D7 reveals differences in the parasite strains at 30 hours post invasion (hpi) and 40 hpi (Figure 7.1.2A and B). Mean ion intensity of lipid metabolites shows significant differences in several lipid species at the 30hpi timepoint (Figure 7.1.2C). Changes in both neutral lipid and phospholipid pools are observed. Of note, triglyceride (TG) species TG(18:1/18:2/20:3) and TG(16:0/16:0/20:4) and phosphatidylcholine (PC) species PC(16:0/20:5) are significantly reduced in the KO (Table 7.1.1). There are significant increases in phosphatidylcholine species PC(16:0) and

phosphoethanolamine (PE) species PE(P-18:0/20:4). Similar trends can be seen in the 40hpi timepoint, though the differences are not significant (Figure 7.1.2D and Table 7.1.1). Stratifying the lipids detected in positive ion mode by headgroup, we see significant changes in the PE class overall (Figure 7.1.3).

Additional significant differences are found in analysis of the targeted hydrophilic metabolites (Figure 7.1.1B). Linear regression of the ACS5 KO versus 3D7 reveals differences in the parasite strains at 30 hours post invasion (hpi) and 40 hpi (Figure 7.1.4A and B). Mean ion intensity of lipid metabolites shows significant differences in several hydrophilic metabolites at both the 30hpi and 40hpi timepoints (Figure 7.1.4C and D). Of note, TCA metabolites succinate and α-ketoglutarate are significantly reduced in the ACS5 KO at both timepoints, while glutamate is significantly reduced at 30hpi and increased at 40hpi relative to the 3D7 parent.

Changes are also observed in CDP-ethanolamine, a precursor to PE biosynthesis (Figure 7.1.4 and Table 7.1.2). With only a single biological replicate, it is difficult to speculate further about these changes. However, it is tempting to see these findings as evidence of perturbations to PE biosynthesis pathways.

Figure 7.1.1. A. Heatmap comparing positive ion lipid profile for ACS5 KO and 3D7 parental strain at 30-36hpi (“30”) and 36-42hpi (“40”). B. Heatmap comparing targeted hydrophilic metabolite profile for ACS5 KO and 3D7 parental strain at 30-36hpi (“30”) and 36-42hpi (“40”). Fold change was calculated from the mean log 2 differences in 2 (30-36hpi timepoint) or 3 (36-42hpi timepoint) technical replicates. (n=1 biological replicate)

A.

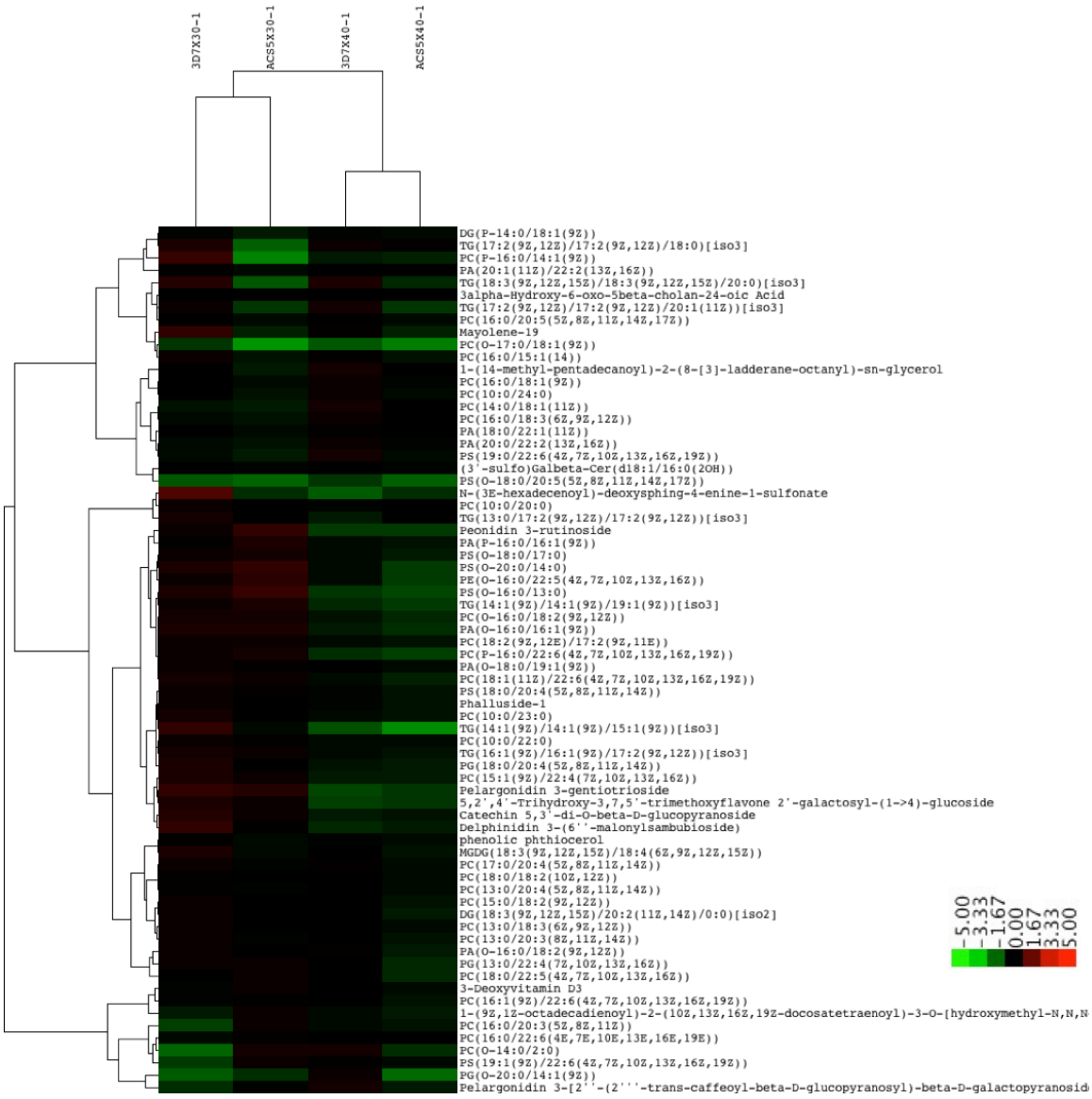

Figure 7.1.1 (continued).

B.

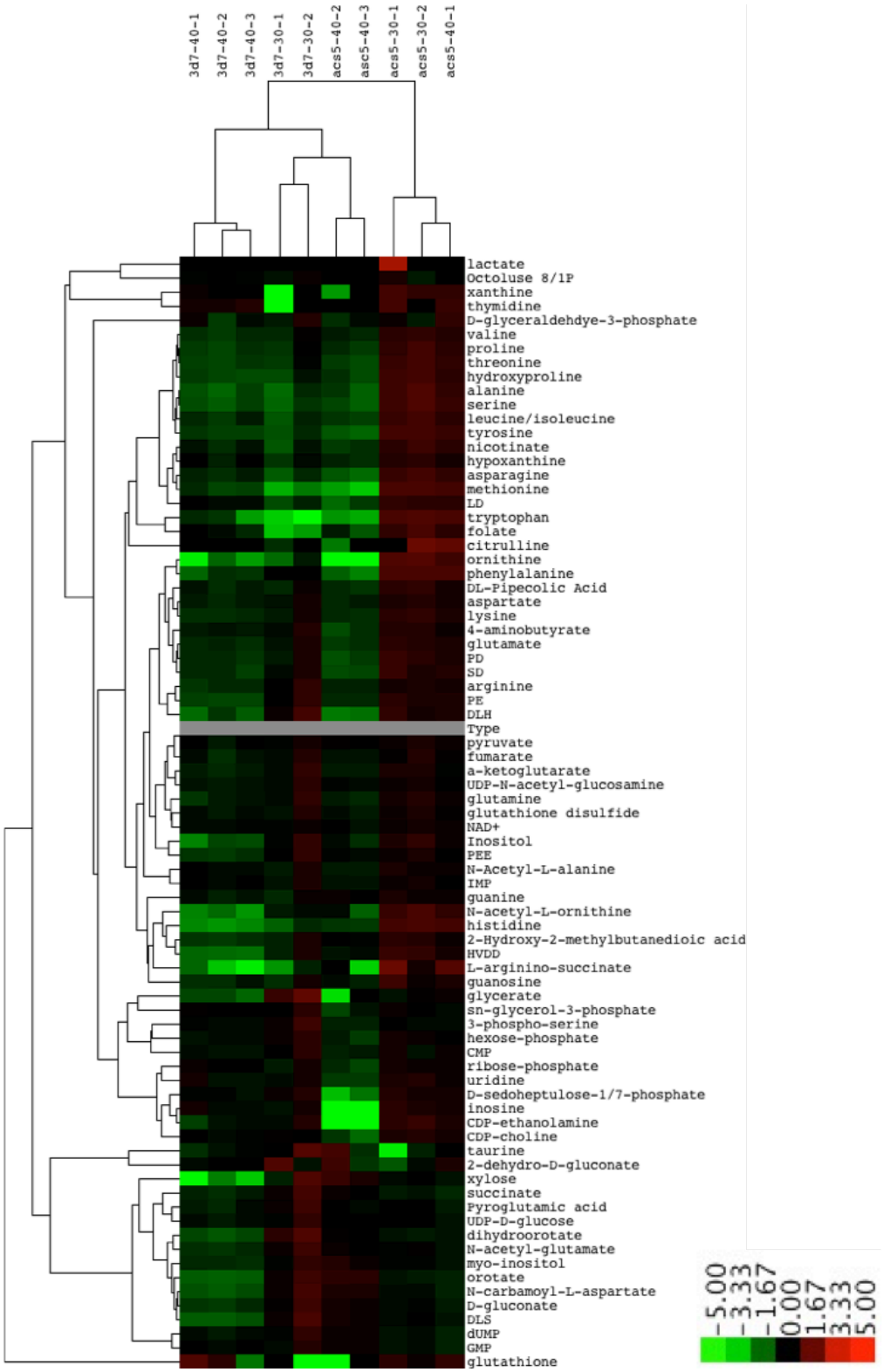

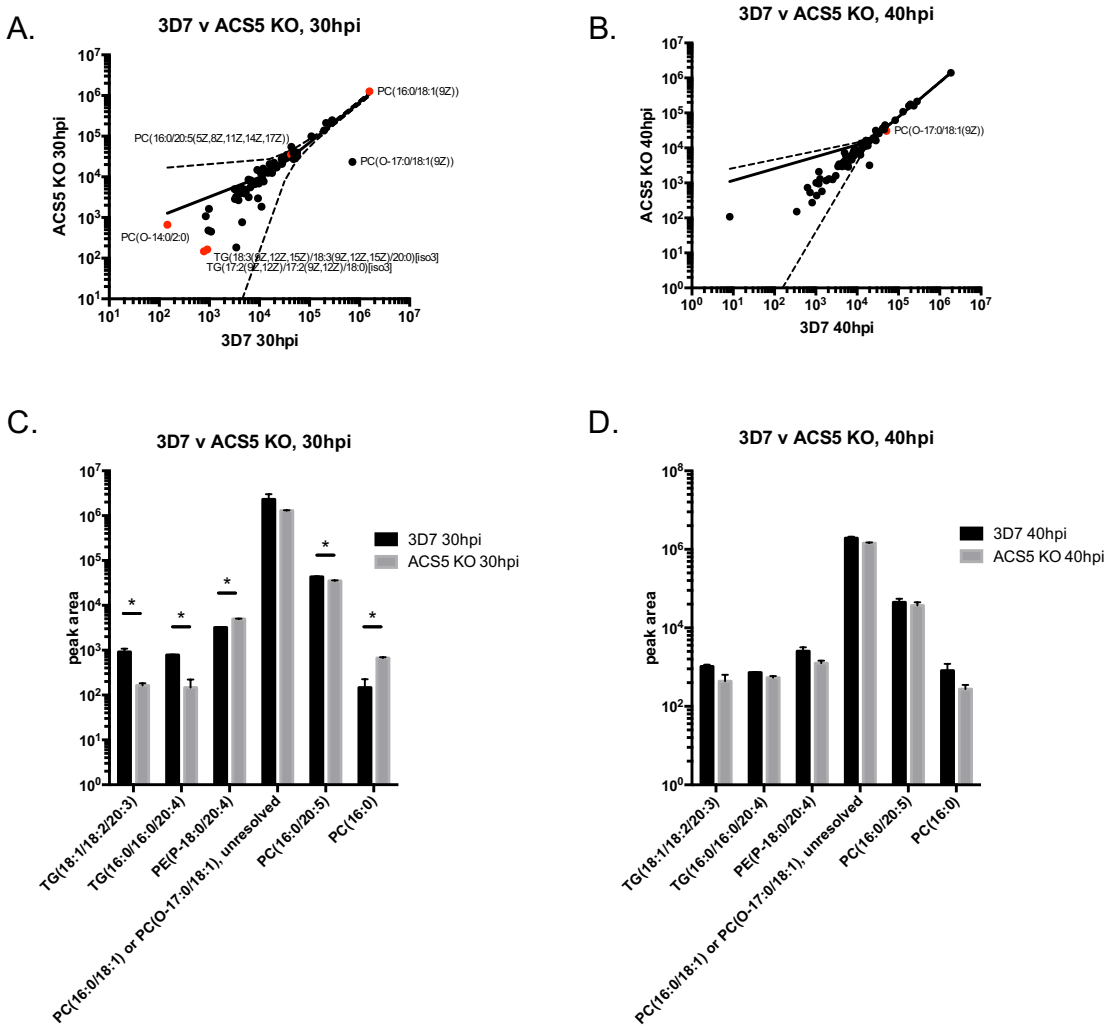

Figure 7.1.2. Significant differences in the lipid profile of the ACS5 KO and its 3D7 parent. Linear regression of ACS5 KO vs 3D7 at (A) 30-36 hours post invasion (hpi) and (B) 36-42 hpi. Mean ion intensity of lipid metabolites at the (C) 30hpi timepoint and (D) 40 hpi timepoint. All metabolites shown are MS/MS confirmed.

hydrophobic metabolites, positive mode						
	30 hpi			40 hpi		
metabolite	**3D7 mean**	**ACS5 KO mean**	**p value**	**3D7 mean**	**ACS5 KO mean**	**p value**
TG(18:1/18:2/20:3)	906.538	163.517	0.0470402	1042.21	437.091	0.109492
TG(16:0/16:0/20:4)	780.55	147.198	0.0136347	723.488	535.564	0.0823555
PE(P-18:0/20:4)	3195.66	4964.83	0.0030244	2556.11	1253.26	0.124026
PC(16:0/18:1) or PC(O-17:0/18:1), unresolved	2299866	1292693	0.285601	1922867	1439892	0.0627044
PC(16:0/20:5)	42839.3	35337.3	0.032416	44693.7	37091.8	0.594846
PC(16:0)	145.043	667.643	0.0242472	814.88	274.88	0.246084

Table 7.1.1. Comparison of mean peak area for top lipid species showing significant differences between ACS5 KO and 3D7 samples. Significant differences in the lipid profile of the ACS5 KO and its 3D7 parent were determined using t-tests. P values <0.05 are highlighted in red. All metabolites shown are MS/MS confirmed.

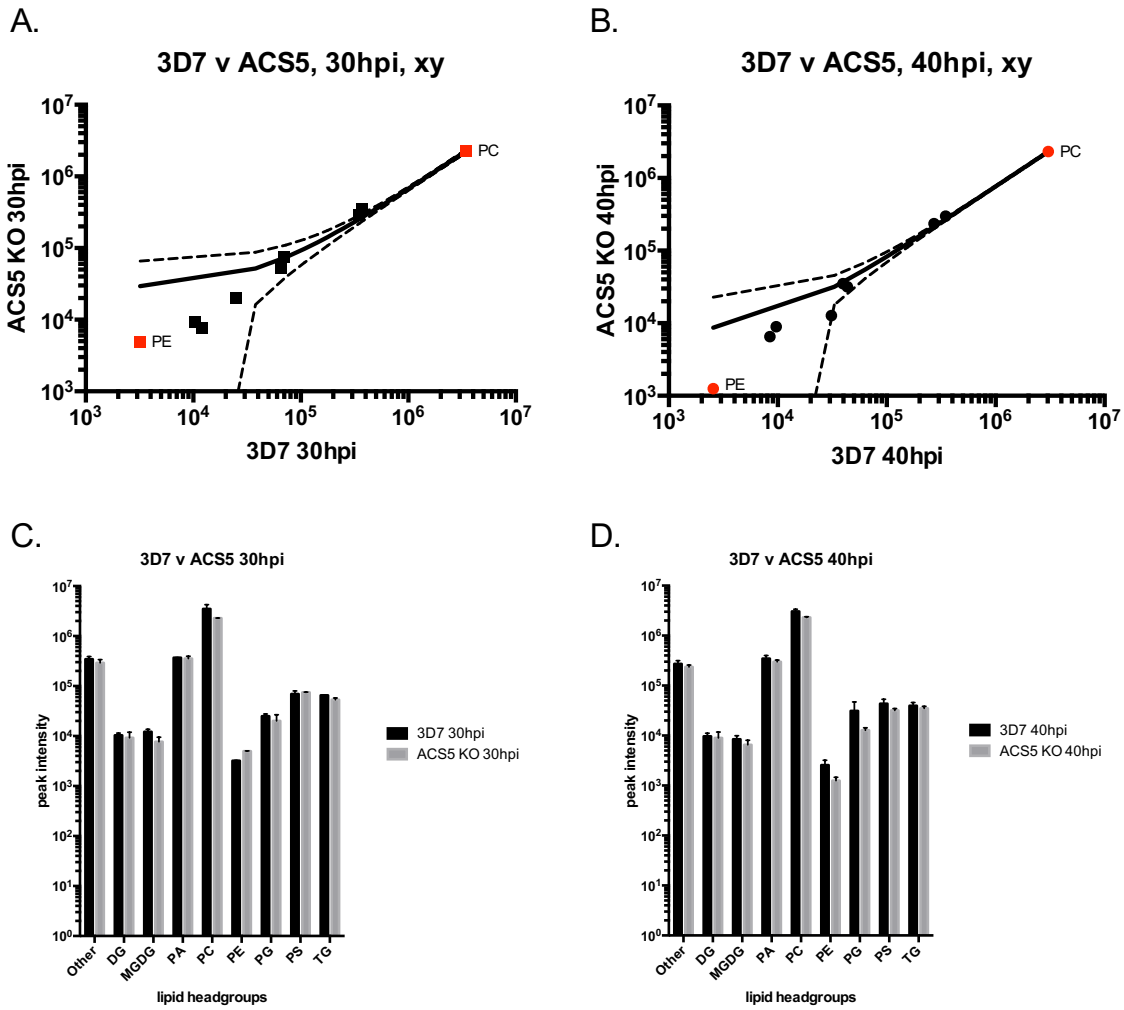

Figure 7.1.3. Significant differences in the positive ion lipid profile of the ACS5 KO and its 3D7 parent, stratified by headgroup. Linear regression of ACS5 KO vs 3D7 at (A) 30-36 hours post invasion (hpi) and (B) 36-42 hpi. Mean ion intensity of lipid metabolites, summed as lipid classes, at the (C) 30hpi timepoint and (D) 40 hpi timepoint. These metabolites have not been MS/MS confirmed.

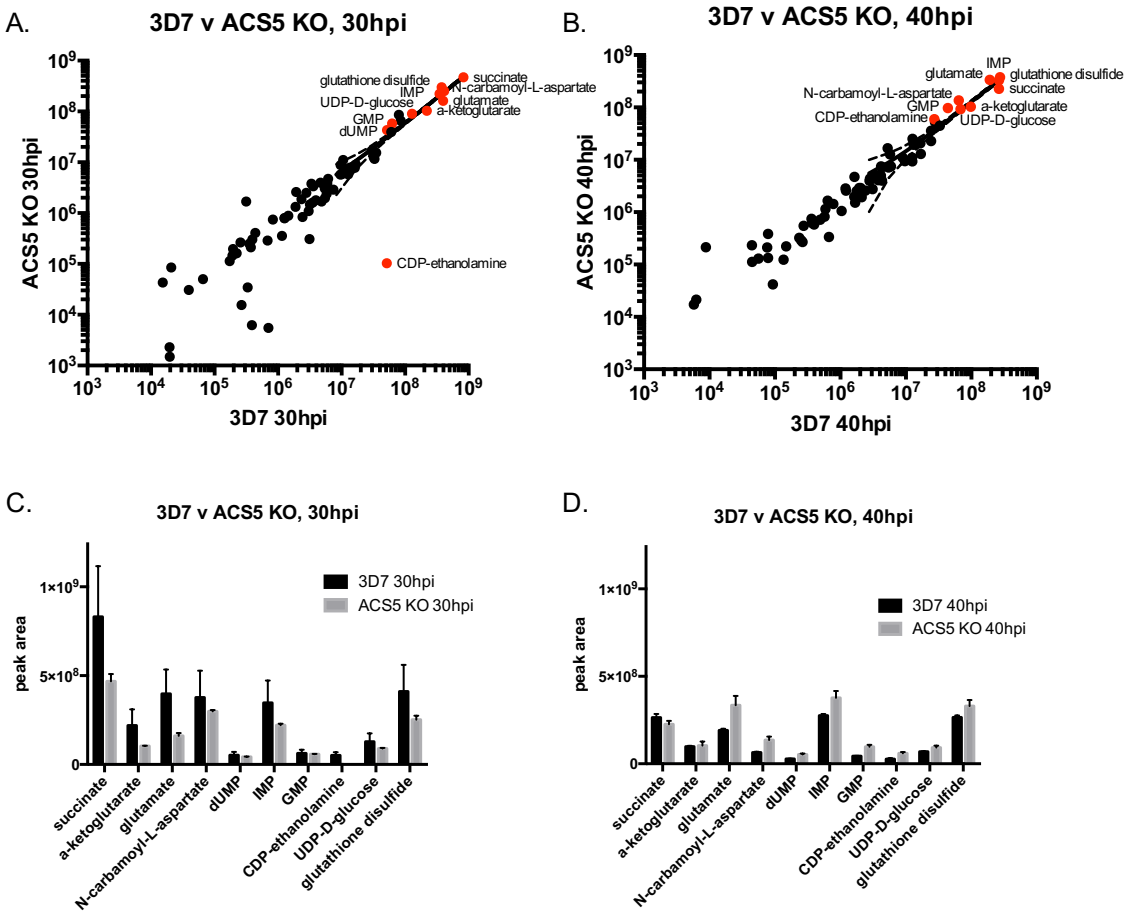

Figure 7.1.4. Significant differences in the hydrophilic profile of the ACS5 KO and its 3D7 parent. Linear regression of ACS5 KO vs 3D7 at (A) 30-36 hours post invasion (hpi) and (B) 36-42 hpi. Mean peak area of hydrophilic metabolites at the (C) 30hpi timepoint and (D) 40 hpi timepoint. Peak identity was confirmed by comparison to a known list of standards.

hydrophillic metabolites, targeted						
	30 hpi			40 hpi		
metabolite	3D7 mean	ACS5 KO mean	p value	3D7 mean	ACS5 KO mean	p value
succinate	831386100	468162100	2.55854E-12	263708400	225956000	0.000304081
a-ketoglutarate	219018800	103553100	0.0168301	97893220	103545300	0.584846
glutamate	397464800	161366000	1.98536E-06	190730700	334934100	1.02158E-34
N-carbamoyl-L-aspartate	376558000	298695900	0.105237	64492800	135942400	2.67857E-11
dUMP	52023320	42957680	0.849776	27790930	52717140	0.0164503
IMP	347161900	221445300	0.00937	275313100	376489200	6.55857E-20
GMP	62364390	57830040	0.924523	43789500	96959230	4.74755E-07
CDP-ethanolamine	51581320	102667	0.283006	27194570	59406890	0.00199834
UDP-D-glucose	128130100	89929130	0.42525	68636300	92710990	0.0204744
glutathione disulfide	410613100	251508500	0.00108527	264823900	330012700	9.69042E-10

Table 7.1.2. Comparison of mean peak area for top hydrophilic species showing significant differences between ACS5 KO and 3D7 samples. Significant differences in the hydrophilic profile of the ACS5 KO and its 3D7 parent were determined using t-tests. P values <0.05 are highlighted in red.

The most significant difference in lipid species was observed in phosphatidylethanolamine (PE) (P-18:0/20:4), which was significantly increased in the ACS5 KO at 30-36hpi (Figure 7.1.2, Table 7.1.2). To identify any global changes in a particular class of lipids in the ACS5 KO, we grouped our lipid results into broad classes. Analysis of the lipid profile stratified by class showed significant increases in the overall PE pool in the ACS5 KO (Figure 7.1.3). PE is the second most abundant phospholipid in *P. falciparum*, following phosphatidylcholine (PC), and is synthesized *de novo* by the parasite from diglycerides and CDP-ethanolamine (Vial et al. 2003; Holz 1977). Corresponding changes in CDP-ethanolamine levels were observed in the 30-36hpi and 36-42hpi timepoints of the targeted hydrophilic metabolic analysis (Figure 7.1.4, Table 7.1.2). These preliminary results support altered PE metabolism in the ACS5 KO.

There were additional changes in the PC profile, suggesting that ACS5 knockouts have an altered repertoire of PCs. When summarized by headgroup, there was a trend toward decreased overall PC pool in the ACS5 KO, though this was not statistically significant (Figure 7.1.3). Intriguingly, PC can be generated from PE, which was also significantly perturbed by the ACS5 KO.

Other intriguing differences were found in the targeted hydrophilic data set (Figures 7.1.1 and 7.1.4, Table 7.1.2). The significant decreases observed in TCA metabolites (succinate, a-ketoglutarate, and glutamate) at the 30-36hpi timepoint are compelling, and could explain the growth defect observed in the ACS5 KO. These significant decreases in TCA metabolites could explain how the ACS5 KO is particularly sensitive to starvation conditions, relative to the 3D7 parent. Baseline deficiencies in TCA function could make these parasites unable to respond to changes in available carbon sources. Additional biological replicates will confirm these findings, and help us to understand the metabolic changes in the ACS5 KO that inhibit parasite growth.

Supplemental methods for Chapter 4.

LC-MS/MS sample preparation and extraction

Methods adapted from Simon Cobbold and Ian Lewis (Cobbold et al. 2013). Parasite-infected RBCs were enriched by Vario MACS magnet purification with25CS or 25LD columns (Miltenyi Biotec). Parasites were counted by hemocytometer, and approximately 10^7-10^8 cells were used per sample. Cell pellets were washed 3x in cold PBS before extractions. Hydrophilic metabolites were extracted by the addition of 1mL 90% methanol (90 methanol:10 water), followed by immediate vortex. Samples were spun down (3500g for 2m), and the supernatant transferred to a new tube. Extraction was repeated, and a final

clarifying spin (10m at 13000rpm) removes any cell debris. Combined supernatants were dried down under N_2 gas and stored at -80°C. Hydrophobic extractions were performed by the addition of 50:50 methanol:water (containing 0.05M HCl and 5uM +5 Aspartate internal standard), followed by the addition of 0.5mL chloroform. The samples are vortexed, then spun down (13000rpm for 2m). The chloroform layer was transferred to a glass vial and chloroform extraction is repeated. Combined chloroform extractions are dried down under N_2 gas and stored at -80°C.

LC-MS/MS analytical methods

Hydrophilic samples

Samples were resuspended in HPLC grade water to a concentration of $1x10^5$-$1x10^6$ cells per microliter. A pooled QC sample was generated for each run to identify instrument drift, samples were randomized, and 10uL was injected for analysis. Negative ion LCMS was performed using the method described in (Lu et al. 2010; Cobbold et al. 2013). Chromatographic separation was achieved using a Phenomenex Synergi C18 Hydro-RP column (2.5 uM x 100A, 100 x 2mm) with the ion pairing agent tributylamine in mobile phase A. Solvent A is 97% water/3% methanol containing 10mM tributylamine and 15mM acetic acid; solvent B is methanol. The gradients have been modified from this original method to enhance the detection of later eluting compounds - 0 min = 0%B, 5 min = 20%B, 7.5 min = 55%B, 15 min = 65% B, 17.5 min = 95% B, 21-25 min = 0%B with data acquisition stopping at 22.5 minutes. The eluate was delivered into a Thermo Exactive Plus Orbitrap using a ESI-ion source. A scan range of m/z = 85-1000 was used for the study of small molecule metabolites. Other MS settings are resolution 140,000 at 1Hz scan, automatic gain control (ACG) target $3x10^6$, and maximum injection time of 100mS. Positive ion LCMS was performed through the Penn State metabolomics core facility.

Chromatographic separation (225uL/min flow rate) was achieved using a Prominence 20 UFLCXR system with a Waters BEH C18 column (1.7 uM, 100 x 2mm) maintained at 55 C. Solvent A is water with 0.1% formic acid and solvent B is acetonitrile with 0.1% formic acid. The gradients are – 0 min = 3%B, 10 min = 45%, 12 min = 75%B, 18-21 min = 3% B with data acquisition stopping at 20 minutes. The eluate was delivered into a 5600 (QTOF) TripleTOF using a Duospray™ ion source. A scan range of m/z = 50-1250 was used for the study of small molecule metabolites. The mass spectrometer was operated in IDA (Information Dependent Acquisition) mode with a 100 ms survey scan from 50-1250 m/z, and up to 10 MS/MS product ion scans (100 ms) per duty cycle using a collision energy of 50V with a 20V spread.

Hydrophobic samples

Samples were resuspended in a 1/1/0.3 chloroform/methanol/water solution to 4.2 x 10^4 cells/uL. A pooled QC sample was generated for each run to identify instrument drift, samples were randomized, and 5uL was injected for analysis. Positive and negative ion LCMS was performed through the Penn State metabolomics core facility. Chromatographic separation (225uL/min flow rate) was achieved using a Prominence 20 UFLCXR system with a Waters CSH C18 column (1.7 uM, 100 x 2.1 mm) maintained at 55 C. Solvent A is 40% water, 60% acetonitrile with 10mM ammonium formate and 0.1% formic acid and solvent B is 90% isopropanol, 10% acetonitrile with with 10mM ammonium formate and 0.1% formic. The initial condition were 60% A and 40 % B, increasing to 43% B at 2 min, 50% B at 2.1 min., 54% B at 12 min, 70% B at 12.1 min and 99% B at 18 min., held at 99% B until 20.0 min before returning to the initial conditions. The eluate was delivered into a 5600 (QTOF) TripleTOF using a Duospray™ ion source. The capillary voltage was set at 5.5 kV in positive ion mode and 4.5 kV in negative ion mode, with a declustering potential of 80V. The mass spectrometer was operated in IDA (Information Dependent Acquisition)

mode with a 100 ms survey scan from 100 to 1200 m/z, and up to 20 MS/MS product ion scans (100 ms) per duty cycle using a collision energy of 50V with a 20V spread.

LC-MS/MS analysis

Targeted (Orbitrap Hydrophilic and FFA)

Thermo Fisher .raw files were converted to .mzXML and analyzed as described in (Lu et al. 2010; Kamphorst et al. 2011). Metabolite identification was confirmed using an in-house generated knowns list, consisting of m/z and RT for pure standard compounds (292 total) run on the same analytical platform. Stable isotope labeled compounds were extracted using the RT for the unlabeled standard using the isotope extraction function of the open-source program "Metabolomics Analysis and Vizualization Engine". Isotope enrichment was determined by comparing the observed M+1/M and M+2/M ratios to the calculated theoretical $M = (1\text{-}0.011)^{N}$, $M+1 = N(0.011)(1\text{-}0.011)^{N-1}$, and $M+2 = (N(N\text{-}1)/2)(0.011^{2})(1\text{-}0.011)^{N-2}$ metabolites fractions, where N is the number of carbons and 1.1% is the natural abundance of ^{13}C. Extracted ion chromatogram (EIC) peak areas were exported as .csv files for further data processing (background subtraction and normalization), visualization, and statistical analysis.

Untargeted (All platforms)

Thermo .raw files were converted as above, while AB Sciex .wiff files were converted to .mzXML using ProteoWizard MSconvert with vendor preferred settings. Analysis was performed using the open source mzMine software. Putative identifications were created using a 20ppm cutoff against the KEGG, HMDB, and LipidMAPS databases depending on sample type. MS/MS spectrum matching was used for metabolite confirmation, where possible. EIC peak areas were exported as .csv files for further data processing (background subtraction and normalization), visualization, and statistical analysis.

7.2 Supplemental material for Chapter 5

Supplemental results for Chapter 5

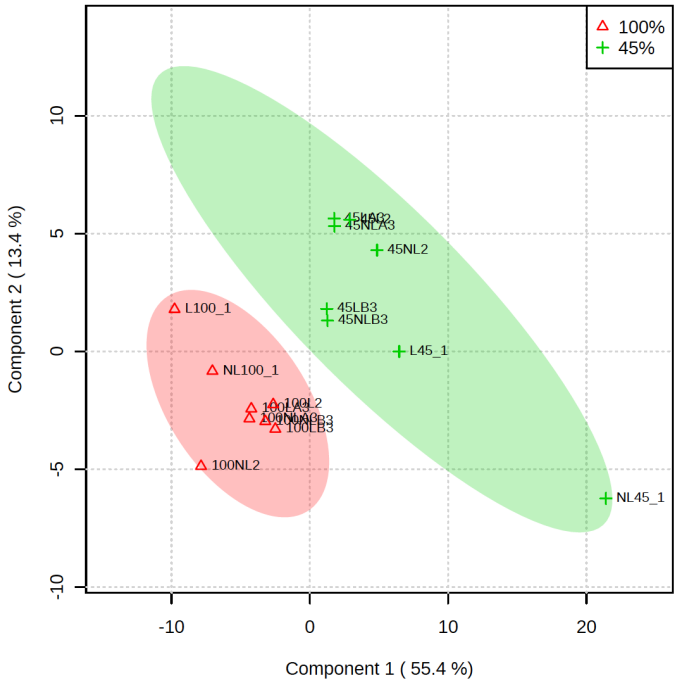

Figure 7.2.1. Partial least-squares discriminant analysis (PLS-DA) of 100% vs. 45% glucose/glutamine conditions.

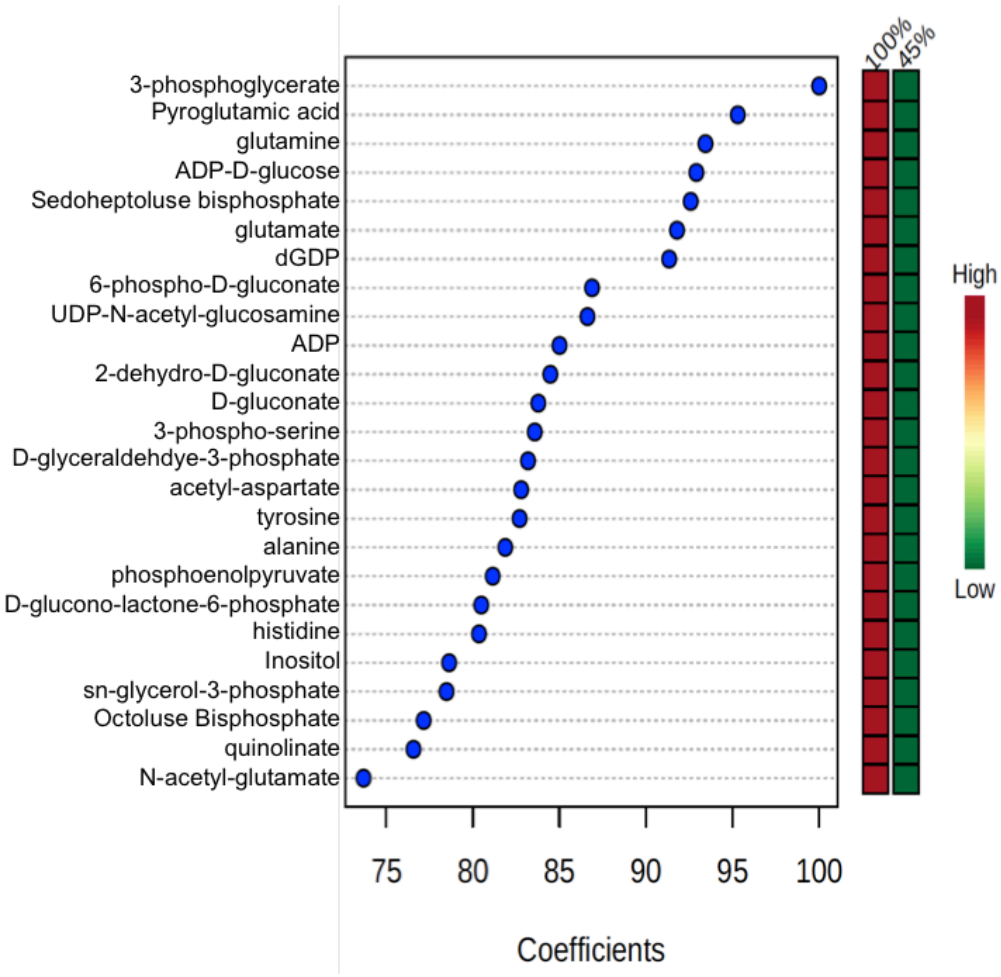

Figure 7.2.2. Major metabolites separating the two conditions by PLS-DA show enrichment for intermediates of the glycolytic and pentose-phosphate pathways, confirming t-test results.